INL/RPT-24-80743
Revision 0

Nuclear Thermal Energy Storage Configurations for Industrial Combined Heat and Power Supply: Conceptual Study and Engineering Designs

September 2024

Václav Novotný
Junyung Kim
So-Bin Cho
Aidan Rigby
Rami M. Saeed
Idaho National Laboratory

IES
Integrated Energy Systems

INL/RPT-24-
Revision 0

Nuclear Thermal Energy Storage Configurations for Industrial Combined Heat and Power Supply: Conceptual Study and Engineering Designs

Václav Novotný
Junyung Kim
So-Bin Cho
Aidan Rigby
Rami M. Saeed
Idaho National Laboratory

September 2024

Idaho National Laboratory
Integrated Energy Systems
Idaho Falls, Idaho 83415

http://www.ies.inl.gov

Prepared for the
U.S. Department of Energy
Office of Nuclear Energy
Under DOE Idaho Operations Office
Contract DE-AC07-05ID14517

Page intentionally left blank

EXECUTIVE SUMMARY

Audience

The report is aimed at the U.S. Department of Energy Office of Nuclear Energy and its federal manager; the Integrated Energy Systems program and its national technical director; representatives of strategic development in industries with high energy demands; advanced nuclear reactor developers; independent system operators; and electric utility companies.

Key Research Question

This report evaluates the prospects of thermal energy storage (TES) within the framework of an industrial energy park, where industrial processes rely on the heat and power supplied by nuclear systems. TES is explored as an enabling technology for enhancing load flexibility and energy system efficiency, thereby improving the feasibility of nuclear integration.

Research Overview

This report explores the potential for TES integration in an industrial energy park featuring various industrial processes (e.g., chemical plants, oil refineries, or iron and steel production facilities) to manage varying (or constant) heat and electricity demands. It also investigates different power conversion system layouts (e.g., TES integration between the nuclear primary loop and the steam cycle conversion system) to enhance energy efficiency and performance. Finally, it shows concept designs of the industrial energy park with combined heat and electricity demands from several industrials and system capacity optimization results.

Key Findings

The industries examined in this report primarily rely on moderate-temperature heat provided by gas- or coal-fired boilers and combined heat and power (CHP) plants, delivered through standard process steam systems. High-temperature energy demands are often industry-specific and typically exceed the capabilities of high-temperature gas-cooled reactors (HTGRs).

While it is technically feasible to replace process steam from fossil-based heat sources with nuclear energy, certain industries, such as methanol production and pulp and paper, face technoeconomic challenges in integrating nuclear energy without major changes or a technological shift. This is mainly due to the limited external energy demand remaining after the use of internal byproducts, waste heat recovery, and simple efficiency improvements. Achieving a full decarbonization of these processes with nuclear energy would require significant technological advancements, involving experimental technology and substantial investments, making widespread adoption in existing industrial plants unlikely in the near term.

This study reviews TES options in the context of enabling a flexible CHP supply while maintaining a steady nuclear heat input. Heat storage systems that interface between the reactor primary fluid and the CHP system offer superior performance and flexibility. Specifically, steam extraction downstream of the reheater with a two-tank molten-salt TES appears as the best solution regarding thermodynamic system benefits and system drawbacks. Using selected system configurations, a conceptual design of an industrial energy park was developed for industries with varying energy demands, such as steel production plants utilizing electric arc furnaces and chemical plants, as well as for those with constant energy demands, like petroleum refineries. This design highlights the capabilities of TES and explores its potential business cases. The study also conceptually develops the potential for integrating additional energy sources with nuclear systems through the implementation of TES.

The potential of the HTGR-TES-CHP system was also evaluated considering key uncertainties, such as industrial demand profiles, external grid access availability, and eligible tax credit levels, using the Holistic Energy Resource Optimization Network. We analyzed the sensitivity of net present value to these uncertainties to determine the optimal number of nuclear reactors (and CHP systems) and the suitable TES capacity. The results were interpreted from a decision-maker's perspective, focusing on three key areas: deployment strategy (oversized units vs. undersized units with TES support), industrial process characteristics (thermal-intensive single profiles vs. electricity-intensive combined profiles), and operational goals (maximizing profits vs. minimizing natural gas [NG] consumption or external grid dependence).

The optimization results indicate that the HTGR-TES-CHP system significantly reduces reliance on NG boilers for individual industrial processes by 9%–60% (in NG capacity factor), with an average reduction of 38%, compared to the standalone NG boiler operation case (business as usual). For combined industrial processes, the reduction ranges from 37%–77%, with an average of 60%. Additionally, the system greatly reduces dependence on external grids. In meeting industrial electrical demands, a 33%–100% self-sufficient internal electricity supply is achieved for a single industrial process, with an average of 74%, compared to the business-as-usual scenario, where 100% of the electricity is imported. For combined processes, 35%–100% of internal electricity demands are met by the reactor, with an average of 73%.

At last, we estimated the relative NG price levels at which the proposed HTGR-TES-CHP system can cost-effectively enter the market currently dominated by existing NG boilers. For a moderate HTGR CAPEX level ($2,500/kWth, $6,329/kWe), the analysis suggests that NG prices must be 2.5–7× higher than HTGR variable operating and maintenance costs for single industrial process and 5.5–9.5× higher for a combined process scenario. Tax credit modeling shows that the investment tax credit significantly reduces the price threshold needed to break even, making the system competitive with NG boilers in certain cases.

Why This Matters

The concept of industrial energy parks that utilize nuclear energy and TES matters for several reasons:

Balancing Energy Demand and Supply—TES can help flatten demand by storing excess energy during low-demand periods and releasing it during high-demand periods. This is particularly important for industries with fluctuating energy needs (e.g., chemical plants). In industries requiring stable energy demands (e.g. petroleum refining), integrating TES with nuclear CHP plants can modulate any excess power coming from oversized plants and export it to the electricity grid, thereby taking advantage of electricity arbitrage. In industries with variable energy demands (e.g. chemicals and iron and steel), TES can help manage demand fluctuations, ensuring a stable energy supply and reducing reliance on non-nuclear or external energy sources.

Increasing Efficiency—TES integration will enable nuclear power plants to operate more efficiently, especially when TES is employed between the nuclear primary loop and the steam cycle conversion system. TES enables enhanced flexibility in steam cycle configurations and design parameters.

Reducing Fossil Fuel Dependency—TES integration can reduce the need for backup fossil-fuel-based heating systems, decreasing the overall reliance on nonrenewable energy sources.

Maintaining Steady Electricity Export—TES can help maintain a steady electricity export, even after meeting an oscillating heat and electricity demand. This type of stability is important for grid reliability. Flexible systems with TES can provide further ancillary grid services as well.

How to Apply the Results

The power conversion and TES system layout, along with the corresponding energy balance models, can be applied during the design, licensing, construction, and operations of future industrial energy park projects. They also serve as a basis for further technoeconomic assessment efforts.

Page intentionally left blank

ACKNOWLEDGEMENTS

This manuscript has been authored by Battelle Energy Alliance, LLC under Contract No. DE-AC07-05ID14517 with the U.S. Department of Energy. The U.S. Government retains and the publisher, by accepting the article for publication, acknowledges that the U.S. Government retains a nonexclusive, paid-up, irrevocable, worldwide license to publish or reproduce the published form of this manuscript, or allow others to do so, for U.S. Government purposes.

Page intentionally left blank

CONTENTS

EXECUTIVE SUMMARY v
ACKNOWLEDGEMENTS ix
ACRONYMS xvii
1. INTRODUCTION 1
2. ENERGY STORAGE TECHNOLOGIES FOR INDUSTRIAL ENERGY PARK 9
3. ENERGY DISPATCH STRATEGIES 11
3.1 Systems with Varying Energy Dispatch 11
3.2 Systems with Constant Energy Dispatch 12
3.3 Combination of Systems 12
4. SELECTED INDUSTRIES AND THEIR CHARACTERISTICS 13
4.1 Chemicals 13
4.2 Petroleum Refinery 14
4.3 Iron and Steel Production 15
4.4 Food and Beverage 16
4.5 Pulp and Paper Mills 16
4.6 Summary of Selected Industries 17
5. POWER CONVERSION AND STORAGE SYSTEM LAYOUTS 18
5.1 No Steam Extraction—Electric Power Only 19
5.2 Steam Extraction—No Reheater 20
5.3 Steam Extraction—Upstream of the Reheater 20
5.4 Steam Extraction—Downstream of the Reheater 21
5.5 Backpressure 23
5.6 High-Temperature Heat Delivery System 24
5.7 Summary of Power Conversion Systems 26
6. INDUSTRIAL ENERGY PARK—EXAMPLES AND ENGINEERING DESIGNS 28
6.1 Energy Demand 28
6.2 Configuration of Energy Sources 28
7. SYSTEM CAPACITY OPTIMIZATION AND TECHNOECONOMIC ANALYSIS 34
7.1 Technoeconomic Analysis 35
7.2 Impacts of Loads Aggregation 38
7.3 Impacts of External Grid Access Availability 45
7.4 HTGR Energy Delivery Requirements 47

8. CONCLUSIONS 50
9. REFERENCES 52
Appendix A Review of CHP Applications in Nuclear Power Plants 60
Appendix B Thermal Energy Storage Systems 65
Appendix C Power Conversion and Storage System 67
Appendix D Conceptual Demonstration of Industrial Energy Park with Individual Industry 78
Appendix E Framework for Analysis of Reactor with TES System Based on Specified Electrical Power Demand 89
Appendix F Holistic Energy Resource Optimization Network 94
Appendix G Input Cost Parameters for HERON Optimization 96
Appendix H Core HERON Optimization Results 97

FIGURES

Figure 1. Number of national net zero pledges and share of global CO_2 emissions covered. 2
Figure 2. Global CO_2 Emissions by Sector. 2
Figure 3. Primary energy-related CO_2 emissions in the U.S. [5] 3
Figure 4. The path to net-zero industrial CO_2 emissions in the United States for five carbon-intensive industrial subsectors, with contributions from each decarbonization pillar 4
Figure 5. Breakdown of energy use onsite at the U.S. manufacturing facilities, along with the distribution of process heat temperature ranges by industrial subsector in 2018 (modified from [6,7]). 5
Figure 6. Distribution of process heat demand across all industry branches in the European Union-28 in 2012, as distinguished by temperature level (modified from [8]). 6
Figure 7. Cumulative process heat demand by temperature. 6
Figure 8. Conceptual design of nuclear – industrial energy park. Rendering is modified based on TerraPower NATRIUM. 8
Figure 9. Generic layout of possible integration points for implementing TES into a nuclear/CHP system. 9
Figure 10. Layout for integrating a molten-salt TES into a nuclear reactor system: 10
Figure 11. Illustration of a nuclear-TES-CHP system for industries that feature variable demand. 11
Figure 12. Illustration of a nuclear-TES-CHP system for industries with constant demand. 12
Figure 13. Steam and electricity supply profile for Case A (an anonymous chemical company). 13
Figure 14. Steam and electricity supply profile for Case B (Eastman Chemical Company). [26] 14
Figure 15. Reference petroleum refinery process. [27] 15
Figure 16. EAF electric load profile (modified from [28]). 16

Figure 17. PFD of the no-steam-extraction configuration for a nuclear-TES plant that fully decouples the nuclear island from the power conversion cycle. 19
Figure 18. PFD of steam extraction—no reheater from the nuclear-decoupled system. 20
Figure 19. PFD of steam extraction upstream of the reheater from the nuclear-decoupled system. 21
Figure 20. PFD of steam extraction downstream of the reheater from the nuclear-decoupled system. 22
Figure 21. Efficiency characteristics of the nuclear-decoupled systems 23
Figure 22. PFD of backpressure CHP system from the nuclear-decoupled system. 24
Figure 23. Industrial heat delivery system for providing heat at temperatures that exceed the possibilities of main or extracted steam. 25
Figure 24. PFD of HT heat delivery system from the nuclear-decoupled system. 26
Figure 25. Combined energy demand profiles of the energy park. 28
Figure 26. A general representation of the energy system that also includes other non-nuclear resources. 29
Figure 27. Proposed configuration of nuclear based system for the energy park. 30
Figure 28. Cost vs. Energy Storage Discharge Duration. [34] 30
Figure 29. Heat and electricity demand and supply from HTGRs and their power conversion systems for the industrial energy park. 31
Figure 30. Energy balance profiles and State of charge (SoC) of energy storage systems. 32
Figure 31. Parametric analysis on TES storage capacity. 33
Figure 32. Parametric analysis on H_2 storage capacity. 34
Figure 33. Schematic representation of the HERON simulation 37
Figure 34. NPV maximizing configurations for the HTGR-TES-CHP system for a single industrial process (under varying deployment cases) 40
Figure 35. NPV maximizing configurations for the HTGR-TES-CHP system for combined industrial processes (under varying deployment cases) 40
Figure 36. Crossover points where the HTGR-TES system outperforms standalone NG boilers in cost-effectiveness (NPV) for a single industrial process. 44
Figure 37. Crossover points where the HTGR-TES system outperforms standalone NG boilers in cost-effectiveness (NPV) for combined industrial processes. 45
Figure 38. NPV percentile distribution with varying external grid access availability under different deployments (combined industrial processes). 46
Figure 39. Natural gas boiler capacity factor (NGCF) distribution with varying external grid access availability under different deployments (combined industrial processes). 47
Figure 40. Two conceptual IES layouts that integrate an HTGR with packed-bed TES. 65
Figure 41. Baseline CHP system with extraction turbine (no integrated TES) 68
Figure 42. Efficiency characteristics of the baseline CHP system with extraction turbine (assuming ideal controlled extractions). 68

Figure 43. Baseline CHP system with backpressure turbine. 69
Figure 44. Efficiency characteristics of the baseline CHP system with a backpressure turbine. 70
Figure 45. Nuclear-TES coupling approach using steam for charging. 70
Figure 46. Nuclear-TES coupling approach in which steam is used for charging the TES and a dedicated balance of plant is used for TES discharging: 72
Figure 47. Conceptual layout of TES integration on the heat extraction branch. 73
Figure 48. A nuclear-TES coupling approach with extraction-charged TES, which then discharges into a process steam line: 74
Figure 49. Configuration with a PCM TES that uses turbine extraction steam for charging and discharges into a process steam line. 75
Figure 50. A nuclear-TES coupling approach with extraction-charged TES with PCM, which then discharges into a process steam line. 76
Figure 51. Heat and electricity demand and supply from HTGRs and their power conversion systems (for chemical plant A). 79
Figure 52. Net excess (positive) or deficit (negative) electricity at chemical plant A after providing all heat via the configuration proposed in Table 13. 80
Figure 53. Heat and electricity demand profiles, supply from proposed systems, and resulting net balance for chemical plant B. 81
Figure 54. Net surplus (positive) or deficit (negative) electricity and heat at chemical plant B, which features the configuration proposed in Table 15. 81
Figure 55. Case involving the integration of Xe-100 reactors into EAF operation over a 24-hour period. Positive power implies energy export. 83
Figure 56. System configurations for nuclear and TES integration into chemical plant A (with relatively higher electricity demand). 84
Figure 57. Net electricity balance for chemical plant A—both with and without TES—when the operation demand is a steady 35 MWe export (positive sign = export; negative sign = import). 84
Figure 58. System configurations for nuclear and TES integration into chemical plant B (with relatively higher heat demand). 85
Figure 59. Net heat balance for chemical plant B (the case with six backpressure turbine systems), both with and without TES (positive sign = curtailment; negative sign = backup boilers). 85
Figure 60. Net electricity balance for chemical plant B (the case with six backpressure turbine systems), both with and without TES (positive sign = export; negative sign = import). 86
Figure 61. State of charge for the specific TES implemented at chemical plant B. 86
Figure 62. Two configurations for implementing TES into the petroleum refinery system: on a CHP extraction system and on an electricity-only system. 87
Figure 63. Example of a TES system applied to the excess power from the petroleum refinery integration—in daily cycling operation and with an arbitrary export demand profile. 87
Figure 64. Configuration of nuclear-TES coupling to an EAF. 88

Figure 65. Electricity demand from the EAF facility, and the electricity supply from the nuclear-TES system. 88
Figure 66. Adaptation of hourly set point demands to new dispatch profile based on a chose electrical power ramp rate of 7.5%/min. 90
Figure 67. Power demand and electrical power output tracking across the course of a week. 90
Figure 68. Effect of chemical plant A dispatch profile on the HPT inlet within the dynamic modelling. 91
Figure 69. SHS system tank levels for week of dispatch examined. 91
Figure 70. Core Inlet temperature variation with the dispatching of the thermal energy storage in the weekly demand case analyzed. 92
Figure 71. Core Thermal Power Deviation variation with the dispatching of the thermal energy storage in the weekly demand case analyzed. 92
Figure 72. Bi-level optimization scheme used in HERON with multiple realizations. [109] 94
Figure 73. Crossover points where the HTGR-TES system outperforms standalone NG boilers in cost-effectiveness (NPV) for a single industrial process (HTGR CAPEX: $2500/kWt, $6329/kWe). 97
Figure 74. Crossover points where the HTGR-TES system outperforms standalone NG boilers in cost-effectiveness (NPV) for a single industrial process (HTGR CAPEX: $1750/kWt, $4430/kWe). 98
Figure 75. Crossover points where the HTGR-TES system outperforms standalone NG boilers in cost-effectiveness (NPV) for combined industrial processes (HTGR CAPEX: $2500/kWt, $6329/kWe). 99
Figure 76. Crossover points where the HTGR-TES system outperforms standalone NG boilers in cost-effectiveness (NPV) for combined industrial processes (HTGR CAPEX: $1750/kWt, $4430/kWe). 100
Figure 77. NPV percentile distribution with varying external grid access availability under different deployments (single-industrial process). 100
Figure 78. Natural gas boiler capacity factor (NG CF) distribution with varying external grid access availability under different deployments (single-industrial process). 101
Figure 79. Change in optimal sizing of BOP and TES with varying import and export levels and external grid access availability (single industrial process). 102
Figure 80. Change in optimal sizing of BOP and TES with varying import and export levels and external grid access availability (combined industrial processes). 103

TABLES

Table 1. Summary of selected target industries for industrial energy park. 18
Table 2. Summary of Power Conversion Systems – NR-TES-CHP type. 27
Table 3. Modeled scenarios for different industrial load input and external grid access availability. 38

Table 4. Optimizing system sizing, NPVs, and performance parameters for a single industrial process under varying operational goals: maximizing NPV, minimizing the natural gas boiler capacity factor (NG CF), and maximizing internal electricity supply. 42

Table 5. Optimizing system sizing, NPVs, and performance parameters for combined industrial processes under varying operational goals: maximizing NPV, minimizing the natural gas boiler capacity factor (NG CF), and maximizing internal electricity supply. 42

Table 6. Breakdown of the HTGR-TES system operation for combined industrial processes under varying operational goals: maximizing NPV and minimizing the natural gas boiler capacity factor (NGCF). 48

Table 7. Change in minimum allowable HTGR heat price under varying investment tax credit (ITC) levels for combined industrial processes. (HTGR CAPEX: $3250/kWt, $8228/kWe) 49

Table 8. Change in minimum allowable HTGR heat price under varying investment tax credit (ITC) levels for combined industrial processes (HTGR CAPEX: $1750/kWt, $4430/kWe) 50

Table 9. Existing and past operating nuclear CHP plants for desalination. [14] 60

Table 10. Existing and past operating nuclear CHP plants for DH. [55] 61

Table 11. Existing and past operating nuclear CHP plants for process heat. 63

Table 12. Summary of Power Conversion Systems – NR-POWER / NR-CHP /NR-CHP-TES-POWER / NR-CHP-TES type. 77

Table 13. System parameters for scenarios that integrate an HTGR with chemical plant A. 78

Table 14. Parameters of applied HTGR systems with different CHP configurations. 78

Table 15. System parameters of the scenarios that integrate HTGR with chemical plant B. 80

Table 16. Parameters of applied HTGR systems with different CHP configurations. 80

Table 17. System parameters of scenarios that integrate an HTGR with the reference refinery. 82

Table 18. Parameters of applied HTGR systems with different CHP configurations. 82

Table 19. Cost assumptions for HERON optimization. 96

Table 20. Breakdown of the HTGR-TES system operation for a single industrial process under varying operational goals: maximizing NPV and minimizing the natural gas boiler capacity factor (NGCF). 103

Table 21. Change in minimum allowable HTGR heat price under varying investment tax credit (ITC) levels for a single industrial process. (HTGR CAPEX: $3250/kWt, $8228/kWe) 104

Table 22. Change in minimum allowable HTGR heat price under varying investment tax credit (ITC) levels for a single industrial process (HTGR CAPEX: $2500/kWt, $6329/kWe). 105

Table 23. Change in minimum allowable HTGR heat price under varying investment tax credit (ITC) levels for a single industrial process (HTGR CAPEX: $1750/kWt, $4430/kWe). 105

Table 24. Change in minimum allowable HTGR heat price under varying investment tax credit (ITC) levels for combined industrial processes. (HTGR CAPEX: $2500/kWt, $6329/kWe) 106

ACRONYMS

APC	announced pledges case
BOP	balance of plant
CAPEX	capital expenditure
CHP	combines heat and power
DRI	directly reduced iron
EAF	electric arc furnace
ERCOT	Electric Reliability Council of Texas
GHG	greenhouse gas
HP	high pressure
HT	high temperature
HTF	heat transfer fluid
HTGR	high-temperature gas-cooled reactor
IRA	inflation reduction act
ITC	investment tax credit
LT	low temperature
NDC	nationally determined contribution
NG	natural gas
NGCF	natural gas capacity factor
NPV	net present value
O&M	operation and maintenance
PCC	power conversion cycle
PCM	phase change materials
PFD	process flow diagram
RAVEN	Risk Analysis Virtual ENvironment
SMNR	small modular nuclear reactor
TES	thermal energy storage
VRE	variable renewable energy

Nuclear Thermal Energy Storage Configurations for Industrial Combined Heat and Power Supply: Conceptual Study and Engineering Designs

1. INTRODUCTION

Decarbonization is essential in the fight against climate change, as it directly addresses the reduction of greenhouse gas (GHG) emissions, which are the primary drivers of global warming and its associated impacts. The science is clear: to prevent the most severe consequences of climate change—such as more frequent and intense extreme weather events, rising sea levels, and widespread disruptions to ecosystems—significant reductions in GHG emissions are necessary. [1] Decarbonization not only mitigates these risks but also presents an opportunity to transform economies, creating new industries and jobs in clean energy, improving public health by reducing air pollution, and enhancing overall quality of life.

Under the Paris Agreement, all United Nations member states are required to submit nationally determined contributions (NDCs) to the United Nations Framework Convention on Climate Change and implement policies to achieve their stated climate goals. The Paris Agreement encourages countries to achieve a balance between GHG emissions and removals in the second half of the century. The Intergovernmental Panel on Climate Change Special Report on Global Warming of 1.5°C emphasized the necessity of reaching net-zero CO_2 emissions globally by midcentury to prevent the worst impacts of climate change.

There has been a significant increase in the number of governments making net-zero emissions pledges, as shown in Figure 1. The first round of NDCs, submitted by 191 countries, covered over 90% of global CO_2 emissions related to energy and industrial processes. As of April 23, 2021, 80 countries had submitted new or updated NDCs, covering just over 40% of global CO_2 emissions. [2] Many of these updated NDCs included more stringent targets than the initial submissions, with broader coverage across sectors and GHGs.

By April 2021, 44 countries and the European Union had pledged to meet a net-zero emissions target. Of these, 10 countries have enshrined their net-zero targets into law, eight are proposing to do so, and the rest have made their pledges through official policy documents. This growing commitment to net-zero emissions reflects the increasing recognition of the urgent need to address climate change through decisive and coordinated global action. The United States has set goals to achieve 100% carbon-pollution-free electricity by 2035 and to reach net-zero GHG emissions by 2050. [3] These targets are part of a broader strategy outlined in the U.S. long-term strategy, which presents multiple pathways to a net-zero economy by 2050. [4]

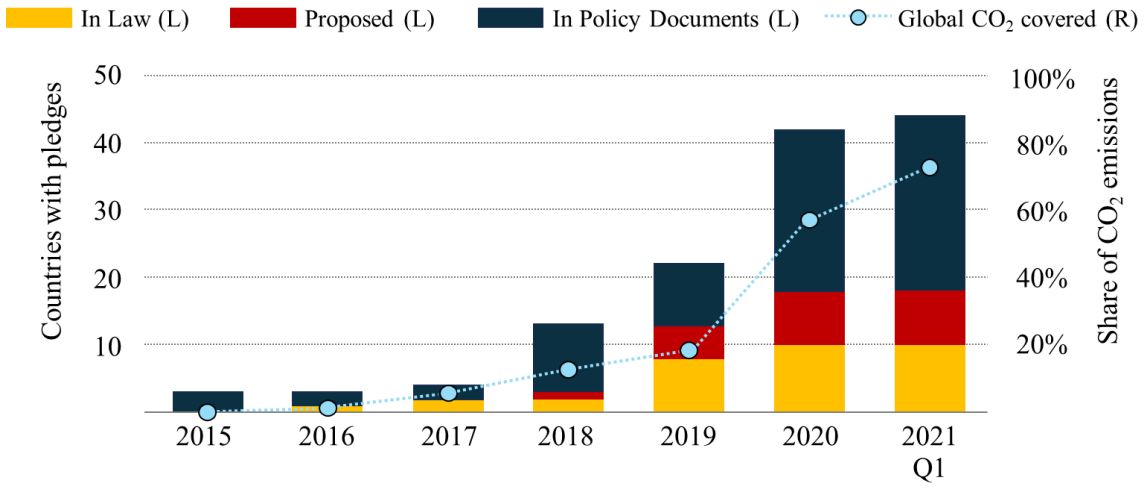

Figure 1. Number of national net-zero pledges and share of global CO_2 emissions covered, where In Law means a net-zero pledge has been approved by parliament and is legally binding, Proposed means a net-zero pledge has been proposed to parliament to be voted into law, and In Policy Documents means a net-zero pledge has been proposed but does not have legally binding status. [2]

The Announced Pledges Case (APC) assumes that all announced national net-zero pledges are achieved in full and on time, whether or not they are currently underpinned by specific policies. It has been estimated in Reference [2] that global energy-related and industrial process CO_2 emissions will fall to 30 Gt in 2030 and 22 Gt in 2050. Extending this trajectory, with similar action on non-energy-related GHG emissions, would lead to a temperature rise of around 2.1°C in 2100 (with a 50% probability). Global electricity generation nearly doubles to exceed 50,000 TWh in 2050. The share of renewables in electricity generation rises to nearly 70% in 2050. Oil demand does not return to its 2019 peak and falls about 10% from 2020 levels to 80 mb/d in 2050. Coal use drops by 50% to 2,600 Mtce in 2050, while natural gas (NG) use expands by 10% to 4,350 bcm in 2025 and remains about that level to 2050. Figure 2 shows global CO_2 emissions and the APC by sector. Based on the APC, industry must reduce emissions by 25% in 2050 compared to 2020.

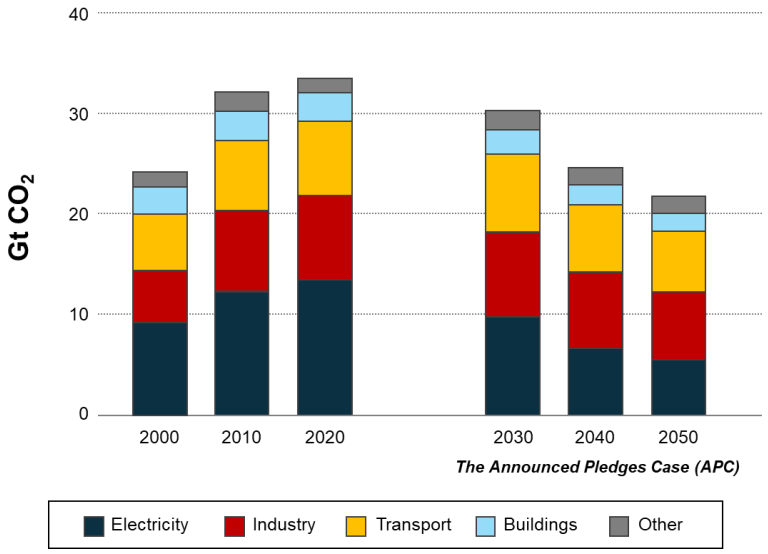

Figure 2. Global CO_2 emissions by sector (modified from Reference [2]).

The U.S. industrial sector, which accounted for 33% of the nation's primary energy use and 30% of energy-related CO_2 emissions in 2020, plays a critical role in the decarbonization effort. [5] The sector is considered difficult to decarbonize due to the diversity of energy inputs and the heterogeneity of industrial processes. Figure 3 presents the energy-related atmospheric CO_2 emissions attributed to each economic sector, breaking down industry by its subsectors. It is worth noting that five subsectors (cement and lime, food products, iron and steel, bulk chemicals, and refining) combined are more than 50% of the CO_2 emissions from industry.

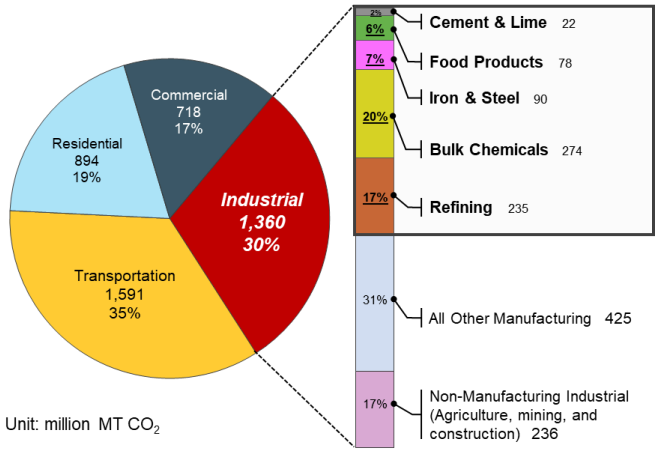

Figure 3. Primary energy-related CO_2 emissions in the United States. [5]

To reduce CO_2 emissions, the United States is focusing on several strategies, including energy efficiency, low-carbon fuels, electrification, and carbon capture, utilization, and storage. Figure 4 indicates that achieving net-zero CO_2 emissions in the top CO_2-emitting industrial subsectors by 2050 will require multiple decarbonization technologies and approaches in parallel. The following industrial subsectors were included in Figure 4: iron and steel, chemicals (only ammonia, methanol, ethylene, and BTX), food and beverage (only bear, beet sugar, cane sugar, fluid milk, red meat, soybean oil, and wet corn milling), petroleum refining, and cement manufacturing.

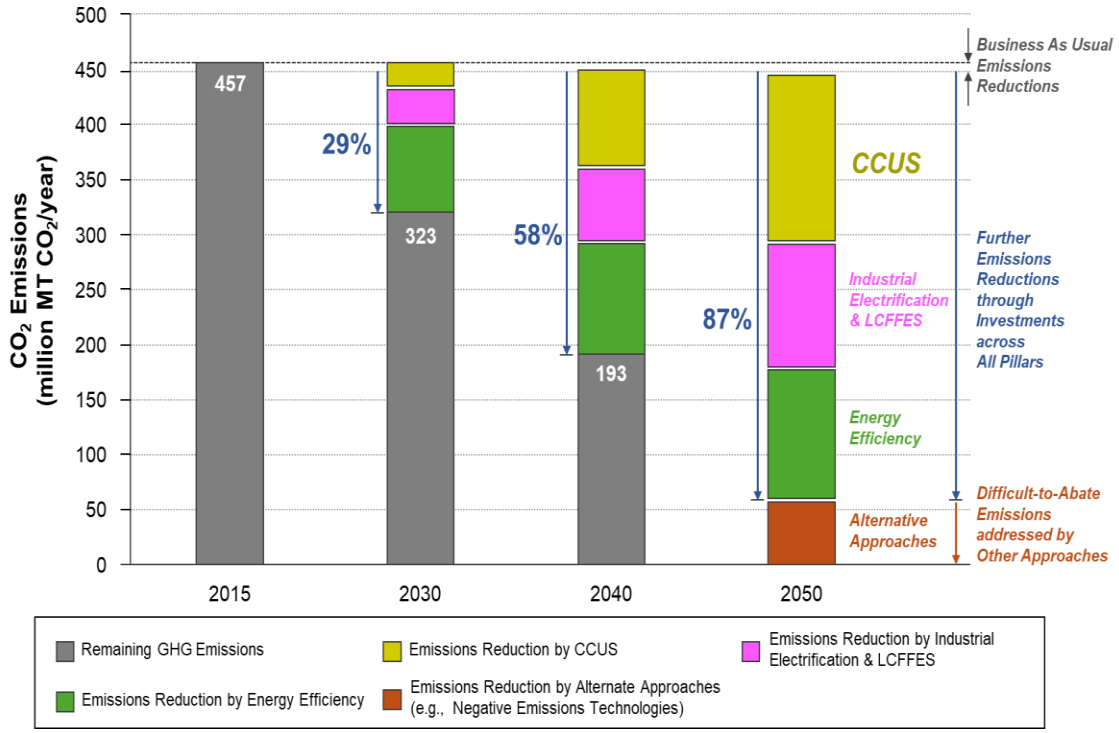

Figure 4. The path to net-zero industrial CO_2 emissions in the United States for five carbon-intensive industrial subsectors, with contributions from each decarbonization pillar: energy efficiency; industrial electrification; low-carbon fuels, feedstocks, and energy sources (LCFFES); and carbon capture, utilization and storage (CCUS). [5]

The difficulty in decarbonizing industrial applications stems from the varied types of energy used (such as petroleum, NG, and coal), the levels of energy demand, and the wide range of temperatures required. Figure 5 illustrates the distribution of energy use at U.S. manufacturing facilities, along with the temperature ranges for process heat across different industrial subsectors. Notably, process heating, which accounts for more than half of the energy consumption at these facilities, requires temperatures below 300°C and constitutes around 70% of the total process heating demand.

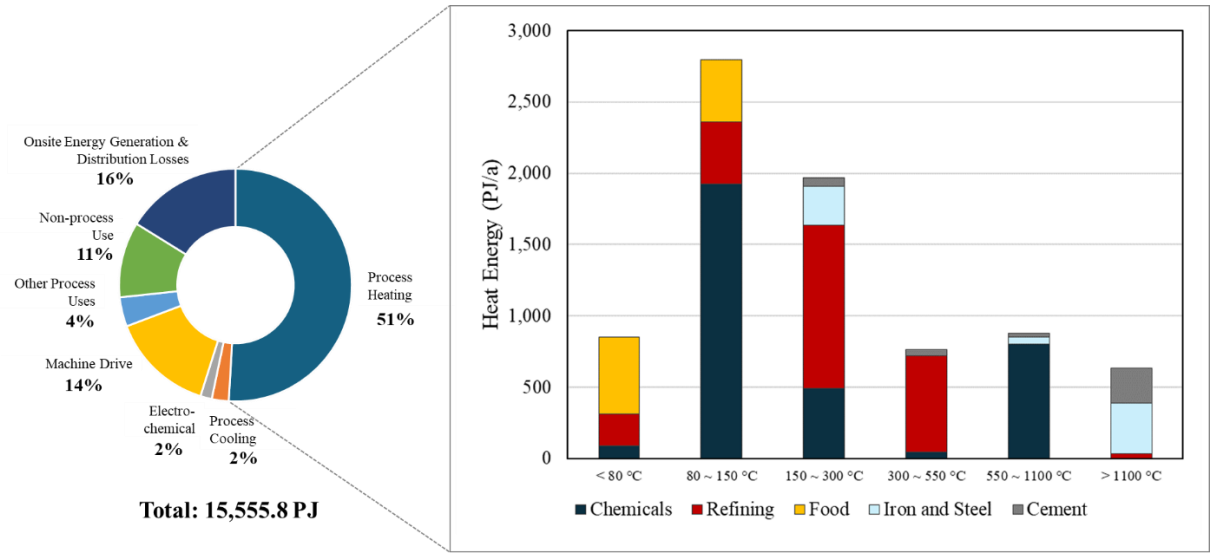

Figure 5. Breakdown of energy use onsite at the U.S. manufacturing facilities, along with the distribution of process heat temperature ranges by industrial subsector in 2018 (modified from References [6,7]).

A comparable summary has been compiled for the European Union as well (conveyed in Figure 6, followed by a cumulative distribution for the European Union in Figure 7). The demand for heat at temperatures exceeding 500°C results from fuels being used as feedstock in high-temperature conversion processes (e.g., coking coal in steel manufacturing) and high-temperature electrical heating (e.g., an electric arc furnace [EAF]). These high-temperature process heating requirements are primarily found in the steel, mineral, and chemical industries. Figure 7 shows the cumulative energy demand over the application temperatures of all manufacturing industries in the United States and European Union. One significant observation is that about two-thirds of all process heat in the United States is used for applications below 300°C, thus confirming that decarbonization efforts should focus on this temperature range. Nearly 90% of the process heat is used for applications below 800°C. In the European Union, the data show that only about 40% of all process heat is used for applications below 300°C.

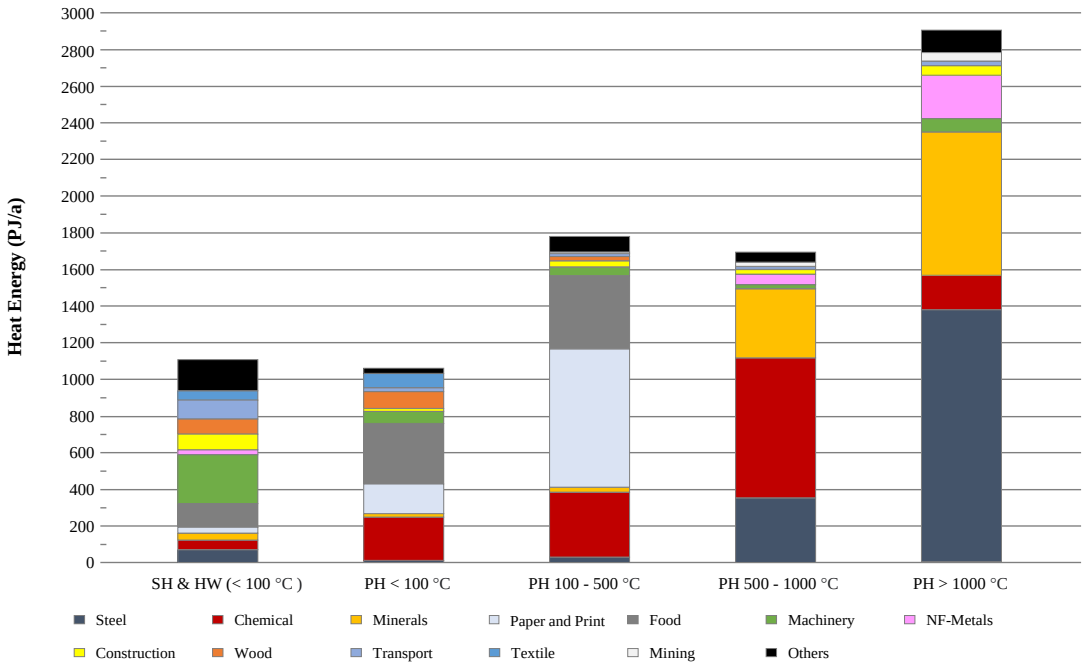

Figure 6. Distribution of process heat demand across all industry branches in the European Union-28 in 2012, as distinguished by temperature level (modified from Reference [8]), where SH, HW, and PH stand for space heat, hot water, and process heat, respectively.

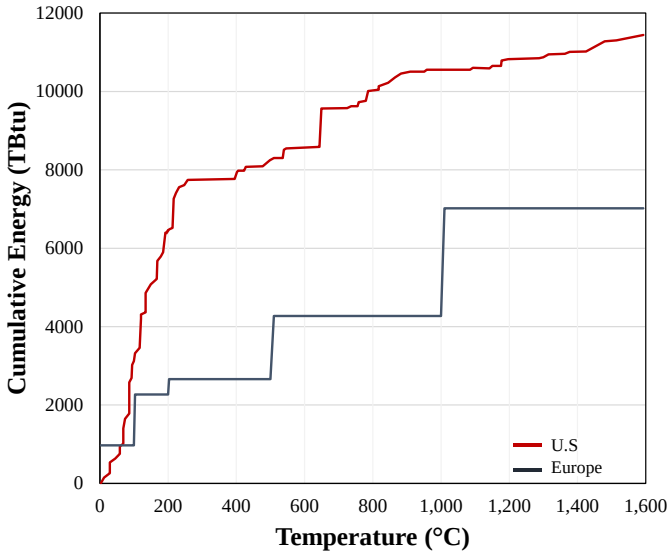

Figure 7. Cumulative process heat demand by temperature (compiled from 2014 data from Reference [7] for the United States, from 2012 data from Reference [8] for the European Union, and refining the granularity of demand from 100°C to 500°C, as specified in Reference [9]).

Traditional CHP technologies involve the combustion of fossil fuels and biomass, utilization of solar energy, or conversion of direct fuel in a fuel cell. After converting the most potent portion of the energy to power, a portion of the heat, eventually waste heat, is utilized for heating applications. While heating systems are built for specific applications, they are still often built from modular and standardized components and systems, which simplifies the retrofitting processes. [10,11] These modifications can often be implemented in a "plug-in" approach without requiring higher engineering efforts. [10] From this perspective, the potential impact of transitioning from fossil-fuel-powered CHP systems to nuclear reactors is considerable. The U.S. Energy Information Administration data reveal that, in 2022, the U.S. industrial sectors consumed nearly 1,044 Petajoules (PJ) of coal, 9,622 PJ of petroleum, and 11,405 PJ of NG. [12] These energy sources supplied the process heat, electricity, or feedstocks for chemical processes. The shift to a nuclear-based CHP could thus significantly reshape industrial energy consumption patterns, leading to carbon emission reductions.

Existing and past nuclear CHP applications have predominantly leveraged nuclear heat at approximately 55°C–130°C for desalination [13], at 128°C–150°C for district heating (DH) [14], and at 190°C–220°C for process heat applications. [15] Light- and heavy-water reactors are widely employed across different applications and regions, with unique designs being deployed locally to meet specific needs based on when the project commenced. For instance, the desalination plant in Aktau (Kazakhstan) employed a liquid-metal-cooled fast reactor with a thermal output of 750 MWth, making it the largest commercial nuclear desalination facility ever operated worldwide. [16] A water-cooled water-moderated reactor (PWR [pressurized-water reactor] or VVER [Vodo-Vodnyj Energetičtij Reaktor]) and Reaktor Bolshoy Moshchnosti Kanalnyy (RBMK–which translates to High Power Channel-type Reactor) were deployed for district heating in Russia and Eastern European countries that were part of the former Soviet Union when the plants were centrally planned. [17] A detailed review of CHP applications in nuclear power plants can be found in Appendix A, Review of CHP Applications in Nuclear Power Plants.

Integrating nuclear power in process heating is most feasible for temperature requirements below 300°C since temperatures beyond this threshold are theoretically attainable by leveraging high reactor outlet temperatures from high-temperature gas-cooled reactors (HTGRs) (e.g., the Xe-100 [18] at 750°C), but integration would be challenging since many industrial processes are designed and optimized for direct fossil fuel combustion. The potential challenges to supplying high-temperature process heat from a nuclear power plant (NPP) within an industrial park include:

- At present, high-temperature heat transfer is predominantly achieved through radiation.
- The heating temperature distribution profiles must be managed. The temperature of the heat transfer fluids (HTFs), after heating the given process, may be higher than the maximum allowed reactor inlet (return from process heating) temperature.
- The process may involve direct fuel conversion, in which fuel composition plays a crucial role, especially in the iron and steel production industry.
- Byproducts from certain industries (e.g., the pulp and paper and petroleum refinery industries) are already being used internally by those industries as fuel. Industrial processes have been optimized to utilize byproducts that would otherwise be wasted.

Due to these challenges, the decarbonization of process heat at temperatures above 500°C is more feasible with direct electrification via low-carbon-sourced energy or (eventually) synthetic fuel combustion than with nuclear heat delivery. For complete decarbonization, some established industrial processes must be modified to change the manner in which byproducts and waste currently used as fuel are reprocessed.

This study begins by identifying industries that are well-suited for replacing or supplementing existing process heating facilities with nuclear power to reduce GHG emissions in the industrial sector. Three criteria were considered in selecting target industries: energy demand, applicability of heat from nuclear energy, and the operating principles of the industries. After reviewing energy requirements from [5], we identified five industries for investigation: chemicals, petroleum refining, iron and steel, food and beverage, and pulp and paper. Next, we explored the applicability of thermal energy storage (TES) within the concept of an industrial energy park. [19,20] Figure 8 shows a conceptual rendering of an industrial energy park. The industrial energy park consists of three major islands: nuclear island, energy island (non-nuclear), and industrial island. Nuclear reactors are on the nuclear island while combined heat and power (CHP) systems (or power conversion cycle [PCC] systems) are on the energy island. Several industrial processes can be placed on the industrial island.

TES can enhance the system's flexibility by responding effectively to varying demands, temperatures, and scales across different industries. Additionally, we examined the operating principles behind industrial processes. For instance, pulp and paper plants, which are significant energy consumers, utilize internally produced byproducts like wood waste and kraft chemical recovery processes to meet their energy and heat needs, often exporting excess electricity. [21] Finally, we conceptually demonstrated the integration of nuclear power into an industrial energy park, an integrated system comprising an energy island, energy conversion island, and industrial island. The concepts and designs presented here are broadly applicable across various other types of resources, industries, and consumers.

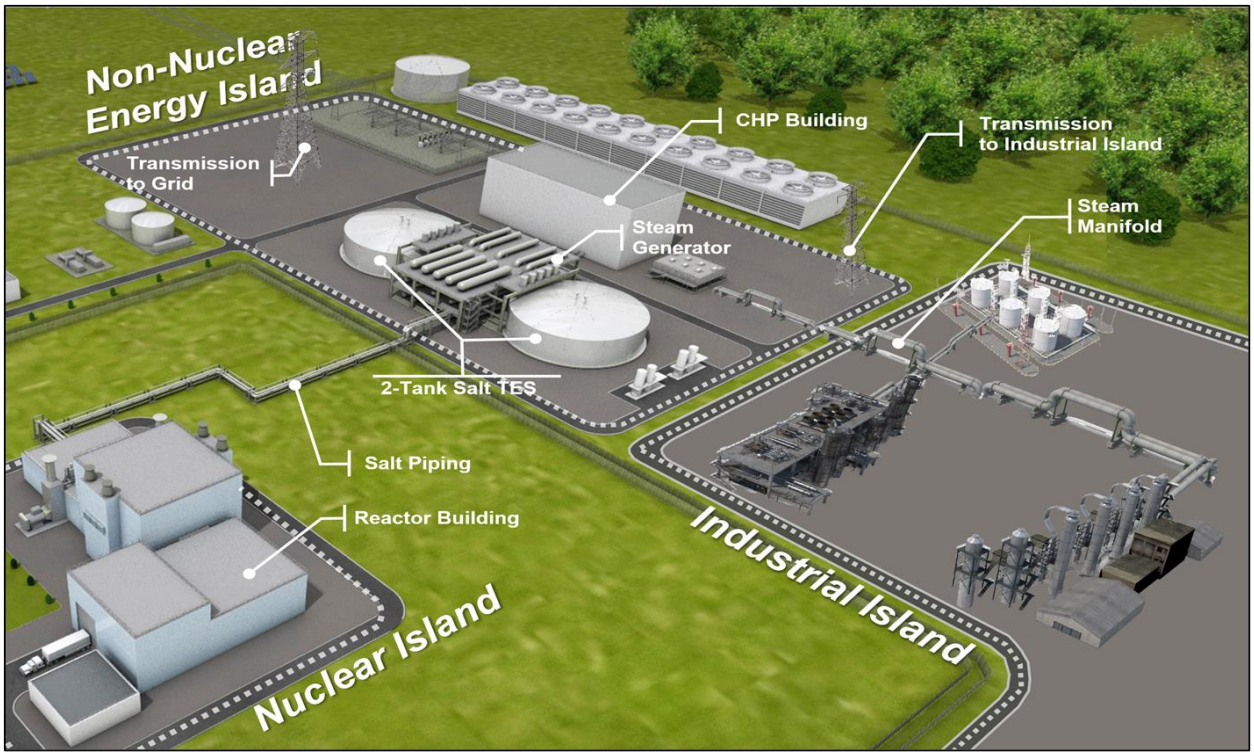

Figure 8. Conceptual design of a nuclear industrial energy park. Rendering is modified based on TerraPower Natrium.

This report consists of eight sections: Section 2 reviews TES technologies for an industrial energy park. Section 3 shows potential energy dispatch strategies. Section 4 then details the main heat and electricity demands of several different industries. While there could be more industries with nuclear integration in the future, the current study only highlights industries that can enable near-term decarbonization. Section 5 illustrates potential power conversion and energy storage system layouts and summarizes key characteristics of each layout. Section 6 demonstrates the concept of an industrial energy park and shows preliminary results. Section 7 shows quantitatively evaluated results of the potential of the HTGR-TES-CHP system under key aspects related to industrial demand profiles, external grid access availability, and eligible tax credit levels using the Holistic Energy Resource Optimization Network. Section 8 presents the overall conclusions.

2. ENERGY STORAGE TECHNOLOGIES FOR INDUSTRIAL ENERGY PARK

TES can be integrated into various points within CHP systems (i.e., before and after the energy conversion system) as shown in Figure 9. The suitability of a given technology varies by application, each introducing its own limitations and exergy losses. Even if the nuclear power source is primarily supplying heat, a power conversion system should be incorporated to maximize exergy efficiency in heat delivery systems. Power conversion systems increase the entire system efficiency by minimizing temperature disparities between the heat source and the application and converting the interim energy into electricity for the industrial process. Figure 9 shows a generic layout for a CHP system, highlighting potential TES integration points.

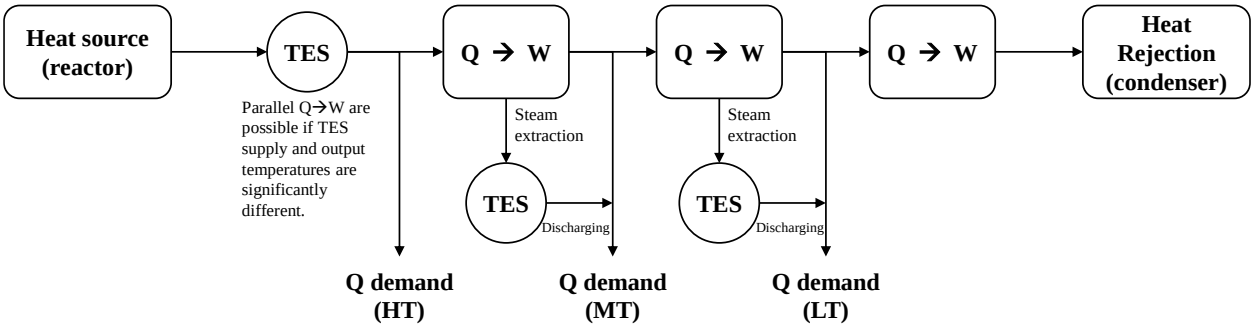

Figure 9. Generic layout of possible integration points for implementing TES into a nuclear CHP system, where HT, MT, and LT stand for high, medium, and low temperature, respectively, and Q and W represent heat (Q) that is converted to work (W) in a piece of turbomachinery.

Heat and power dispatch is controlled by switching the conversion system between heat and power and by adjusting the total discharge rate. It will later be shown in the report that the most suitable system involves directly integrating TES with the primary heat source (e.g., primary loop of an NPP). Integrating TES with the heat output stream(s) is inefficient and hindered by the currently low technology readiness levels of available (or even anticipated) TES systems.

Molten-salt storage is a standard technology utilized in concentrated solar power plants, and it is increasingly used in industrial integrated TES systems to take advantage of fluctuating electricity prices for charging. The upper temperature limits (typically around 500°C–550°C) of the most commonly used salts, such as solar salt or HITEC, [22] are limited due to corrosion or thermal degradation, though they can be used at temperatures over 600°C in some cases. [23] Other salts (e.g., hydroxide with proprietary corrosion control methods) can function up to about 700°C. [24] The $MgCl_2$-KCl eutectic mixture is recommended for high temperature (HT) applications (around 750°C). [25]

The melting points of these salts set the lower operating temperature limit, which they must always be above. While salts such as HITEC have melting temperatures below 200°C, the MgCl2-KCl mixture's melting point is 422°C. Figure 10(a) shows the ideal layout for integrating a molten-salt TES into a nuclear reactor system, but the lower and upper temperature limitations of salt together with nominal reactor inlet and outlet temperatures may necessitate a more complex approach, as reflected in Figure 10b (based on a design found in Reference [25]).

In this report, molten-salt storage technology is utilized throughout this report. Alternatively, other sensible heat storage technologies could be adopted. These other technologies are outlined in Appendix B, Thermal Energy Storage Systems.

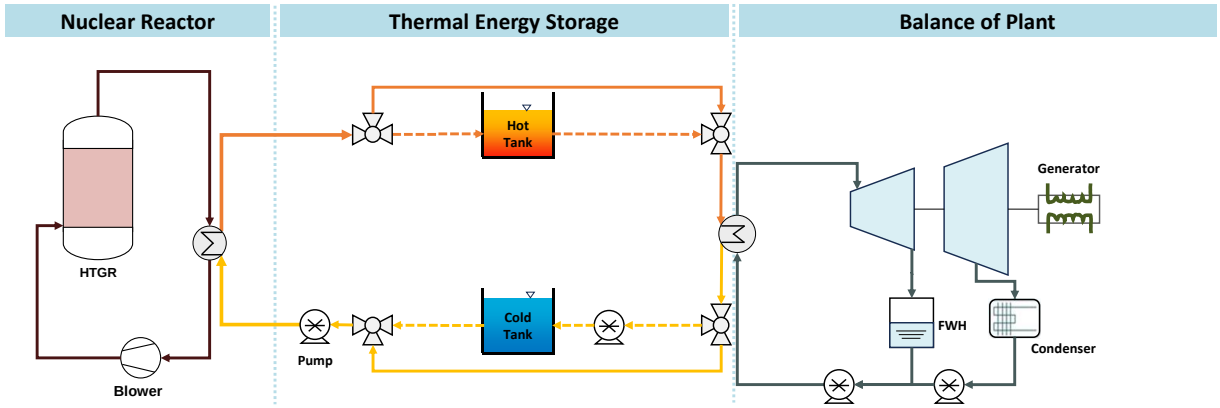

(a)

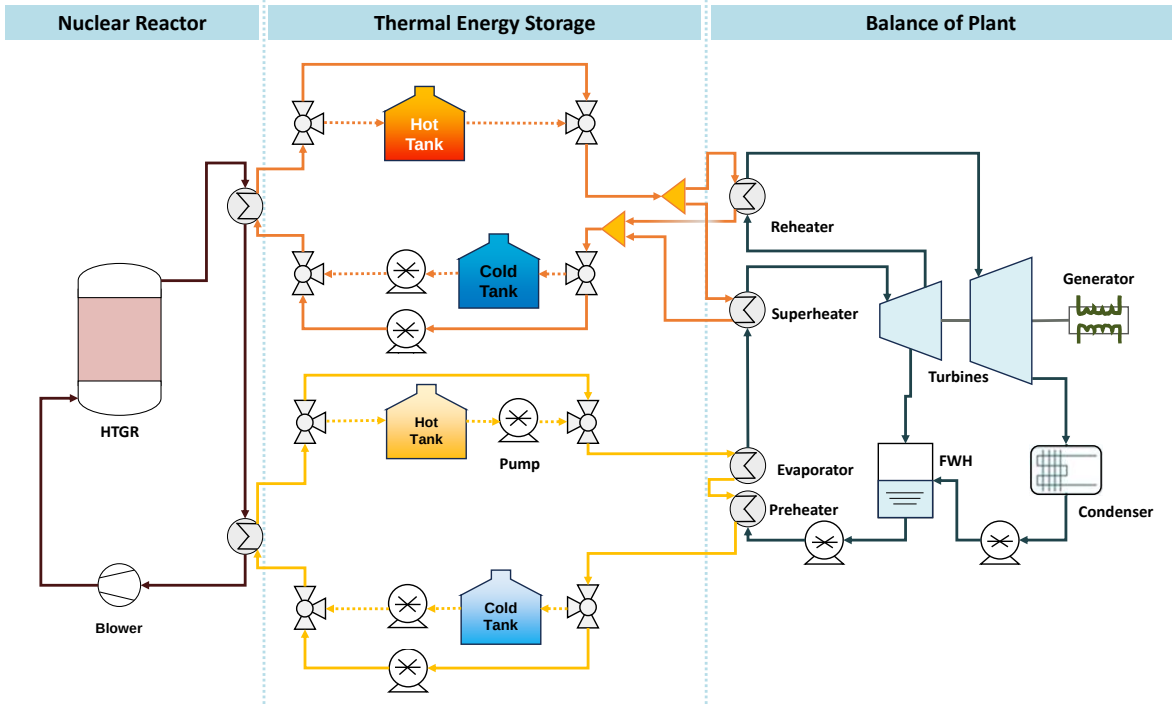

(b)

Figure 10. Layout for integrating a molten-salt TES into a nuclear reactor system: (a) ideal configuration of a molten-salt TES coupled to a primary loop and (b) two-TES system solution, as presented in Reference [25], to address the temperature limitations of TES fluids.

3. ENERGY DISPATCH STRATEGIES

Some industries operate on a baseload schedule, with maintenance shutdowns or rampdowns occurring once every several years, and some industries have highly variable load profiles. Variable profiles greatly benefit from using TES for flexible heat and power production. Systems with steady demand profiles can also benefit from flexible energy dispatch when integrated with small modular nuclear reactor (SMNR) systems.

3.1 Systems with Varying Energy Dispatch

Systems with variability in load demand inherently require a flexible energy supply. Such flexibility can be provided by the grid, an onsite energy production system, or a combination of both. Without TES, when the demand is less than the amount of energy from the onsite supply system, any excess energy produced must either be exported (as electricity) or curtailed (either by lowering the output of an energy source or releasing and wasting its produced energy). The chemical production and food and beverage industries are two industries with varying loads due to their use of batch-processing operations. This concept is illustrated in Figure 11.

A flexible nuclear-TES coupled system could potentially mitigate demand peaks and reduce risks in terms of the external energy supply and grid interactions. TES also improves system efficiency by supplementing plant demands during peak hours, which reduces capacity requirements for primary energy generators (i.e., the SMNR) and avoids expensive energy imports. Furthermore, active grid interaction remains an option, generating revenue via grid auxiliary services and arbitrage opportunities.

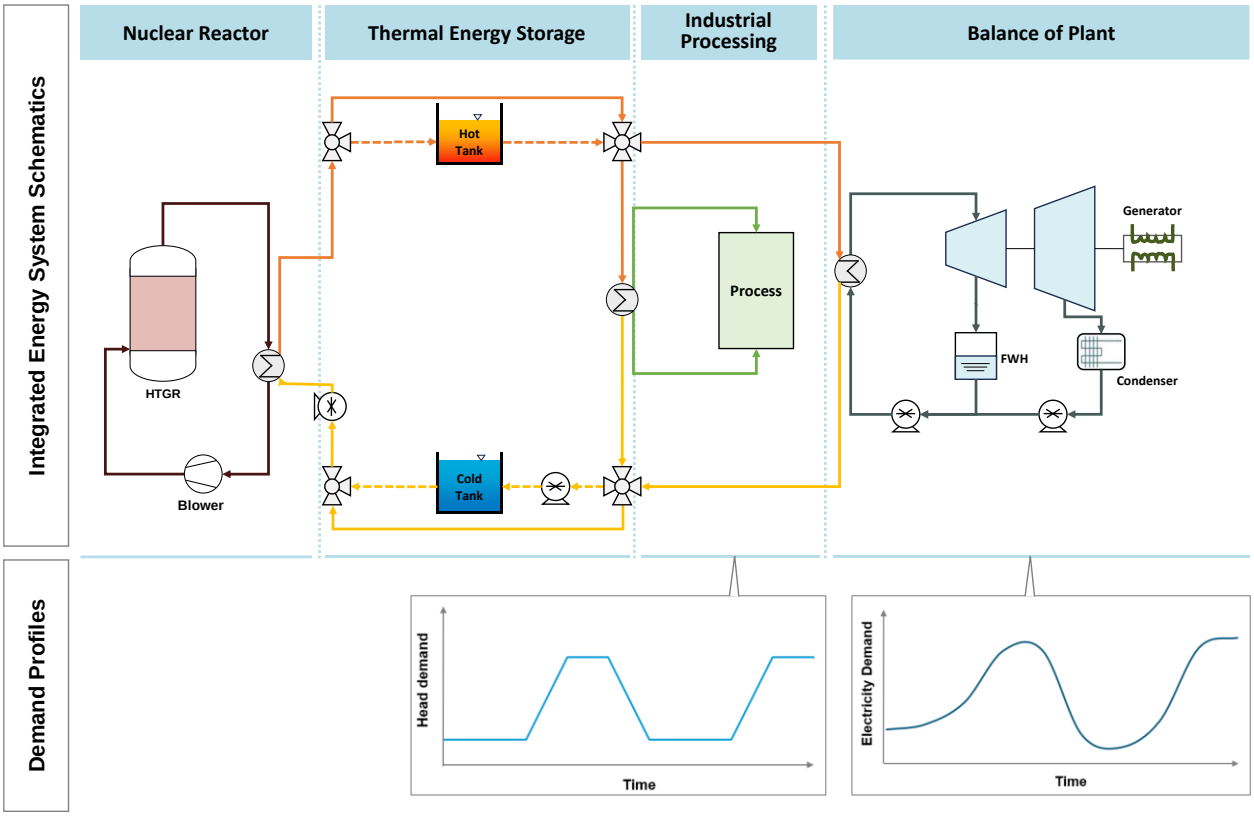

Figure 11. Illustration of a nuclear-TES-CHP system for industries that feature variable demand.

3.2 Systems with Constant Energy Dispatch

Systems with steady energy demands can also benefit from TES. The system design is restricted by the number of specifically sized energy sources (e.g., the number of reactor units), and this can lead to either excessive or deficient electricity. By employing a relatively smaller storage system to capture the excess energy, the system can be used for both electricity arbitrage and auxiliary grid services, thereby generating additional revenue. Figure 12 shows a schematic of an integrated energy system that meets industrial demand while utilizing the excess amount of energy for grid arbitrage and ancillary services.

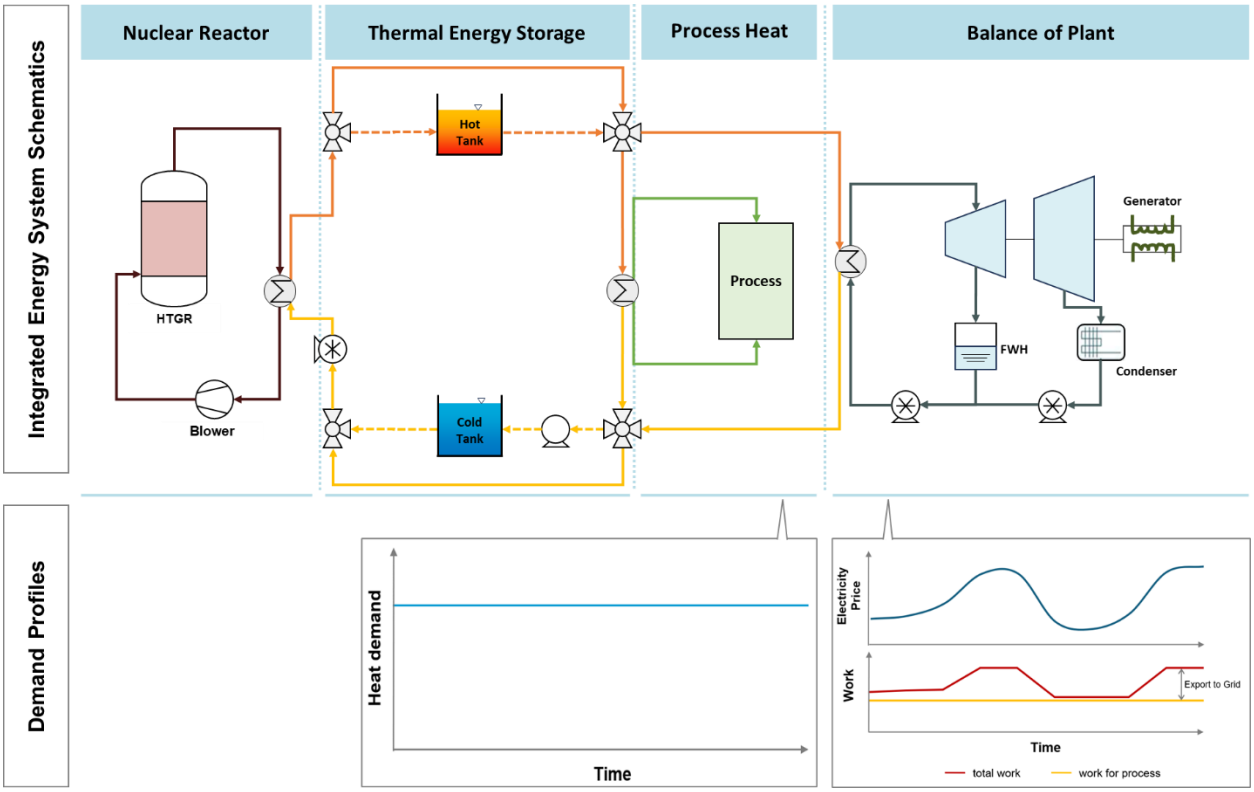

Figure 12. Illustration of a nuclear-TES-CHP system for industries with constant demand.

3.3 Combination of Systems

Stacking constant and variable loads ultimately leads to a variable load system in which the demand can be divided into two portions: baseload and variable. The baseload portion would include the steady demands, as well as the baseload component of heat and power demand within the variable loads. To minimize the total cost of meeting demand, reactor systems should be sized to cover as much of the baseload profile as possible, and the TES-integrated dispatch system should be sized to meet any remaining portion of the baseload profile and all of the variable load profile.

4. SELECTED INDUSTRIES AND THEIR CHARACTERISTICS

This section examines industries that have existed for decades or centuries and optimized their processes over this time to maximize efficiency. It explores the potential application of TES—primarily within the realm of nuclear energy input. For nuclear integration, heat delivery by process steam is the primary focus of this study. This is for two reasons: the technical feasibility of substituting process steam heat supply by nuclear power systems and the fact that dynamic profiles of the higher temperature heat demand of respective industries, generally provided by fossil fuel combustion in furnaces, are not readily available.

4.1 Chemicals

Though chemical plants vary greatly in terms of size and operation regimes, the present analysis focuses on large plants to align with the energy supply of standard SMNRs. These plants are comprised of numerous unit operations, many of which are batch operations or transient systems with frequent shutdowns and maintenance. This makes them promising for TES integration. A chemical plant can already achieve some demand flattening using demand-side management to minimize baseload heat and power demand. When integrating a nuclear energy source, however, the demands should be maintained so as to operate the nuclear plant as near as possible to its steady, full-power state.

For this section, two heat and electricity demand profiles for relatively large chemical plants were obtained. The first, hereafter referred to as Case A, is from an undisclosed source and was created by generating a synthetic history from the source's demand data. The second, hereafter referred to as Case B, is from Eastman Chemical Company's Kingsport plant. [26] Since Case A and Case B pertain to different chemical products and involve different processes, their heat and electricity demand profiles also differ. Case A demands steam at 600, 200, and 75 psig, whereas Case B requires it at 600, 100, and 15 psig. Figure 13 and Figure 14 show the steam demands of Case A and Case B, respectively, over a year.

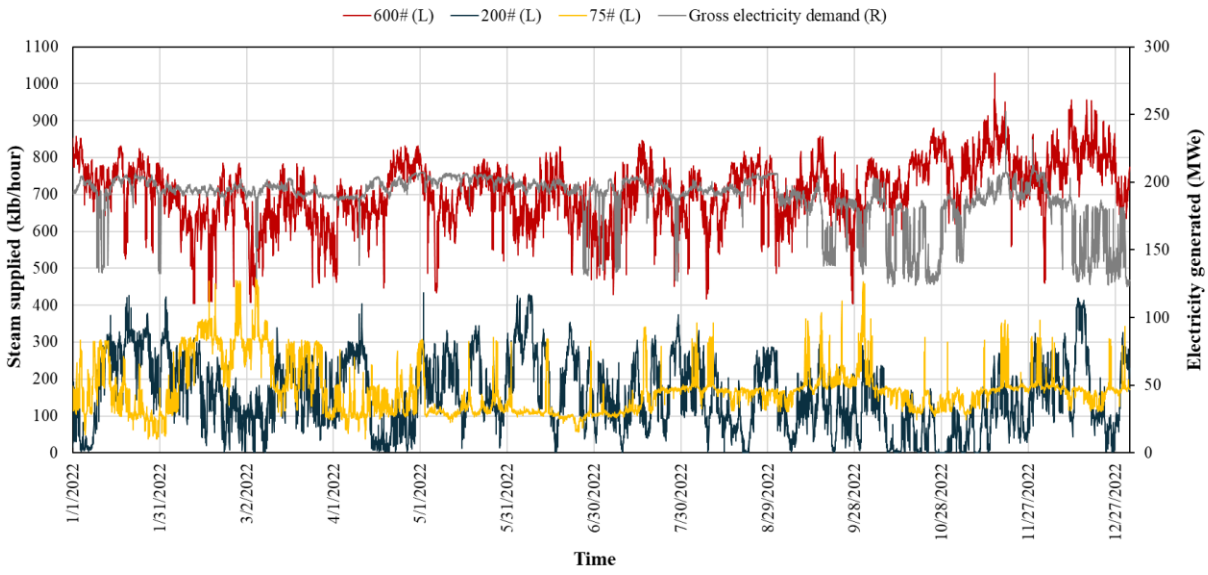

Figure 13. Steam and electricity supply profile for Case A (an anonymous chemical company).

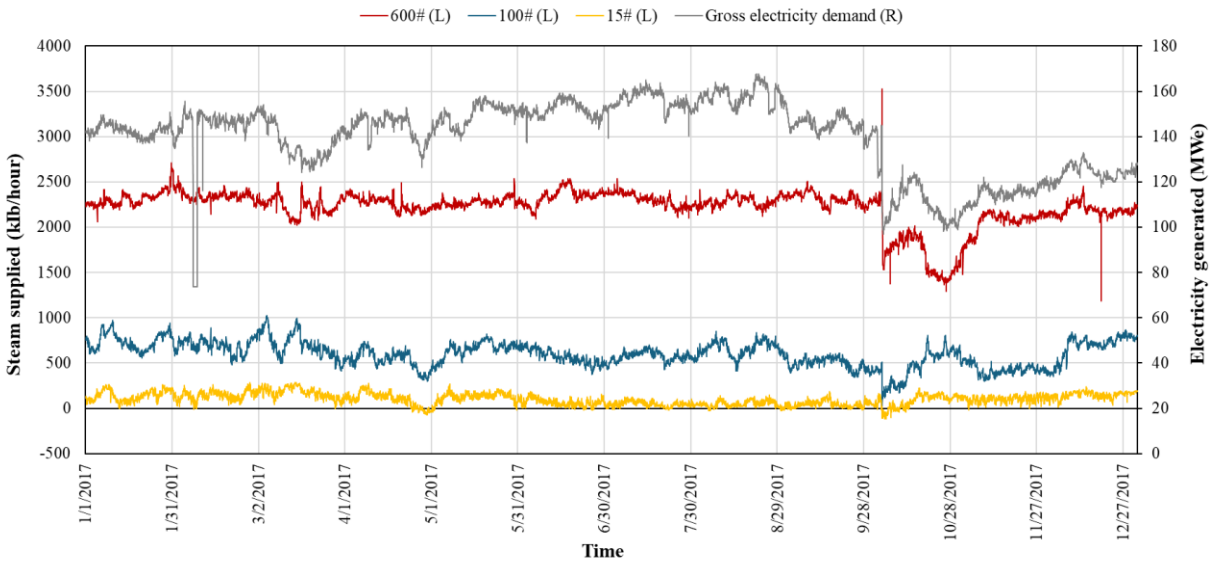

Figure 14. Steam and electricity supply profile for Case B (Eastman Chemical Company). [26]

4.2 Petroleum Refinery

The petroleum refinery industry is a sector characterized by steady operational profiles, where fluctuations primarily arise from periodic equipment maintenance (both planned and occasionally unplanned) occurring at several-year-long intervals. The industry's energy demands—including power, heat, and hydrogen—are relatively stable. [27] This study focuses on the specific case of a reference refinery as shown in Figure 15. Nuclear integration is considered for meeting the demand for power (28 MWe) and process steam (39 MWth) and involving hydrogen production of 129 ton/day via solid oxide electrolysis, which serves as a substitute for the current methane reforming process. The refinery's hydrogen needs are currently met with steam methane reforming but could be supplied by nuclear energy and electrolyzers. Hydrogen could also be used for power generation if an additional storage and electrolyzer capacity is implemented. This option has not yet been explored, because the cost of additional electrolyzer capacity would likely be more than the potential income from electricity sales.

The system design necessitates an integer number of nuclear plants, resulting in a surplus or deficit of overall power. It also aims to expand on existing operational possibilities by integrating a TES system, thus enabling excess power to be stored or discharged based on market conditions, as outlined in Section 3.2.

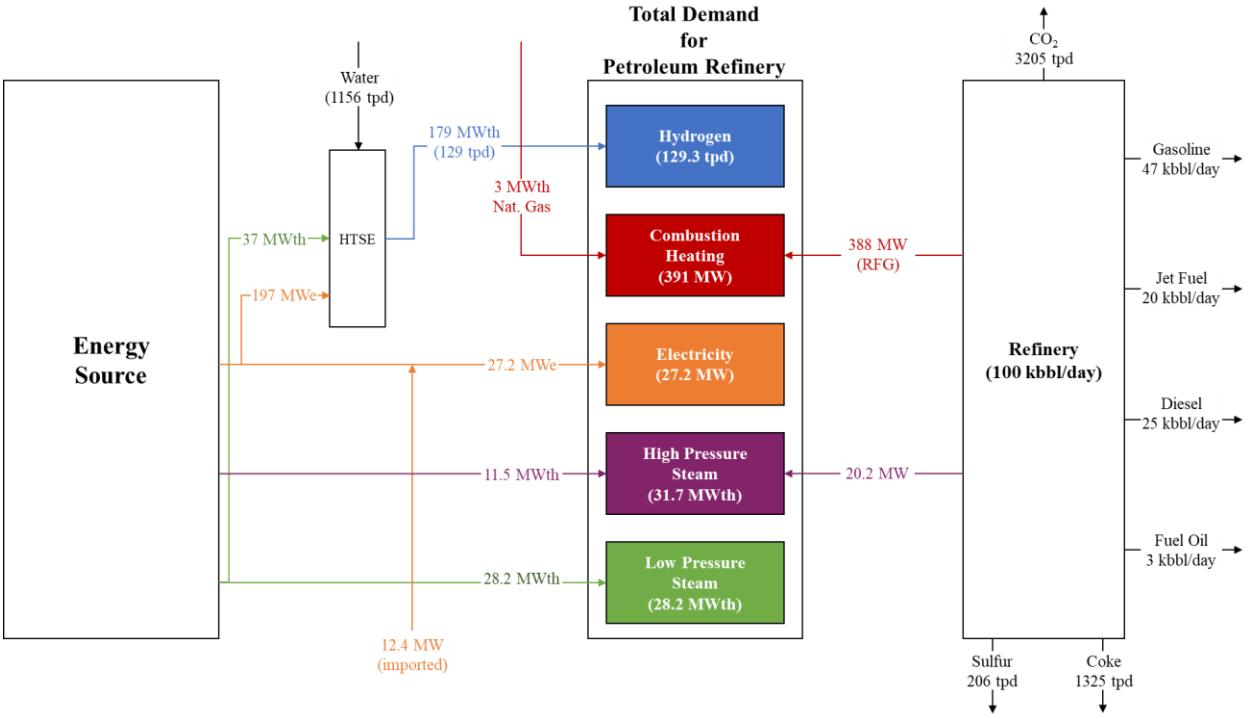

Figure 15. Reference petroleum refinery process. [27]

4.3 Iron and Steel Production

Conventional iron and steel production uses blast furnaces, directly reduced iron (DRI), and EAF. Blast furnaces are known for their stable operations, but their pathways for integrating nuclear energy are too complex or restrictive to be practical. Moreover, most existing plants have already surpassed much of their expected lifespan, making the construction of new blast furnaces unlikely. [27]

DRI technology is a modern alternative to the blast furnace, using hydrogen and carbon monoxide to reduce iron ore. This technology offers a potential pathway for nuclear integration by providing clean hydrogen from electrolysis rather than NG. However, an alternative CO source would be required to replace the NG feed completely. The amount of clean hydrogen that can replace NG is therefore limited by the process requirements and the small number of operating DRI facilities. As with petroleum refineries, DRI plants operate in a steady-state condition [27] and, from the perspective of this study, resemble the refinery's hydrogen supply but with greater uncertainty. Given that the refinery case is well established, this study will not delve into an industry that reflects similar behavior.

EAF operates like large electric heaters with highly variable electricity demands and significant power inputs. Unlike traditional methods, they rely entirely on electricity to supply the necessary heat for the process. As materials melt inside the EAF, additional heat is generated, some of which can be recovered to preheat materials as they are loaded into the furnace. To handle the fluctuating electricity demands of EAF, energy storage solutions are essential, especially when using nuclear energy as a baseload power source. These demand variations, which can range from milliseconds to several minutes, require rapid balancing systems such as flywheels, supercapacitors, magnetic energy storage with active-reactive power compensation, and electrochemical batteries. Given the characteristics of the iron and steel production industry using EAF, this study includes EAF, as integrating TES into the steam cycle could offer a solution for long-term demand fluctuations. A representative EAF demand profile during operation was obtained from Reference [28] was reconstructed and scaled to the relevant system size.

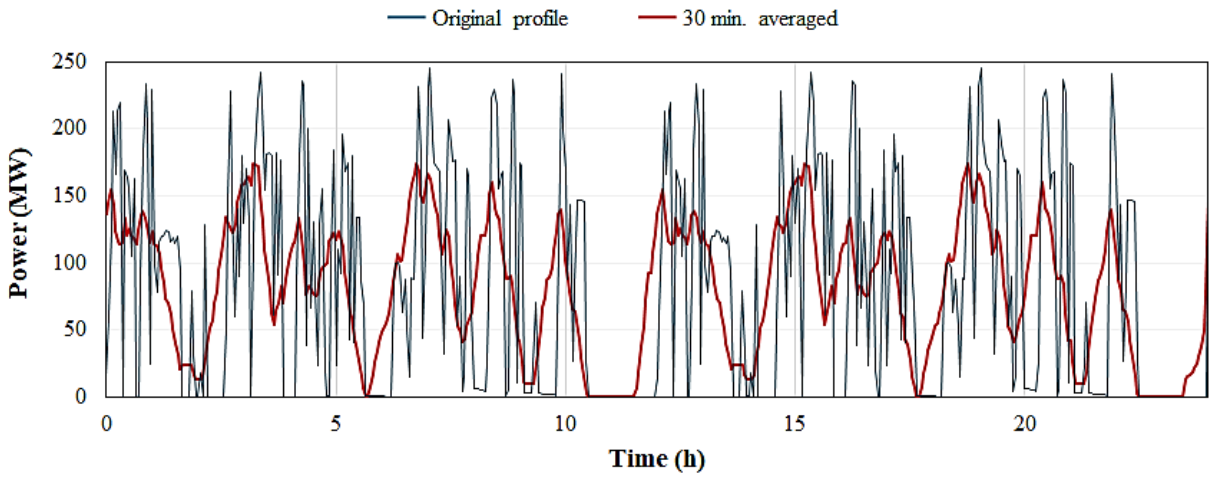

Figure 16. EAF electric load profile (modified from Reference [28]).

Figure 16 presents the resulting demand curve for EAF. The demand curve assumes continuous operation, revealing the potential need for smaller storage capacity with high utilization. In future studies, further investigation into the presence of non-three-shift continuous operation could prompt consideration of additional storage for longer durations during EAF operation. The rapid oscillations require short-term balancing systems, both for active compensation of reactive power and short-period storage systems such as flywheels or electrochemical batteries. Future considerations will include evaluating waste heat recovery and utilization, adopting a more comprehensive approach to actual load scheduling, and eventually exploring demand-side management for the EAF itself.

4.4 Food and Beverage

Food processing frequently relies on batch and transient processes, making it a suitable candidate for TES integration. However, the energy demand of a single plant—even one with relatively large facilities—is typically small in comparison to that of an SMNR. For instance, a brewery with an annual production capacity of 200 million liters consumes an estimated 50 kWh per barrel, [29] resulting in only 7.2 MW of average demand. Another example is the Sierra Nevada Brewing Company in Chico, California, which has an installed capacity of only 1.6 MWe. [30] Similarly, a bakery producing 35,000 kg of bread per day [31] requires an average demand of 3 MW. Such modest energy demands are more suitable for integration with microreactors (~10 MWe or fewer) than SMNRs.

4.5 Pulp and Paper Mills

In this study, a kraft pulp mill was investigated for a target industrial process leveraging the industrial energy park because the kraft process is the predominant method of pulp production in the United States. [32] Although kraft pulp and paper mills generally have steady demand, they do experience transient operations over short periods. Older pulp mills, in particular, often deviate from nominal production capacity, with approximately 10% of their operating time each year spent in low pulp production modes. Additionally, unit processes within these mills can introduce variable demands. For instance, batch digester operations can be variable, though this variability can be mitigated by using parallel digesters. Soot blowers are used frequently for temporary operations, especially in the recovery boiler, but their steam demands are small and brief. [32] Intermittent plant shutdowns are often caused by airborne pulp or paper residue, which must be managed to avoid fires.

The pulp and paper industry are excluded from the primary focus of this study due to two reasons: low energy demand and the technical feasibility of storage options. Most of the energy needs of modern kraft pulp mills are met internally by a CHP steam cycle, utilizing steam from a black liquor recovery boiler and a wood residue boiler. The main external energy source is NG, used for the lime kiln process that requires temperatures of around 800°C~1,000°C—temperatures that cannot be provided by any other system in the plant, nor from the currently considered nuclear energy integration. Recovery boilers in these mills typically operate at maximum pressures of around 10 MPa and temperatures of 510°C—similar to wood residue boilers—and are generally of a drum type. [6] The boiler drums and the overall water content already function as steam accumulators. Steam accumulators can respond in the tens-of-minutes range, aligning well with the ramping time of the boilers themselves. Options for alternative heat storage technologies rather than steam accumulators are limited because the heat is produced in the form of relatively high-pressure steam. Due to a steam saturation temperature of near 310°C at 10 MPa, transferring heat to a sensible heat storage system and then regenerating steam would result in significant exergy losses due to pinch point limitations. Recovered steam from storage would also be low pressure, losing most of its power production potential. Instead of deploying a heat storage system, flexibility in controlling extraction-condensing steam turbines could convert excess steam into additional electricity, which has a reasonable market value for export or can otherwise be utilized within the mill.

4.6 Summary of Selected Industries

The outcomes from analyzing the energy demands of the selected industries are summarized as:

- Industries primarily require moderate-temperature heat, which is currently supplied by standard process steam.
- High-temperature energy demands tend to be industry-specific and often exceed HTGR capabilities.
- Fluctuations in demand typically affect both steam and power requirements.
- Some industries (e.g., pulp and paper industries) are technoeconomically disadvantageous for nuclear energy integration unless they undergo major changes or a technological shift. This is primarily because the industry's external energy needs are too low to practically integrate process steam or because its external energy demands are beyond the feasible temperature range of nuclear reactors.
- Some industries have a size mismatch with SMNRs, making microreactors of potential interest (e.g., the food industry).
- The steam demand of a petroleum refinery was chosen to illustrate steady heat and electricity demand. Additionally, steam and electricity demand is expanded by substituting hydrogen production with electrolyzers.
- Two large chemical production plants were selected to illustrate oscillating heat and electricity demand.
- EAF was selected to illustrate oscillating electricity demand.

Heat and power demand from industrial process may be dynamic in nature and must also interact with the grid in regulated or deregulated markets. This report focuses primarily on implementing TES into three industries (i.e., the petroleum refinery, chemical production, and iron and steel production industries) that have unique characteristics of those heat and electricity demands as well as its impact on overall carbon emissions in the United States.

Table 1. Summary of selected target industries for an industrial energy park.

Industry	Process Heating				Energy Demand Characteristics
	Fuel Demand [TBtu] [33]	Steam Demand [TBtu] [33]	Electricity Demand while PH [TBtu] [33]	CO_2 Emission while PH [mil. MT] [33]	
Chemicals	952	734	22	70.9	Slightly oscillating with seasonal aspects
Refinery	2,042	418	8	149	Constant
Iron and Steel	603	46	97	31.4	Highly fluctuating on hourly basis
Food and Beverage	194	259	12	13.9	Relative low magnitude of demand per plant
Forest Products*	196	15	732	12.7	Demand internally met

* The Forest Products sector includes those subsectors: wood production manufacturing (321); sawmills (321113); veneer, plywood, and engineered woods (3212); other wood products (3219); paper manufacturing (322); pulp mills (322110); paper mills, except newsprint (322121); newsprint mills (322122); and paperboard mills (322130). The number next to the subsector is the North American Industry Classification System (NAICS) code.

5. POWER CONVERSION AND STORAGE SYSTEM LAYOUTS

This section outlines the layouts of power conversion systems that provide electricity and heat for meeting industrial demand, along with a concept for integrating TES to enhance load flexibility. Depending on the required demand temperatures, several configurations are available:

- Above 300°C: Heat is provided directly by the main steam or some other HTF. Conventionally, NG (or other fuel) combustion is mainly used for this temperature range.
- 100–300°C: This range corresponds to standard process steam pressures (i.e., 1~80 bar). Steam can typically be provided via backpressure or extraction turbines.
- Below 100°C: Water heating systems are heated indirectly by extracted steam from turbines or process steam. In an integrated system, condensate from process steam may also be used.
- Below ambient temperatures: While not the main focus of this work, chillers and refrigeration are generally important to industries as well. Cold energy production requires vapor compression chillers or thermally driven (e.g., absorption) chillers.

All concepts in this work are based on the Xe-100 HTGR. The system parameters allow for a supply of HT steam, and a nominal size of 80 MWe serves as a good representation of an SMNR. Note that, for this level of analysis, ideal partial admission behavior is assumed for the turbine's operation at both the inlet and controlled extraction point.

TES opens the possibility of fully decoupled heat conversion between the nuclear reactor and CHP system, allowing for operatively matching both heat and power demands while limiting losses. This unlocks more options for the conversion system. This study focuses on the configurations of CHP systems with TES charged by the primary loop. Other configurations investigated are listed in Appendix C, Power Conversion and Storage System.

5.1 No Steam Extraction—Electric Power Only

Even in CHP settings, some units may be dedicated solely to power production. This TES-integrated approach is a follow-up to the work conducted in Reference [25] to develop a fully decoupled flexible power production system (schematically illustrated in Figure 10). In this approach, two separate TES systems were required to meet the HT range between reactor inlet and outlet while ensuring high efficiency of the power conversion system. If only a single TES system, the system efficiency would be 37%. With the two-TES configuration described in the process flow diagram (PFD) (see Figure 17), system efficiency starts at 41.3% and can increase up to 44.3% with a supercritical steam cycle [25] (values adjusted for parasitic load included in this work).

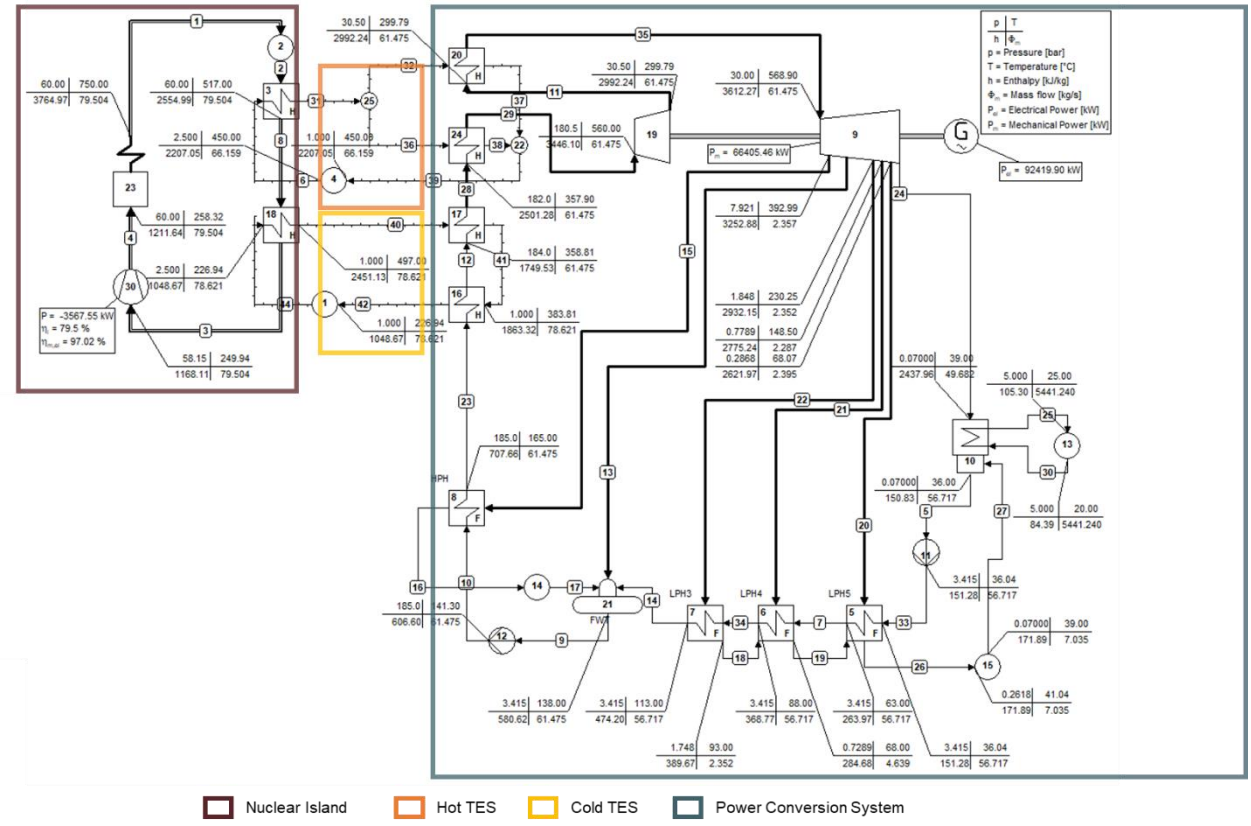

Figure 17. PFD of the no-steam-extraction configuration for a nuclear-TES plant that fully decouples the nuclear island from the PCC. This configuration is based on two separate TES systems.

5.2 Steam Extraction—No Reheater

The two-TES system can also be coupled to a Rankine cycle with the baseline cycle parameters as shown in Figure 41 in Appendix C. The system characteristics follow the ones developed for the baseline system without TES, as the steam cycle has the same parameters. This approach is beneficial for system control as the heat input into the cycle takes place at a constant mass flowrate at any time in all exchangers. Note however that the LT-TES temperature is almost 550°C (see the Component 18 tube outlet temperature in Figure 18). While this temperature is within HITEC salt capabilities with novel atmosphere control for corrosion mitigation, it is notably higher than intended in our design.

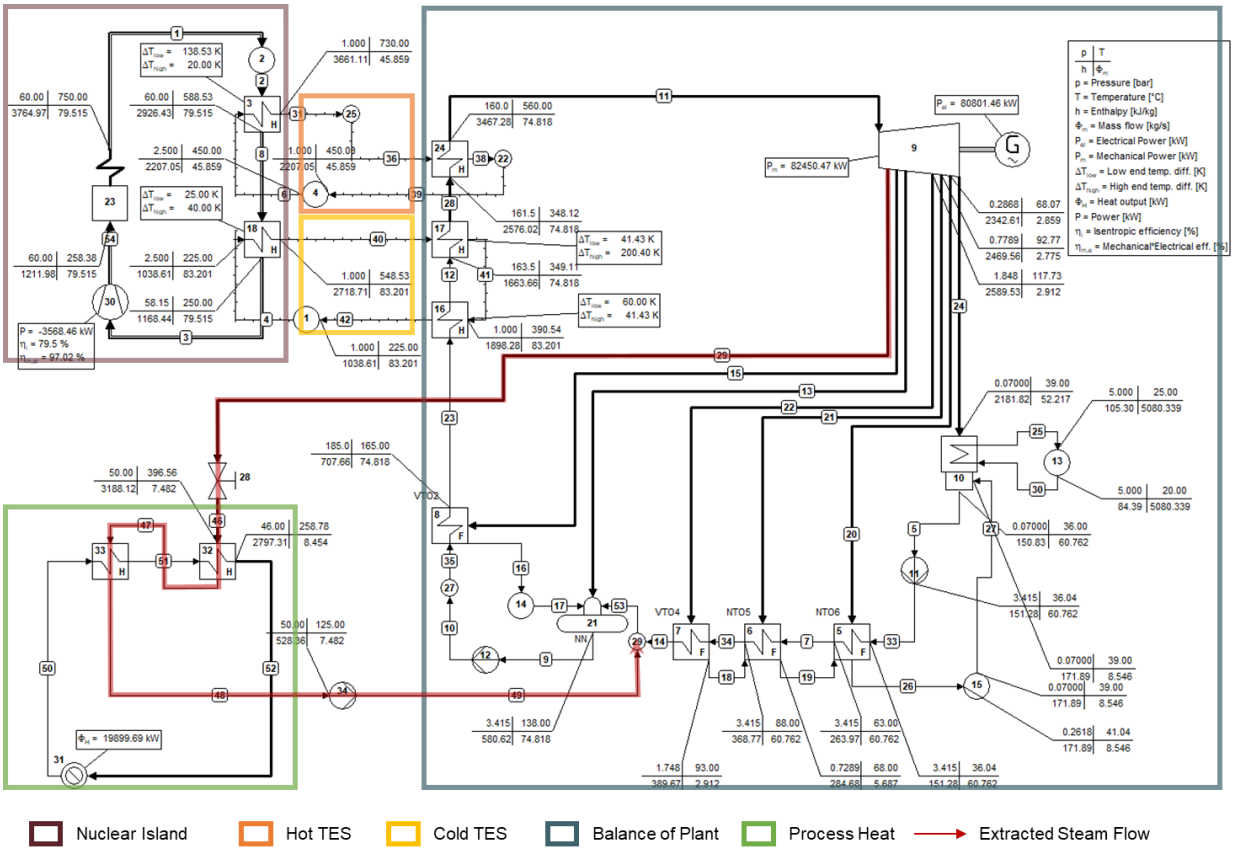

Figure 18. PFD of steam extraction—no reheater from the nuclear-decoupled system.

5.3 Steam Extraction—Upstream of the Reheater

The second steam extraction option involves extracting steam between the high-pressure turbine and the reheating heat exchanger, as illustrated in Figure 19. This setup can achieve a slightly higher power production efficiency than steam extraction—downstream of the reheater, as all the extracted heat (steam) has already contributed to power production. The extracted steam remains superheated at about 360°C, whereas the saturation temperature is around 260°C. However, this approach would require a complex control system. This arises because the decrease in heat transfer from the HT-TES through a reheater (Component 20 in Figure 21) disturbs the balance between the heat transfer from the HT-TES and the LT-TES. The steady-state operation at extraction may lead to heat accumulation in the HT-TES, which can be mitigated by a proportional increase in the LT-TES temperature or flowrate, while a failsafe or balancing method can be employed to transfer excessive heat from the HT-TES into the LT-TES, as proposed in Reference [25].

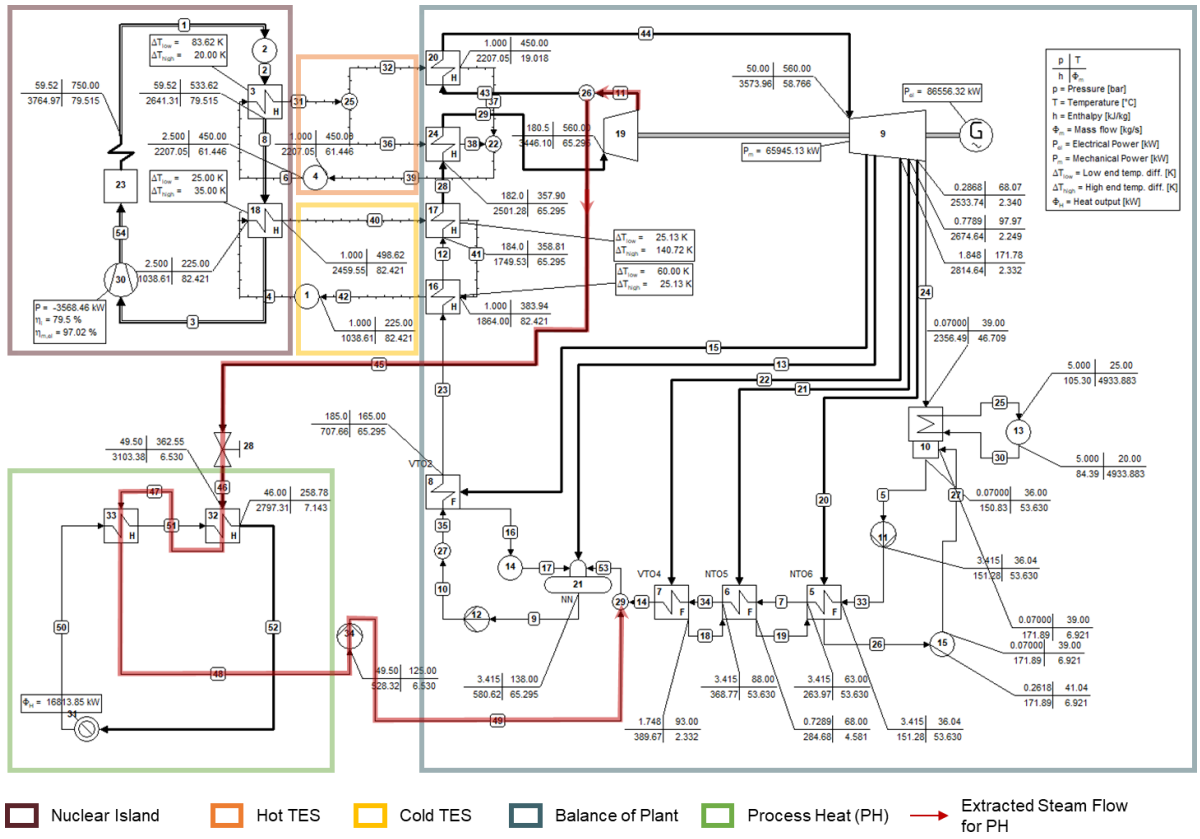

Figure 19. PFD of steam extraction upstream of the reheater from the nuclear-decoupled system.

5.4 Steam Extraction—Downstream of the Reheater

We also propose the CHP configuration of steam extraction downstream of the reheater, considering the reheat cycle for improved performance and large temperature margin of the LT-TES salt. While the extraction point (i.e., downstream of the reheater) is not thermodynamically optimal in terms of pressure, it has some technoeconomic benefits. For example, it is less expensive to extract steam from the intermediate-pressure piping at this location than extracting from a turbine upstream. Moreover, this extraction point at the splitter (Component 26 in Figure 20) is advantageous to adjust reheat pressure to extraction pressure. It's important to note that the target industrial process requires 42 bar steam. However, in the "no steam extraction—electric power only" case, only 30 bar is maintained at the reheater (refer to Component 20 in Figure 17), whereas in the "steam extraction—downstream of the reheater" case, 50 bar is achieved at the reheater (see Component 20 in Figure 20). Opting for a higher reheat pressure results in higher steam density, decreasing the number of pipes in the heat exchanger[a]. Another advantage for adopting extraction downstream of the reheater is the system's controllability, as there is no impact on the energy balance of the heat transfer between the two TES systems and the steam cycle. This configuration has an advantage over others if the CHP system needs to frequently regulate steam across a wide range. For system safety, a desuperheater may be in need for the extracted steam to limit material stresses on the heat delivery components of the process heat system. Note that a comprehensive technoeconomic analysis extends beyond the scope of this work and that this design merely represents one possible approach.

a This leads to an increased required thickness.

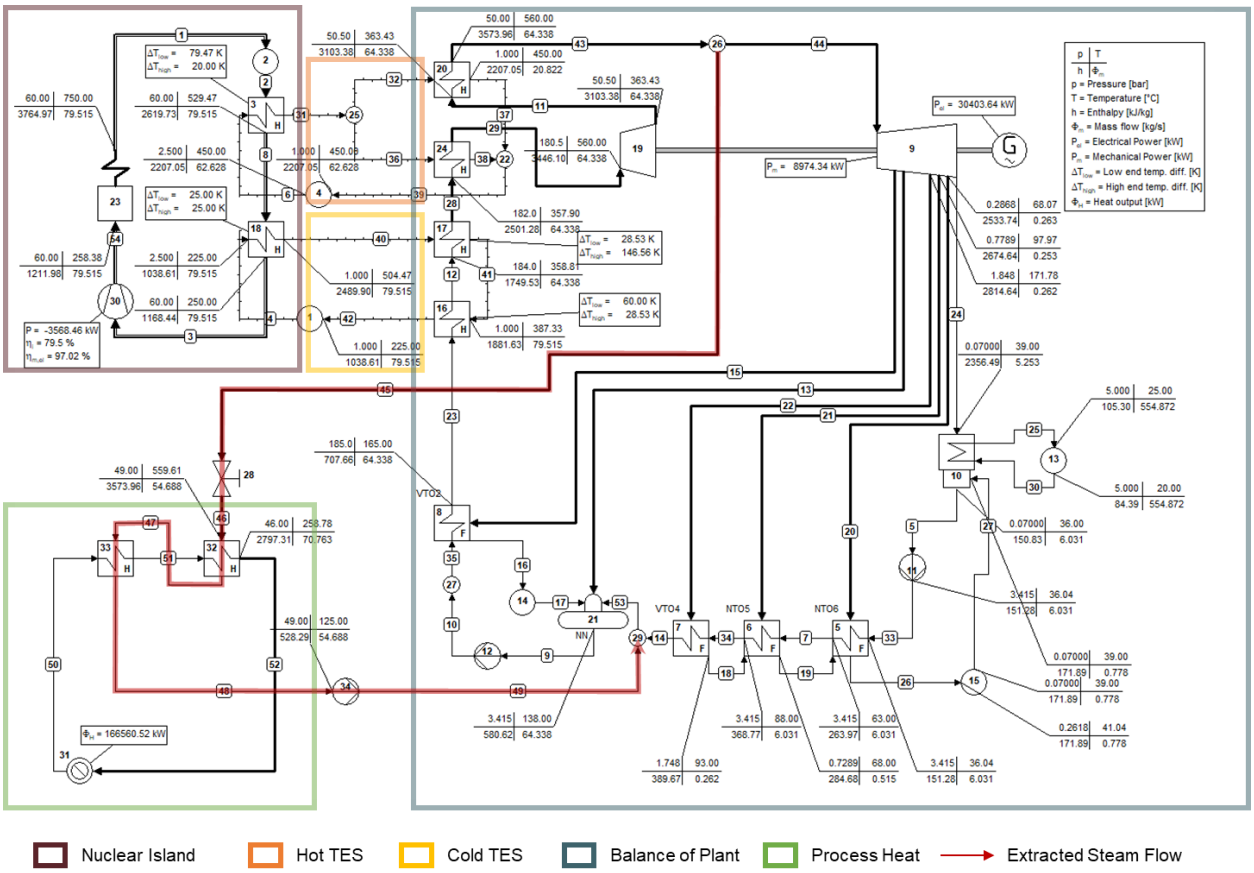

Figure 20. PFD of steam extraction downstream of the reheater from the nuclear-decoupled system.

Figure 21 shows the efficiency characteristics for the steam extraction cases from Section 5.3 and Section 5.4 when comparing the steady operation of both systems and assuming ideal controlled extractions with ideal partial admission. Note that electricity production differs between cases because they require different mass flow rates to meet the same demand. When extracting upstream of reheat, electricity production efficiency is slightly higher as all heat transferred to the steam cycle is utilized for power production. When extracting downstream of the reheater, the reheater heat effectively bypasses power cycle directly to process heat, showing higher values of heat production efficiency.

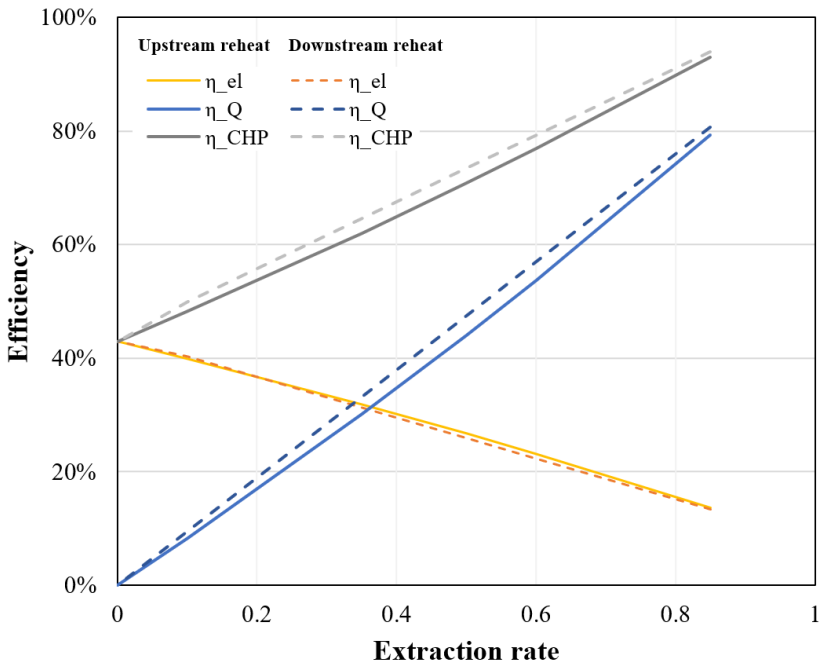

Figure 21. Efficiency characteristics of the nuclear-decoupled systems, with steam extraction at 50 bar upstream and downstream of the reheater. η_{el} = Electrical Power / Reactor Design Thermal Power; η_{Q} = Thermal Output / Reactor Design Thermal Power; $\eta_{\mathrm{CHP}} = \eta_{\mathrm{el}} + \eta_{\mathrm{Q}}$.

5.5 Backpressure

A backpressure system can also be coupled to the TES. This configuration depends on the return condensate temperature remaining low enough to ensure that heat is stored in the LT-TES at a suitable temperature to cool the reactor inlet to its nominal condition. This approach is similar to steam extraction—upstream of the reheater (Section 5.3)—but all the steam is utilized for process heating. Since the condensing section is omitted and the conversion cycle is not limited by the turbine outlet steam quality, a higher turbine inlet pressure (182 bar) is adopted and the heat transfer ratio between the HT-TES and LT-TES is well balanced, resulting in an LT-TES charged temperature of 512°C. Figure 22 presents the PFD and energy balance model of the system. The conversion-to-electricity efficiency is 10.6%, whereas the conversion-to-heat efficiency is 89%. As shown in the diagram, a turbine-bypass valve could be used to adjust heat and power production to meet demand. A desuperheater would be necessary on the bypass line (together with Component 5 in Figure 22) to control the steam temperature and avoid unnecessary thermal stresses.

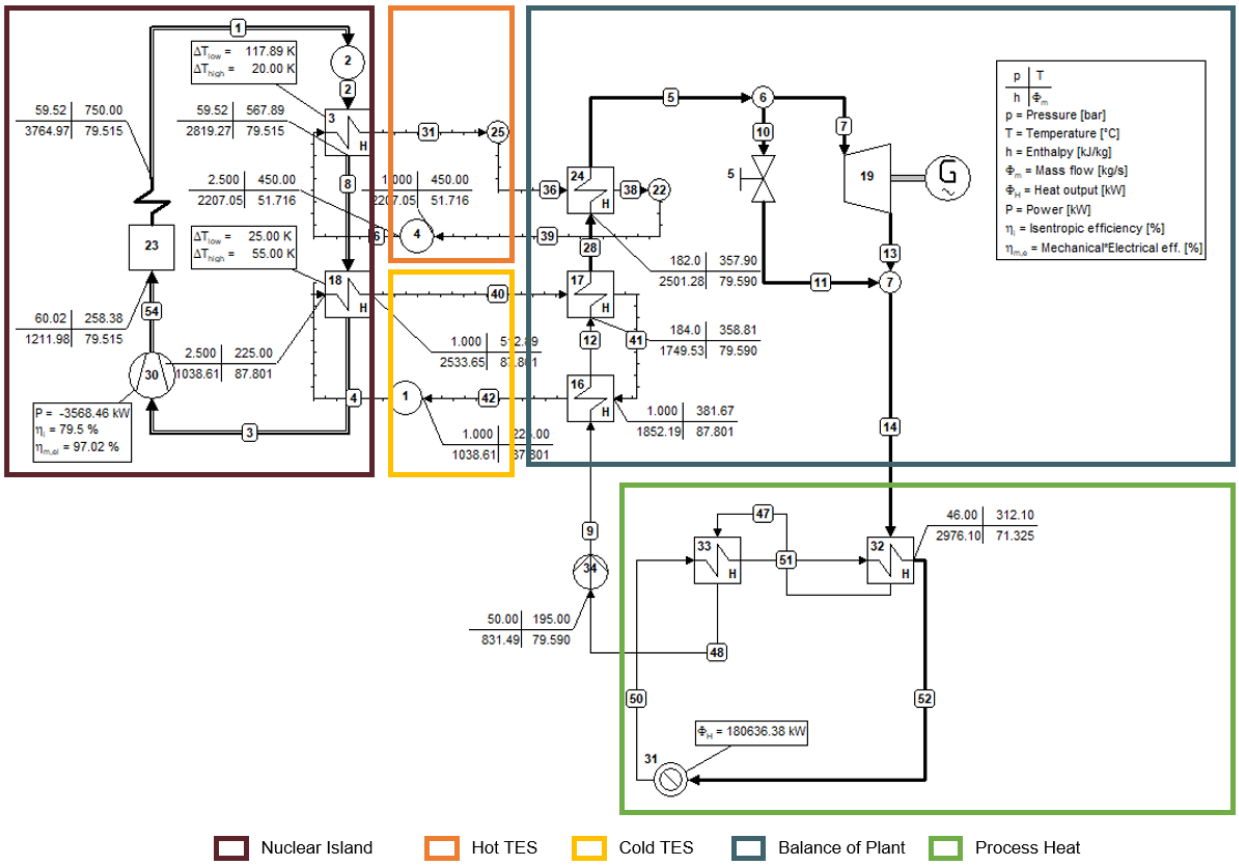

Figure 22. PFD of backpressure CHP system from the nuclear-decoupled system.

5.6 High-Temperature Heat Delivery System

If a specific industry requires fluctuating heat demand at temperatures that cannot be met by the turbines main steam or extracted steam, it may be possible to directly deliver the heat to an industrial process using the TES HTF, as illustrated in Figure 23.

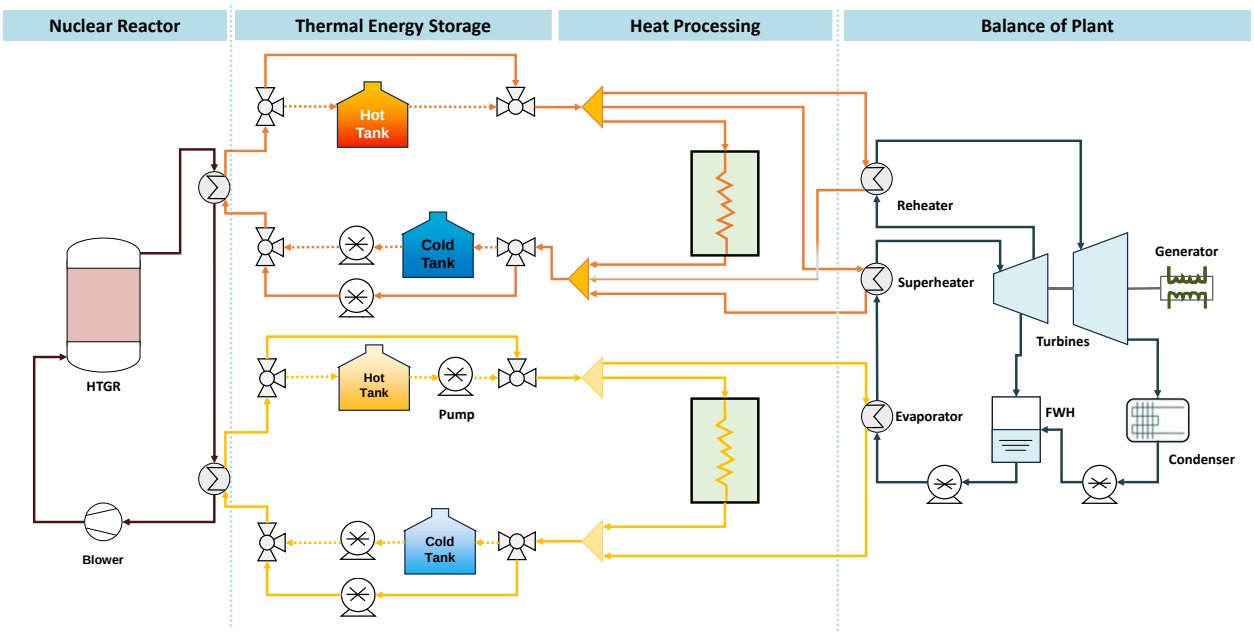

Figure 23. Industrial heat delivery system for providing heat at temperatures that exceed the possibilities of main or extracted steam.

Implementing high-temperature heating can be technically and economically more complex compared to using lower temperature process steam. This complexity arises in part because heat tracing is needed along the heat delivery system to prevent the HTF from freezing. Compared to process steam, there would be a necessity to also redesign delivery systems at industrial sites, some of which rely on radiative heat transfer, and complex control systems may be required, especially if the very HT demand notably exceeds other lower temperature heat demands and power production. There is also no thermodynamic benefit of cogeneration. The decarbonization of HT industries, however, might necessitate such a solution.

The PFD of this configuration with thermodynamic parameters is shown in Figure 24. By parallelizing the PCC and heat delivery, the efficiency of the PCC remains constant, but an overall system is proportionally reduced by the amount of delivered heat.

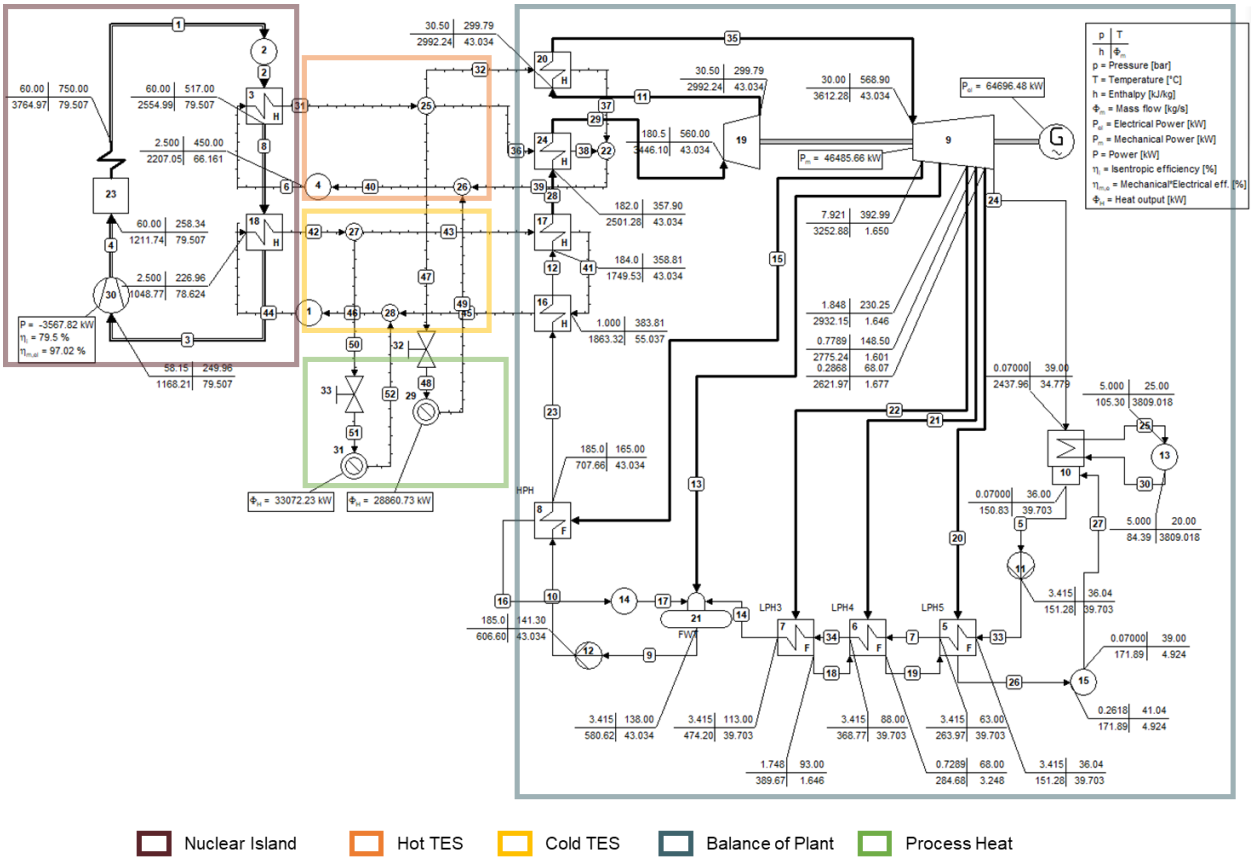

Figure 24. PFD of HT heat delivery system from the nuclear-decoupled system.

5.7 Summary of Power Conversion Systems

All investigated configurations of TES-integrated CHP systems are summarized in Table 2. We have concluded that the best solution is to integrate the TES between the primary loop and PCC. Specifically, steam extraction downstream of the reheater with a two-tank molten-salt TES appears as the best solution regarding thermodynamic system benefits and system drawbacks. Integrating TES into the steam conversion system, though potentially simpler from a nuclear licensing and regulation standpoint, brings notable efficiency losses and limitations on maximal extracted heat rate. The TES system furthermore needs to be modified for each specific industrial need, while TES behind primary loops offers a universal solution for a range of process heat applications and solutions.

There are many other configurations and dispatch algorithms that prioritize factors such as heat demand, electricity demand, curtailment, or excess electricity exports. However, this work does not attempt to cover all possible variations. Instead, it focuses on general illustrative cases of conversion systems applicable in energy parks to outline their potential benefits, technical feasibility for implementation, and limitations.

Table 2. Summary of power conversion systems—NR-TES-CHP type.

Cycle			Energy Efficiency (%)	Heat Production Efficiency (%)	CHP Efficiency (%)	Max Heat Diversion to TES ** (%)	Max Decrease in Power Output (%)	Max Decrease in Heat Output (%)	Pwr. Conversion System Capacity	Note
Reference	Type*	Features								
Figure 17	NR-TES-POWER	Elec. power gen. tes charged by reactor primary loop HX	42.9	0	42.9	100.0	100.00	0	Flexible	—
Figure 18	NR-TES-CHP	Elec. power gen. + process heat w/ extracted steam (no reheater) TES charged by reactor primary loop HX	40.2–10.5	0~83.4	40.2~93.9	100.0	100.00	100	Flexible	Minimum low-pressure flowrate 15% and max decrease in power output might be practically limited by minimal load ~10%
Figure 19	NR-TES-CHP	Elec. power gen. + process heat w/ extracted steam (upstream reheater) TES charged by reactor primary loop HX	42.9~13.7	0~79.3	42.9~93.0	100.0	100.00	100.0	Flexible	Minimum low-pressure flowrate 15% and max decrease in power output might be practically limited by minimal load ~10%
Figure 20	NR-TES-CHP	Elec. power gen. + process heat w/ extracted steam (downstream reheater) TES charged by reactor primary loop HX	42.9~13.3	0~80.7	42.9~94.0	100.0	100.00	100.0	Flexible	Minimum low-pressure flowrate 15% and max decrease in power output might be practically limited by minimal load ~10%
Figure 22	NR-TES-CHP	Elec. power gen. + process heat w/ steam from backpressure turb. TES charged by reactor primary loop HX	10.7~-2.5	89.0~102.5	99.6~99.9	100.0	100.00	100.0	Flexible	Max decrease in power output might be practically limited by minimal load ~5%
Figure 24	NR-TES-CHP	Elec. power gen. + process heat w/ TES medium TES charged by reactor primary loop HX	42.9~-2.5	0~102.5	42.9~99.9	100.0	100.00	100.0	Flexible	For HT heat delivery system, no thermodynamic benefits of cogeneration and max decrease in power output might be practically limited by minimal load ~10%

* NR: nuclear reactor; CHP: combined heat and power system; PCM: phase chance material; POWER: power system.

** Equal to max decrease in CHP output.

6. INDUSTRIAL ENERGY PARK—EXAMPLES AND ENGINEERING DESIGNS

This section presents case studies of a nuclear-TES-CHP integrated industrial energy park, with a focus on selected industrial applications. When multiple industries are co-located, a centralized energy supply system could leverage synergies by balancing demand fluctuations across different industries, while also needing to manage combined peak loads and seasonal variations.

6.1 Energy Demand

The energy demands of the integrated energy park result from a combination of the steady baseload heat and power needs of the refinery, the moderately fluctuating demands of the chemical plant with some seasonal variations, and the highly variable electricity demand of the EAF plant. The individual demand profiles of each industry were aggregated to form the overall demand profiles for the energy park, as shown in Figure 25. It's important to note that, for simplification, all heat demand is assumed to be supplied as steam at 42 bar. Lower pressure demands are managed by letdown turbines and valves at each industrial site, with the corresponding power generation reflected in each industry's power demand profile. The energy demand of each individual industry and conceptual demonstration of industrial energy park without aggregating energy demands from industries can be found in Appendix D, Conceptual Demonstration of Industrial Energy Park with Individual Industry.

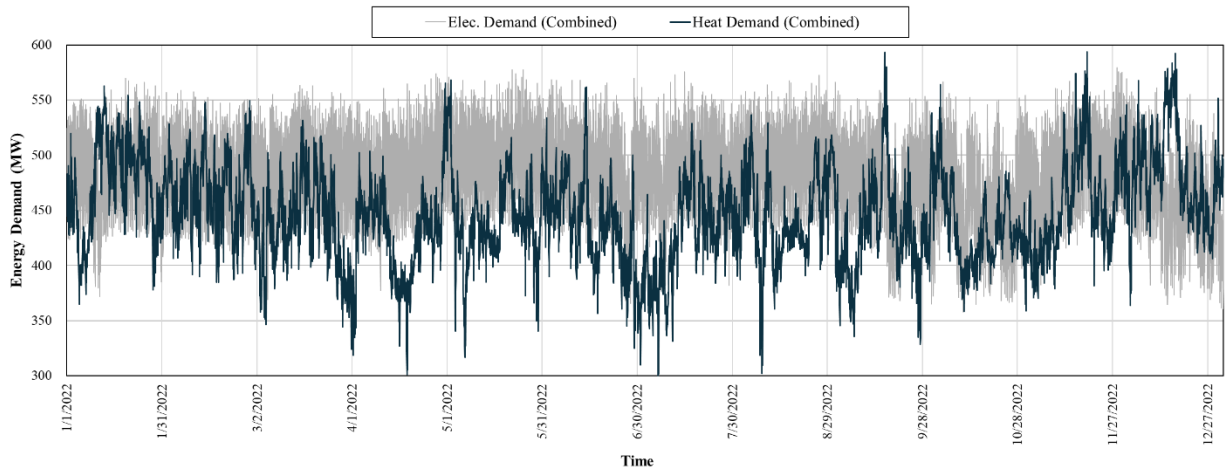

Figure 25. Combined energy demand profiles of the energy park.

6.2 Configuration of Energy Sources

There are numerous options available for meeting the energy needs from the industrial island of the industrial energy park. These range from the conventional approach, which involves a combination of gas-fired boilers, NG combined cycle (NGCC) CHP, and electricity from the power grid to the integration of onsite and offsite renewables and energy storage, the utilization of waste heat streams, and, as the focus of this work, the integration of nuclear resources. Figure 26 provides a schematic, generalized representation of all these resources.

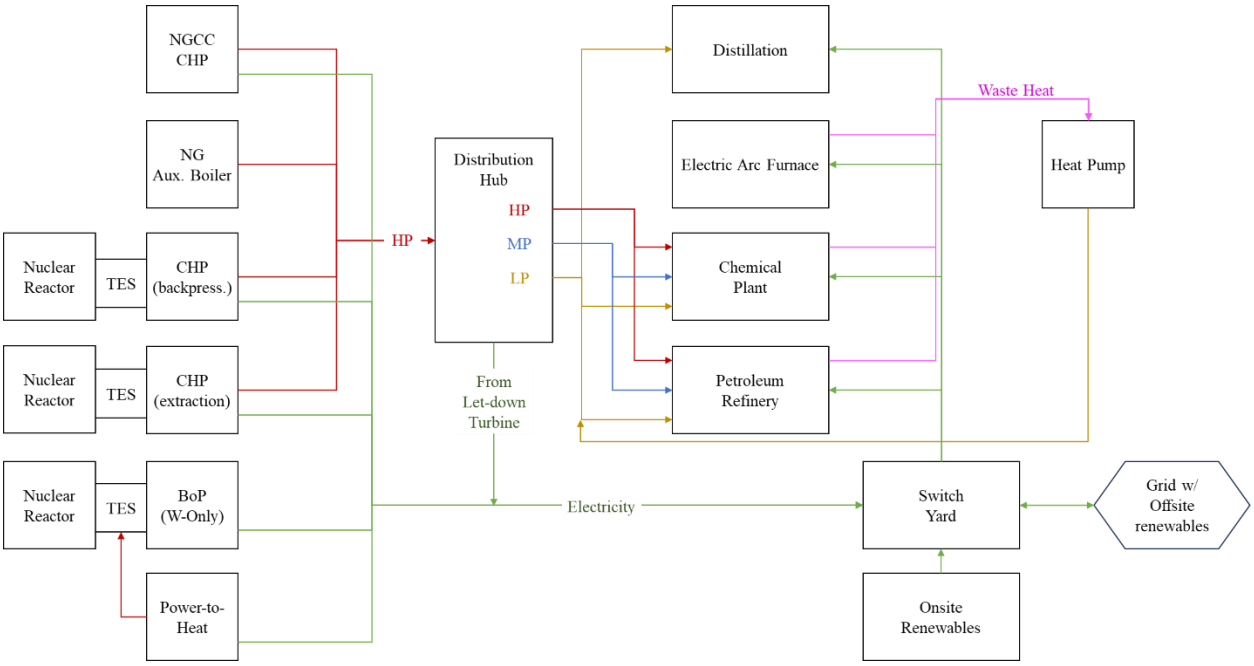

Figure 26. A general representation of the energy system that also includes other non-nuclear resources, where NGCC—natural gas combined cycle, TES—thermal energy storage, CHP—combined heat and power, BOP—balance of plant, HP—high pressure, MP—medium pressure, and LP—low pressure.

The nuclear integration strategy involves first deploying CHP and power only (or work only) systems until most of the demand is satisfied, followed by an analysis of the impact of TES and potentially integrating additional energy storage systems (e.g., H_2 storage). The placement of CHP begins with backpressure units, as long as their combined heat production remains below the minimum demand from the industrial island. Once the backpressure CHP system capacity is saturated, extraction-condensing modules are added until all heat demand is met. Finally, power-only systems are used to cover the remaining electricity demand. It's important to note that, in some scenarios, heat demand peaks may also be covered by NG boilers or by deploying additional backpressure units with some curtailment.

The preliminary configuration for the industrial energy park case study is depicted in Figure 27. It includes eight Xe-100 reactor modules, along with conversion and optional energy storage systems. It comprises one backpressure unit, three extraction-condensing units, and four power-only systems. TES integration is proposed for two of the power-only units to manage balancing medium-duration energy demand fluctuation, while a small power-to-hydrogen system with a simple discharge method via a boiler, parallel to the TES-integrated units' steam generator, is suggested for balancing seasonal demand variations. The installation of a power-to-hydrogen system is due to its low cost compared to TES (see Figure 28). Several assumptions and boundary conditions are made as listed below for the preliminary industrial energy park configuration:

1. 50 kWh/kg for H_2 production.
2. 85% boiler efficiency (combusting stored H_2) based on lower heating value (120 MJ/kg).
3. 40% all heat to power conversion systems efficiency.
4. 200 MWth reactor module output.
5. 100% TES efficiency (heat to heat) with no impact on PCC.
6. Constant (linear with heat extraction) PCC efficiency in off-design.

7. Heat extraction ranges from zero to 85% of the main steam flow (for extraction-condensing PCCs).
8. Unlimited hour-to-hour step variation in system performance.

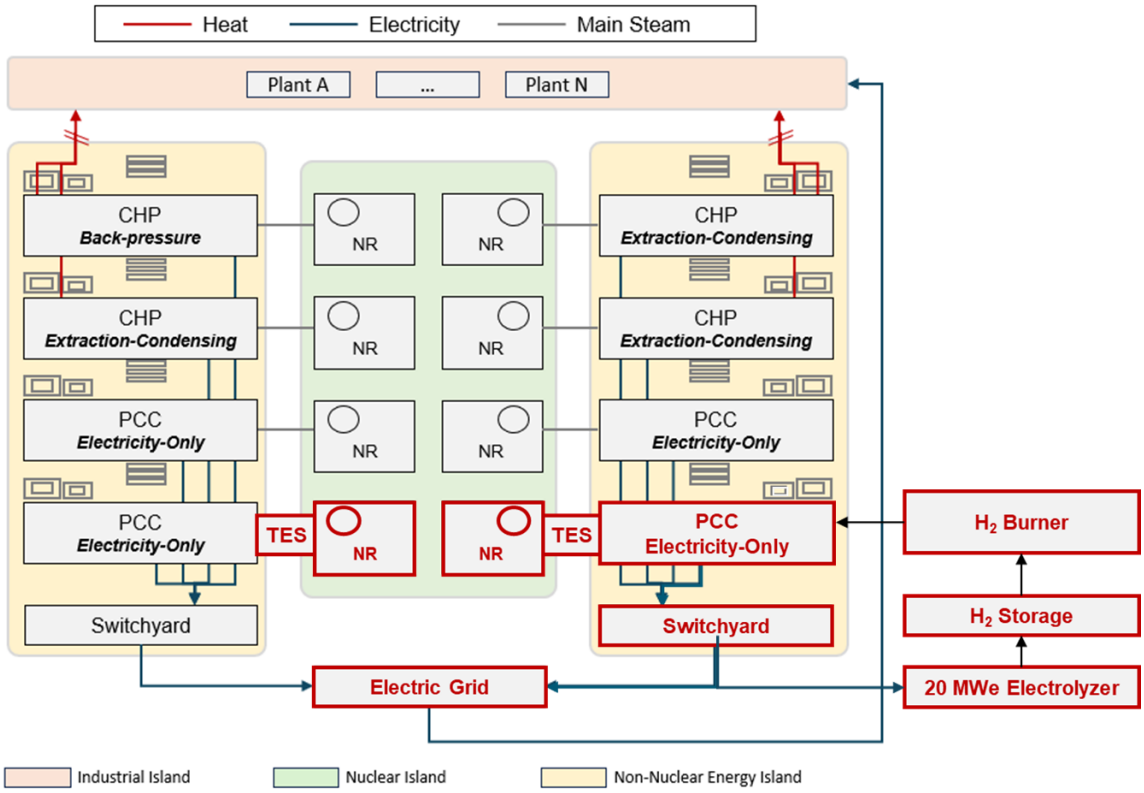

Figure 27. Proposed configuration of nuclear-based system for the energy park: CHP—combined heat and power, PCC—power conversion cycle, TES—thermal energy storage, NR—nuclear reactor.

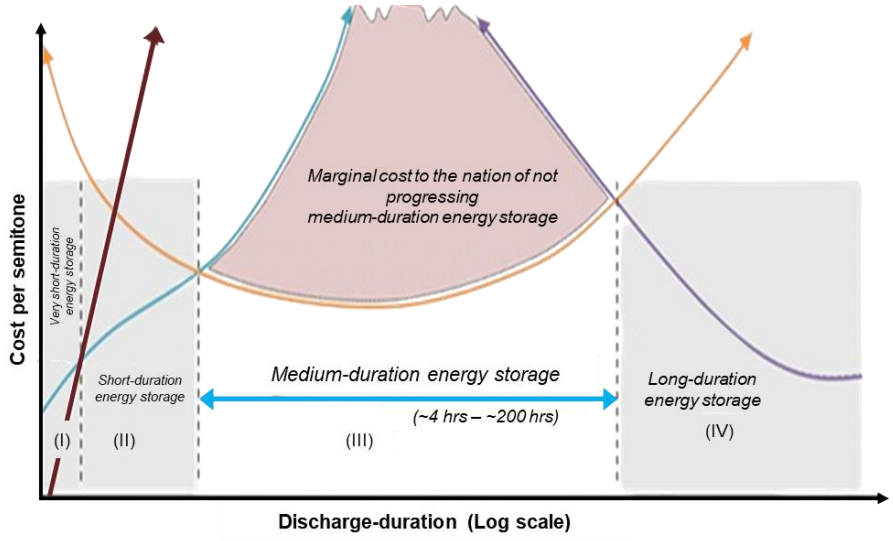

Figure 28. Cost vs. energy storage discharge duration. [34]

Figure 29 illustrates how different production modules meet thermal (see Figure 29(a)) and electrical demands (see Figure 29(b)). In Figure 29(a), the backpressure CHP unit handles a constant thermal load, while the second, third, and fourth units of the extract-condensing CHP unit manage the varying thermal load to maintain a consistently zero net heat balance. Although the net heat balance remains at zero, the net electricity balance fluctuates (see the pink profile in Figure 29(b)) due to the highly variable electricity demand. This fluctuation highlights the need for additional energy storage to stabilize the electricity balance.

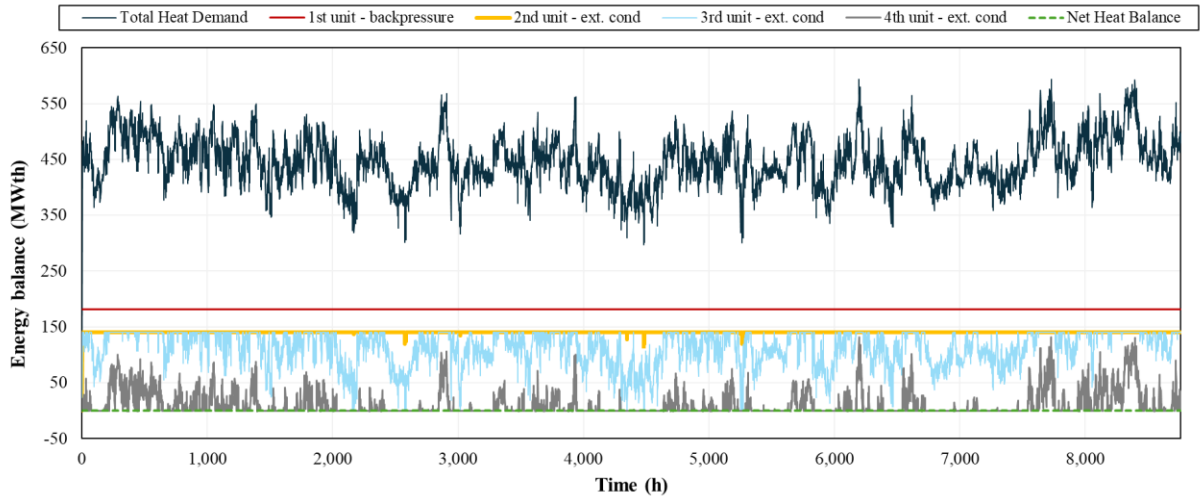

(a)

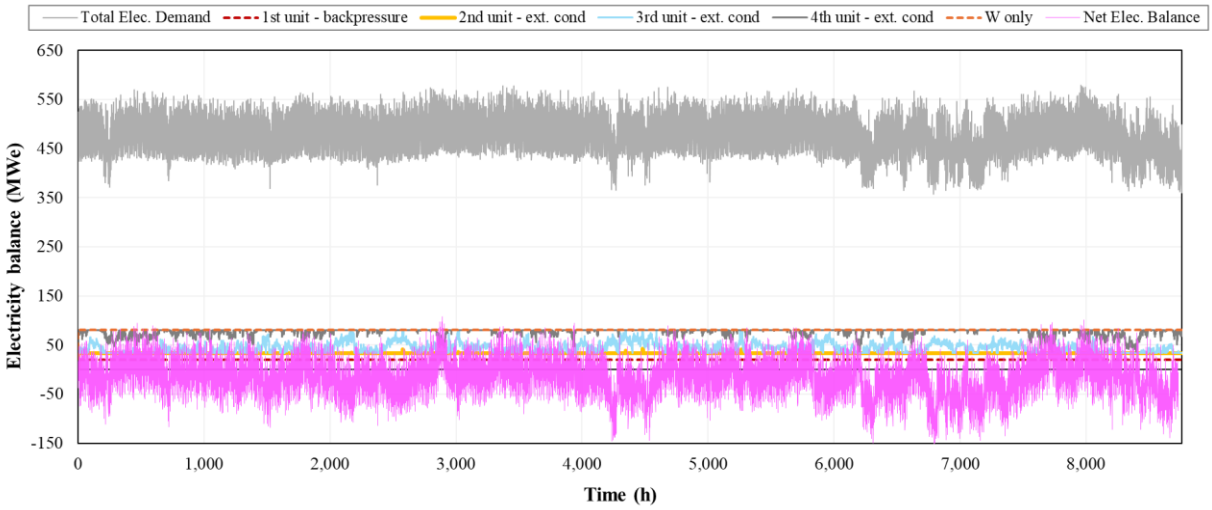

(b)

Figure 29. Heat and electricity demand and supply from HTGRs and their power conversion systems for the industrial energy park: (a) heat demand and supply from distinct reactor units and their power conversion systems and (b) electricity demand and supply from distinct reactor units and their power conversion systems. Negative electricity balance implies energy export to grid.

After integrating the energy storage system, its dispatch can be guided by strategies as outlined in Section 2. The sizing of the system becomes a variable that influences how effectively these objectives can be achieved. In the scenario presented, TES is coupled with two reactor modules, providing a combined maximum discharging power of 225 MWth (equivalent to a 90 MWe boost), with each module's PCC having an installed capacity of 125 MWe. The storage capacity is designed for 10 hours of full discharge. The hydrogen system is designed with a charging capacity of only 20 MWe to minimize electrolyzer capital costs and has a storage capacity of 450 tons of hydrogen, comparable to the largest current liquid hydrogen tanks. [35–37] Figure 30 illustrates the resulting electricity balance and state of charge (SoC) under a control strategy where the TES targets the floating average of net power output, while the H_2 storage system strives to maintain a zero net electricity balance, both within their respective storage capacity limits. Figure 30 shows the energy balance profiles and SoC of the energy storage systems.

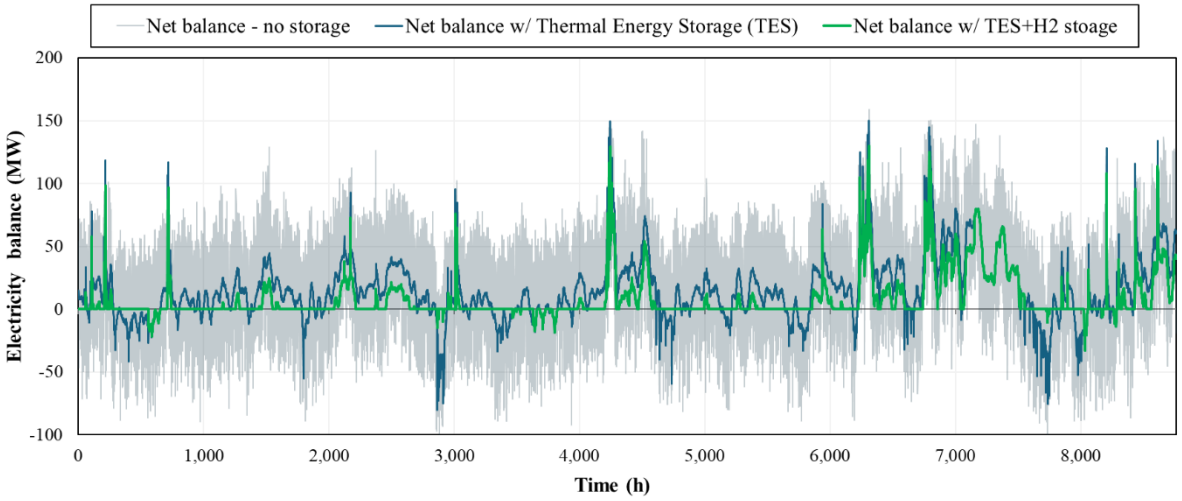

(a)

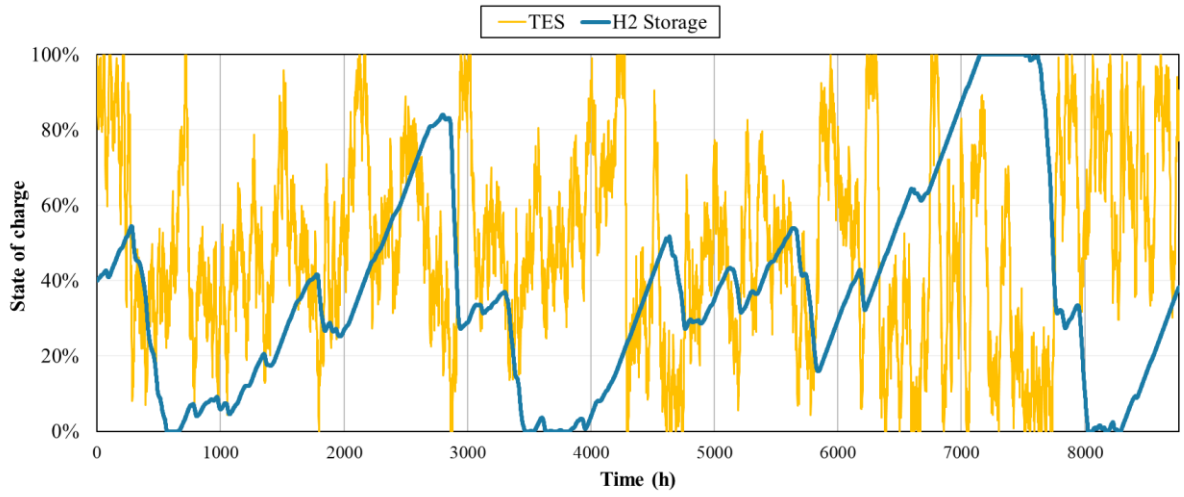

(b)

Figure 30. Energy balance profiles and SoC of energy storage systems: (a) electricity balance after integration of TES and additional H_2 seasonal storage and (b) SoC of these systems throughout the year.

A parametric analysis was conducted on TES storage capacity to quantify its benefits and guide optimal sizing. The results, shown in Figure 31, focus on the TES dispatch algorithm designed to follow the floating average of the net balance in the positive (export) region and to limit import in the negative (import) region. The number of cycles is calculated as the ratio of the total annual discharged energy to the TES system capacity. For a 10 hour storage capacity (i.e., storage capacity = 2.25 GWh_th), the results as shown in Figure 31 indicate an average of one cycle every 3 days and a 77% reduction in imported electricity compared to the scenario without TES. Beyond 10 hours of storage capacity, the additional benefits become negligible.

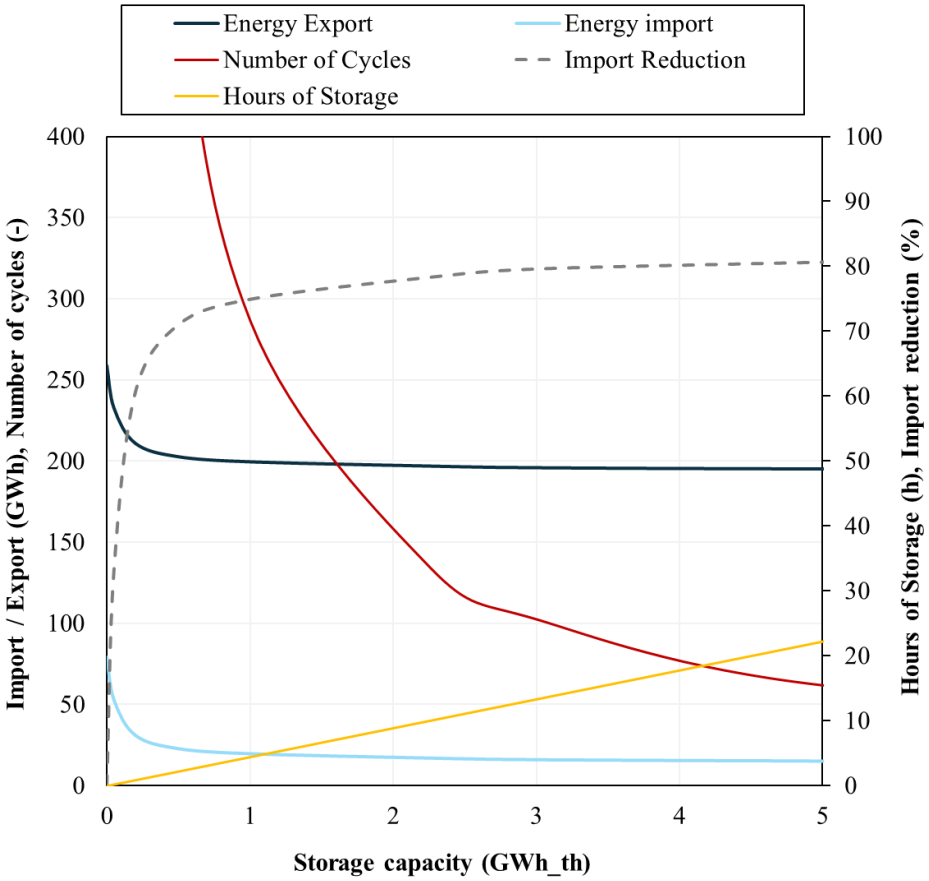

Figure 31. Parametric analysis on TES storage capacity.

A similar analysis was conducted for H_2 as a seasonal storage system, as shown in Figure 32. The number of cycles is quite low, given that the system is designed for seasonal storage, with a capacity of 450 tons corresponding to nearly 13 GWh. It is evident that a thorough technoeconomic assessment is needed to determine the appropriate capacity. The analysis suggests that achieving the final increments in import reduction may be better addressed through internal demand-side management rather than by installing an excessively large storage system for only a minimal reduction in imports.

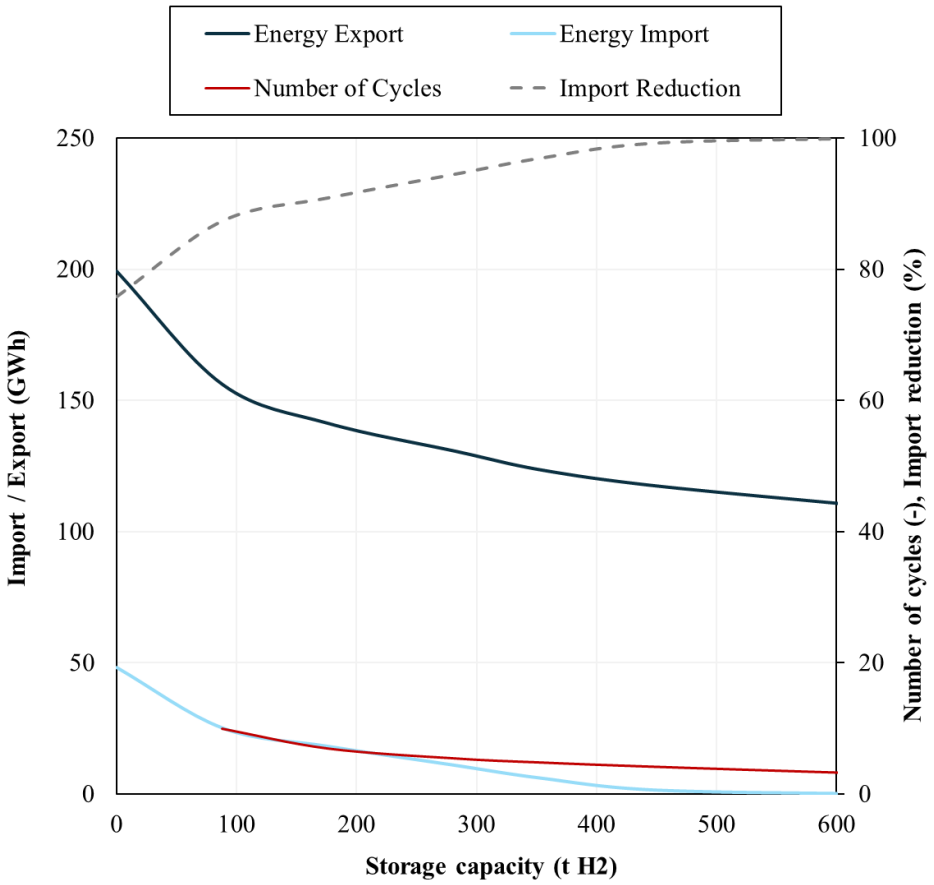

Figure 32. Parametric analysis on H_2 storage capacity.

7. SYSTEM CAPACITY OPTIMIZATION AND TECHNOECONOMIC ANALYSIS

In this section, the industries selected for the TES coupling is further investigated using the Holistic Energy Resource Optimization Network (HERON) framework, a software plug-in for the Risk Analysis Virtual ENvironment (RAVEN) [38]. HERON takes trained synthetic inputs (industrial energy profiles and electricity price signals) along with the technoeconomic specifications of the HTGR, TES, and BOP[b] and translates them into a linear programming formulation, which is subsequently solved in RAVEN. These considerations will ensure that TES is appropriately positioned to provide heat to industrial consumers at optimal value. Details regarding the HERON optimization scheme are available in Appendix F, Holistic Energy Resource Optimization Network.

b BOP in this section implies the CHP or PCC system.

7.1 Technoeconomic Analysis

It is likely that decision makers would compare the benefits of introducing the HTGR-TES system to the business as usual (BAU) operation with their existing fossil-fueled boiler or CHP. To reflect this aspect, our modeling is based on the premise that each modeled industrial process has an NG boiler capable of covering all their demands, and if needed, they can import electricity from external grids. This premise allows us to identify conditions under which the HTGR-TES system becomes competitive or uniquely beneficial to various decision makers' interests and operational goals. To quantify the design space of optimal sizing and the range of the system operation, we trace both the changes in system economics in net present value (NPV) and energy delivery within the system. Additionally, we introduce the concept of external grid access availability as a proxy for varying transmission constraints and variable renewable energy (VRE) availability, which may differ across geographic regions. For instance, setting external grid export to a low value may depicts the optimal system located in a region with high VRE or significant transmission constraints. We differentiate external grid access availability (whether exporting surplus electricity or importing additional supply) to focus on two key scenarios: prioritizing the use of generated electricity for onsite consumption ("behind the meter") and optimizing operations in electricity markets by responding to price signals.

Along with industrial demand profiles, another key economic driver in optimization is electricity price levels. Our proposed system is likely to be sited in areas characterized by high variability in prices and high electricity prices throughout a year, which are conducive to recovering HTGR and TES investments. Based on this premise, we select the 2018 real-time market price data from the Electric Reliability Council of Texas (ERCOT). [39] The hourly data from ERCOT is particularly suitable for testing and exploring off-design operation due to its high price volatility compared to the PJM Interconnection LLC and the Midcontinent Independent System Operator [25]. Details on data collection and statistical analysis for the selected ERCOT real-time market data can be found in Reference [25]. The objective function in HERON aims to find a combination of optimal HTGR, BOP, and TES sizes that cost-effectively meets industrial demands under given external grid access capacities. If we optimize with greater export and import capacities sufficient to position the system as an energy arbitrage player, HERON will identify the NPV-maximizing industrial energy park configuration by placing more emphasis on adjusting the system dispatch in response to electricity price signals. Conversely, if the system operates in an island mode (with minimal external grid access), HERON primarily seeks the least-cost industrial energy park configuration by more factoring in capital expenditure (CAPEX) and operation and maintenance (O&M) costs.

Our analysis treats the HTGR-TES system (coupled to industrial processes) as a utility-scale (on the order of hundreds of MWe) energy prosumer within power networks, flexibly choosing their source of energy supply. Additionally, depending on allowed external grid access capacities, it can add additional revenue streams by shifting output from periods of low prices to periods of high prices. In our modeling framework, the HTGR is introduced as a single 203 MWt unit or in multiple batches with incremental additions of 203 MWt, all operating at full power capacity. The TES is characterized by a round-trip efficiency of 90% and a power capacity that is subject to the BOP capacity. Hence, our optimization range for BOP exceeds the HTGR capacity being considered in HERON, thereby utilizing stored heat energy when energy demands surge. For instance, if HERON seeks a larger BOP, the TES accordingly has a larger power capacity proportional to the BOP capacity. With this setting, we aim to derive the operation and design requirements that would maximize market potential from this simulation.

Our study also assesses the impact of the Inflation Reduction Act of 2022 (IRA) [40]. These tax credits can lower financing barriers around the CAPEX of nuclear technologies through investment tax credit (ITC) and production tax credit (PTC). The ITC for qualified projects reduces the upfront capital costs per capacity ($/MW). The PTC decreases the present value of variable O&M costs, such as fuel costs ($/MWh), which can be earned for 10 years from the year the facility begins operations. The ITC and PTC provide two levels of incentives: a base rate and a bonus credit if projects meet specific provisions for wages and labor, domestic content requirements, and/or are located in geographically targeted communities [41]. Guaita and Hansen provide guidance on applying the ITC (IRA Section 48E) and PTC (IRA Section 45Y) for nuclear technology [42]. Recent studies identify that any reactor with a capacity exceeding 30.45 MWe would benefit more from the ITC regardless of the tax credit levels [43]. Thus, our analysis is solely concerned with the ITC impact on HTGR technology. The specific rates examined in HERON are: 6%, 30%, 40%, and 50% for ITC.

Key simulation assumptions and constraints are implemented in HERON for this study. First, we do not model multidecade project lifespans. Instead, we optimize over 1 year with annualized CAPEX for each component. This approach allows for the incorporation of technologies with different lifetimes without requiring decades of modeling. Second, we use a price-taker model under perfect foresight in price information. In other words, the saturation of storage suppliers and the resulting diminishing energy arbitrage returns are ignored. This approach is useful for identifying a lower bound on storage capacity requirements and an upper bound on energy arbitrage returns [44]. Similarly, we exclude transmission constraints and VRE availability in the region, as we assume these factors are already reflected in the price signals. Additionally, we do not include CAPEX and fixed O&M costs for NG boilers; these costs are assumed to be precommitted expenses before the introduction of the HTGR-TES system into the site. Our calculations use a discount rate of 7% to determine the NPV of the technologies considered.

Figure 33 shows the schematic of the overall optimization process in HERON; optimizations are conducted from the key perspectives of decision makers, considering deployment case (i.e., the number of reactor units), industrial process characteristics (i.e., which demand does the process need more—electricity or heat?), and optimization goals. Simulation outputs are interpreted with an emphasis on performance indicators (highlighted in the green boxes). Note that the deployment case is graphically represented for the single industrial process examined in this study. The pie charts show the ratio of the electrical and heat demands for each individual profile[c].

Table 3 summarizes the frameworks and formulated scenarios for different industrial energy profiles and external grid access availability. For *BAU-Single* and *BAU-Combined* scenarios are BAU cases that solely rely on NG boilers to meet the energy demand. NG boilers for *Single* and *Combined* scenarios are cases of nuclear-TES configurations supplying energy to meet single and combined multiple energy demand profiles and assumed to be operating onsite and capable of covering peak demand. The maximum thermal demand for chemical and combined loads is 510 MWt and 563 MWt, respectively. Since NG boilers are considered a given (with no CAPEX accounted for during HERON simulation), their size makes no difference as long as it is greater than the peak demand for the base case with respect to dispatch schedule and the resulting NPV. Having a larger NG boiler could expand the operational range when combined with an HTGR-TES system. However, the NPV difference between cases with 560 MWt and 570 MWt in such configurations is not statistically significant at the 5% significance level (t-test). In other words, the 10 MWt difference is negligible when interpreting results across single and multi-load scenarios. For *single* scenario, four-unit and five-unit nuclear reactor configurations are labeled as medium-sized and self-sufficient cases, respectively. The four-unit configuration aims to meet mean internal energy demands (thermal and electricity combined), while the five-unit configuration is designed to meet peak energy demands. Under this classification, any configuration lower than four units is

c Electrical demand is converted to thermal equivalent.

considered undersized, and any configuration greater than five units is considered oversized. This classification will be used in our subsequent analysis. In the combined scenario, eight and 10 units are identified as medium-sized and self-sufficient deployments. In exploring the optimal TES size, the TES charge duration ranges from 0 to 9 hours. For instance, if the total reactor capacity is 406 MWt, and HERON seeks an industrial energy park configuration that gives the highest NPV by examining capacities ranging from 0 to 3,654 MWht in increments of 406 MWht. When operating the reactor at full capacity (nameplate capacity), having TES requires a larger size of BOP than the reactor unit(s) capacity to use stored thermal energy. In light of this, the optimization step for BOP ranges from 0% to 100% with 12.5% increments (0/8 ~ 8/8) of added TES capacity. This assumes that the TES can discharge all its stored energy in 1 hour (1 hour discharge duration). For instance, if the total reactor capacity is 406 MWt and TES is 2,030 MWt (charge duration 5 hours), HERON examines a BOP size from 406 to 2,436 MWt with 253.75 MWt increments. Cost parameters for our modeling are available in Appendix G, Input Cost Parameters for HERON Optimization.

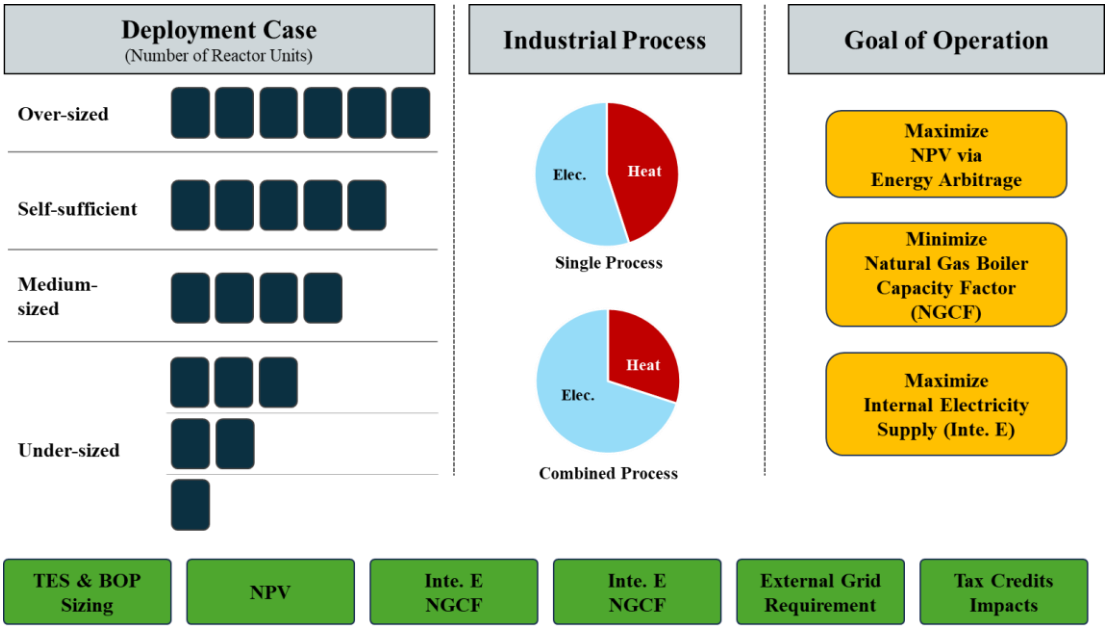

Figure 33. Schematic representation of the HERON simulation: optimizations are conducted from the key perspectives of decision makers, considering deployment case (i.e., the number of nuclear reactor units), industrial process characteristics (ratio of thermal and electricity demands), and operational goals. Simulation outputs are interpreted with an emphasis on performance indicators. The deployment case is graphically represented for a single industrial process examined in this study. The pie charts show the electrical and thermal industrial demands for each individual profile, with electrical demands converted to thermal equivalents.

Table 3. Modeled scenarios for different industrial load input and external grid access availability.

Scenario	Input Signal Type			NG Boiler[a] [MWt]	HTGR-TES System			Ext. Grid Access	
	Int. Heat Demand	Int. Elec. Demand	Elec. Price		HTGR[b] [Unit]	TES[c] [hour]	BOP[d] [%]	Export [MWe]	Import [MWe]
BAU-Single	Chem.	Chem.	ERC	560	0	0	0	0	300
Single					1–6	0–9	0–8	0–1,000	0–1,000
BAU-Combined	Chem., Refinery	Chem., Refinery, EAF	ERC	570	0	0	0	0	600
Combined					5–11	0–9	0–8	0–2,000	0–2,000

ERC: Electric Reliability Council of Texas.

7.2 Impacts of Loads Aggregation

In this section, we identify key cost-effective deployment options for the HTGR-TES system for industrial process decarbonization. Acknowledging varied decision makers' priorities and regional constraints, we consider key uncertainties, including the number of industrial loads (single vs. combined), the level of decarbonization (full supply from nuclear or partial supply from nuclear), and additional value-adding services when external grid access is available (i.e., energy arbitrage).

We focus on a demand-side analysis in two stages. First, we examine the system impact of the single process (chemical plant), which exhibits seasonal and daily variations, with thermal demand being more intensive than electrical demand (average demand for thermal and electricity at 362 MWt and 169 MWe and standard deviations of 44 MWt and 11 MWe, respectively). In parallel, we investigate the impact of combined loads by introducing electricity-intensive but static refinery loads as well as electricity-only EAF loads. The combined loads are characterized by their high average thermal and electrical demand (477 MWt and 446 MWe) and high standard deviations (44 MWt and 43 MWe), compared to the single process profiles[d]. Second, based on their total equivalent loads (thermal and electrical loads in MWt based on a BOP efficiency of 39.5%), we emphasize our findings for cases undersized, medium-sized, self-sufficient, and oversized as more representative of scenarios decision makers would face in investment. Medium-sized and self-sufficient cases represent total reactor capacities (MWt) sized to meet respective mean and peak total equivalent loads[e]. Undersized and oversized cases represent reactor capacities that are one incremental step (203 MWt) lower or higher, respectively. These case-specific aspects will be discussed in the next sections.

[d] Refinery profiles have average thermal and electrical demand at 84 MWt and 230 MWe, with zero standard deviation for both, as well as electricity-only EAF loads, which have an average of 82 MWe and a standard deviation of 33 MWe.

[e] The mean total thermal equivalent loads for the single and combined profiles are 755 and 1,606 MWt, respectively. The peak total thermal equivalent loads for the single and combined profiles are 972 and 2004 MWt, respectively.

Figure 34 and Figure 35 summarize cases where reactor capacities are optimally sized to maximize NPV with industrial demands and external grid access availability in each scenario (*single* vs. *combined*) described in Table 3. We present the BAU scenarios, where existing NG boilers meet industrial demands, for comparison (see the case where the installed HTGR capacity is zero). For illustration, we selected the goal of operation of NPV-maximization, with a maximum allowable electricity import and export of 1,000 MWe for a single industrial process scenario and 2,000 MWe for a combined industrial process scenario.

Figure 34(a) and Figure 35(a) demonstrate that TES capacity generally increases with reactor capacity, up to 1,015 MWhth for the *single* energy demand case and 2,030 MWhth for the *combined* energy demand case. This trend is driven more by ERCOT price signals than by industrial demands. As reactor capacities increase, resulting in excess thermal energy, a larger TES capacity is required to maximize electricity sales in response to price signals until the revenue from electricity sales no longer exceeds the combined costs of TES CAPEX and Charger CAPEX. In contrast, BOP capacity is influenced less by reactor size and more by external grid access capacities, as it is geared toward capturing energy arbitrage opportunities. Under a price-taker model, coupling with TES consistently enhances NPV through energy arbitrage activities. When there are no limits on external grid capacity, larger TES and BOP sizes than their total thermal equivalents are preferred.

Figure 34(b) and Figure 35(b) show that introducing the HTGR-TES-CHP system significantly lowers the contribution of NG boilers and grid imports to meet internal thermal and electricity demands. This effect is due to the HTGR-TES's lower variable O&M costs compared to NG boilers (see Table 19 in Appendix G) and is pronounced in Figure 35(b) as the industrial thermal demands are extended. The substitution of NG boilers and grid imports with HTGRs becomes saturated (Figure 34(b) and Figure 35(b)) when the total HTGR capacity reaches a medium size (812 MWt for the *single* case and 1624 MWt for the *combined* case). At these capacities, the base industrial loads (the constant portion of total thermal equivalents) are covered by the output from these medium-sized reactors. With the larger TES (Figure 34(a) and Figure 35(a)), fluctuating loads are also met by HTGR, marginally reducing the contribution of NG boilers and grid imports (Figure 34(b) and Figure 35(b)).

Figures 34(c) and 35(c) show normalized NPV by components. The black line represents the benefit-cost ratio. We first identified the cost components, including HTGR CAPEX, HTGR fixed O&M cost, HTGR variable O&M cost, TES CAPEX, BOP CAPEX, Charger CAPEX, NG variable O&M cost, and the cost of electricity imported from the grid, alongside a benefit component, which is the sales revenue of electricity to the grid. The cost and benefit components are accumulated, and if the electricity sales (shown by the purple area) approach the black line, the case is considered profitable. Since no monetary value is assigned to meeting industrial energy demands, all cases result in a negative NPV (indicating that the accumulated percentage of all cost components exceeds 50%). The average ERCOT electricity price (synthetic input) of $42/MWh and the variable O&M cost for NG are higher ($15/MWh) compared to that of an HTGR ($12/MWh). Consequently, the monetized changes resulting from the substitution of NG boilers and grid imports with HTGR are therefore more noticeable (Figure 34(c) and Figure 35(c)).

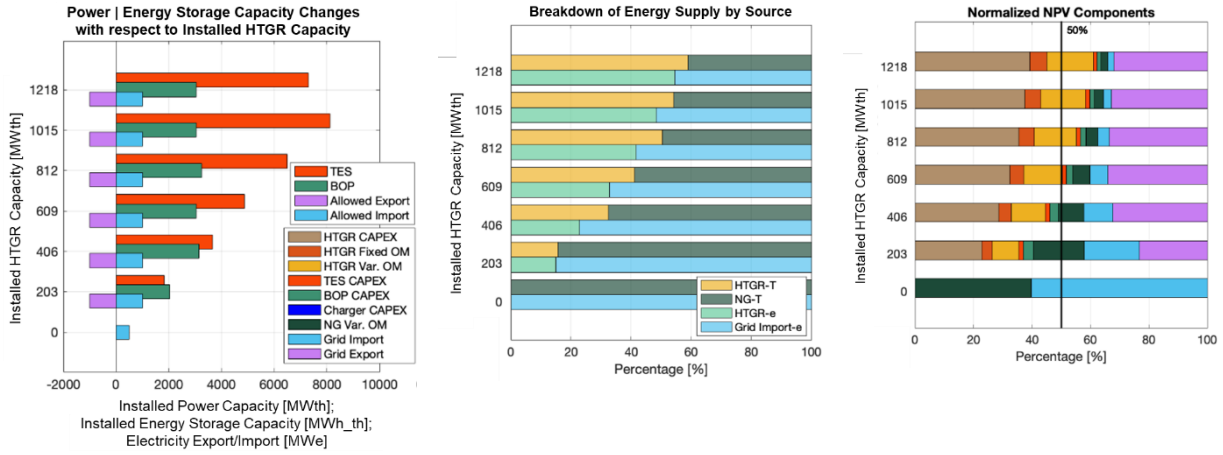

(a) (b) (c)

Figure 34. NPV-maximizing configurations for the HTGR-TES-CHP system for a single industrial process (under varying deployment cases): (a) optimal sizing for TES, and BOP capacities for varying reactor units (in total capacities), (b) the breakdown of energy supply by source to meet industrial thermal and electricity demand, and (c) normalized NPV by components. The black line in (c) indicates the benefit-cost ratio.

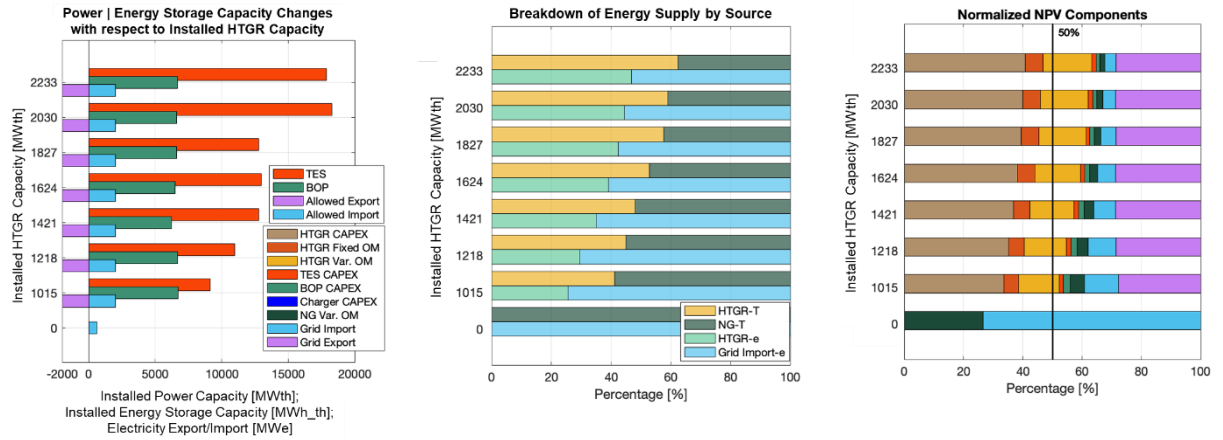

(a) (b) (c)

Figure 35. NPV-maximizing configurations for the HTGR-TES-CHP system for combined industrial processes (under varying deployment cases): (a) optimal sizing for TES, and BOP capacities for varying reactor units (in total capacities), (b) the breakdown of energy supply by source to meet industrial thermal and electricity demand, and (c) normalized NPV by components. The black line in (c) indicates the benefit-cost ratio.

The optimal capacity of TES and BOP depends on the specific operational goals: maximizing NPV, minimizing the natural gas boiler capacity factor (NGCF), and maximizing internal electricity supply from the HTGR as illustrated in Figure 33. Therefore, we quantify the cost-optimal trade-offs between these varying operational goals and the sizes of TES and BOP in terms of NPV, NGCF, and the share of internal electricity supply (as shown in Table 4 and Table 5). Since the heat and electricity provided to industrial processes are not monetized, the outcomes are identical for maximizing NPV and maximizing net electricity revenue. Similarly, minimizing NGCF is equivalent to maximizing internal thermal supply in our model.

We focus on cases with three to six HTGR units for the *single* case and seven to 11 HTGR units for the *combined* case. When examining energy supply by source below this level, we observe that HTGRs are primarily being used for electricity sales (while the industrial demands being covered by NG boiler and grid import). This is not the primary objective of the industrial energy park and leads to suboptimal performance in terms of industrial decarbonization. Therefore, our discussion will concentrate on the four previously mentioned deployment cases.

Numerical results shown in Figure 34 and Figure 35 are presented in Table 4 and Table 5 along with outcomes under the differing operational goals. Several insights are found from this investigation:

1. Under the operational goal of maximizing NPV, the internal electricity supply from HTGR is low. In other words, achieving a high NPV involves leveraging the low cost of NG and exploiting electricity arbitrage opportunities, given the available export and import capacities, rather than focusing on minimizing grid imports or heat supply from NG boilers.
2. Targeting the minimization of NGCF and maximization of internal electricity supply lower the NPV primarily due to reduced electricity sales. Although the CAPEX for TES and BOP are also reduced under these goals, the loss in electricity sales outweighs those CAPEX savings. The loss in electricity sales does not suggest that nuclear heat is priced higher to recover the investment. Rather, the goals of low NGCF and high internal electricity supply increase the total amount of nuclear heat energy (MWht) supplied for internal demands. This, in turn, lowers the unit nuclear heat energy price required to break even on the investment ($/MWht), which will be discussed in Section 7.4.
3. The installed reactor capacities significantly impact the respective sizes of TES and BOP under the different goals. When minimizing NGCF, the optimal TES size tends to decrease if the HTGR is average-sized or smaller, compared to when the goal is maximizing NPV. This is because the generated heat energy is directly used by the industrial process rather than stored, which also reduces the required BOP size. An oversized BOP is necessary for *self-sufficient* and *oversized* cases to balance internal electricity demand variations, regardless of single or combined scenarios. Under the goal of maximizing internal electricity supply, we find that a larger BOP size is needed. Given that the minimum BOP size to meet the peak electricity demand is 597 and 1,504 MWth for the single and combined profiles, respectively, any additional oversizing is for energy arbitrage purposes. This trend of oversizing the BOP for energy arbitrage is more pronounced in self-sufficient oversized cases.
4. Lowering the NGCF (or increasing the nuclear heat supply for the processes) generally increases the internal electricity supply. However, simply increasing internal supply does not necessarily result in a low NGCF (i.e., high internal thermal demand supply). This is related to the consideration of external grid capacities to achieve individual goals. To lower the NGCF, electricity export is minimized, and to achieve a high internal electricity supply, electricity import is set to minimum. The former setting increases internal electricity supply to utilize excess nuclear energy, while the latter can still balance oversupply by selling to external grids. Therefore, the NGCF is less affected by this constraint.
5. If the internal demand is electricity-intensive, the decoupling between internal nuclear heat supply and internal electricity supply will be intensified (as observed in the 2,030 and 2,233 MWt cases in Table 5). For instance, the electricity load share in the combined loads accounts for a higher share (70%) of their total equivalents compared to that of a single industrial process (57%). Additionally, 48.2% of the electrical load is static (refinery plant, baseload load of chemical plant), leading to a lower substitution of grid imports in meeting internal electricity demands, as the system flexibility in heat allocation to TES and BOP is limited. This indicates that dissecting individual electricity demands in a granular manner can be an important factor if the system aims to primarily supply electricity internally.

Table 4. Optimizing system sizing, NPVs, and performance parameters for a single industrial process under varying operational goals: maximizing NPV, minimizing the NGCF, and maximizing internal electricity supply.

HTGR		TES Capacity [MWht]	BOP Capacity [MWt]	External Grid Access		NPV [mill. $]	NGCF [%]	Internal Electricity Supply[b] [%]	Target Goal
Units	Capacity [MWt]			Export [MWe]	Import [a] [MWe]				
3	609	4,872	3,045	1,000	500–1,000	-146.0	38.0	32.8	Max.NPV
		1,218	914	100	200–1,000	-227.1	12.6	61.9	Min.NG CF
		3,654	2,893	1,000	0	-207.3	55.1	100	Max.Inte. E
4	812	6,496	3,248	1,000	500–1,000	-184.8	32.1	41.7	Max.NPV
		1,624	1,218	200	200–1,000	-266.8	10.5	72.3	Min.NG CF
		6,496	3,248	1,000	0	-216.5	41.9	100	Max.Inte. E
5	1,015	8,120	3,045	1,000	500–1,000	-226.9	29.6	48.3	Max.NPV
		1,015	1,269	200	200–1,000	-325.4	4.3	93.3	Min.NG CF
		4,060	3,045	1,000	0	-248.1	32.7	100	Max.Inte. E
6	1,218	7,308	3,045	1,000	500–1,000	-272.0	26.5	54.6	Max.NPV
		3,654	2,132	500	100	-333.5	11.6	78	Min.NG CF
		7,308	3,045	1,000	0	-288.2	28.3	100	Max.Inte. E

NPV, maximizing NPV; NGCF, minimizing the natural gas boiler capacity factor; Inte. E, maximizing internal electricity supply.

[a] Discrete level of 0, 100, 200, 500, and 1,000 MWe for export and import capacities are examined. When cases yield the same highest NPV with different import capacities, the ranges are indicated together.

[b] Internal electricity supply reflects the percentage of electricity for a single industrial process met by the HTGR prior to grid connection.

Table 5. Optimizing system sizing, NPVs, and performance parameters for combined industrial processes under varying operational goals: maximizing NPV, minimizing the NGCF, and maximizing internal electricity supply.

HTGR		TES Capacity [MWht]	BOP Capacity [MWt]	External Grid Access		NPV [mill. $]	NGCF [%]	Internal Electricity Supplyb [%]	Target Goal
Units	Capacity [MWt]			Export [MWe]	Import a [MWe]				
7	1,421	12,789	6,217	2,000	1,000–2,000	-400.2	43.5	35.0	Max.NPV
		1,421	1,776	100	1,000–2,000	-536.1	6.9	80.4	Min.NG CF
		1,421	1,599	100	100	-542.7	13.8	88.1	Max.Inte. E
8	1,624	12,992	6,496	2,000	1,000–2,000	-440.9	39.5	39.2	Max.NPV
		1,624	2,030	200	1,000–2,000	-580.6	7.6	84.3	Min.NG CF
		1,624	2,030	200	100	-585.2	9.9	91.2	Max.Inte. E
10	2,030	18,270	6,598	2,000	1,500–2,000	-528.2	34.4	44.5	Max.NPV
		4,060	3,045	500	1,000–2,000	-654.5	7.6	77.9	Min.NG CF
		10,150	7,105	2,000	0	-586.2	46.1	100	Max.Inte. E

HTGR		TES Capacity [MWht]	BOP Capacity [MWt]	External Grid Access		NPV [mill. $]	NGCF [%]	Internal Electricity Supplyb [%]	Target Goal
Units	Capacity [MWt]			Export [MWe]	Import a [MWe]				
11	2,233	17,864	6,699	2,000	1,000–2,000	-573.5	31.5	46.9	Max.NPV
		4,466	2,791	500	1,000–2,000	-713.7	7.3	84.4	Min.NG CF
		11,165	6,420	2,000	0	-621.7	41.1	100	Max.Inte. E

NPV, maximizing NPV; NGCF, minimizing the natural gas boiler capacity factor; Inte. E, maximizing internal electricity supply.

[a] Discrete level of 0, 100, 200, 500, 1,000, 1,500, and 2,000 MWe for export and import capacities are examined. When cases yield the same highest NPV with different import capacities, the ranges are indicated together.

[b] Internal electricity supply reflects the percentage of electricity for a single industrial process met by the HTGR prior to grid connection.

Figure 37 and Figure 38 show crossover points of the NG-to-HTGR variable O&M cost ratio ($= \frac{\text{NG price}}{\text{HTGR variable O\&M costs}}$) at which the proposed HTGR-TES-CHP system can cost-effectively penetrate the market currently solely served by NG boilers. We explored NG price sensitivity to NPV under various operational goals for three cost estimate scenarios for HTGR: conservative, moderate, and low (see Table 19 in Appendix G). The results are presented for four deployment cases—undersized, medium-sized, self-sufficient, and oversized. A line placed above the BAU case indicates that the system configuration already demonstrates better economic outcomes at a certain relative cost level (gas-to-HTGR variable O&M ratio). A gentle slope indicates less sensitivity to a NG price change.

In the BAU case, NPV increases linearly with rising NG prices, showing a steep slope. Maximizing NPV consistently produces higher NPVs, while the NPVs from minimizing NG consumption and maximizing internal electricity supply goals follow closely behind. Interestingly, these relative NPV levels shift as NG prices increase, and these changes depend on factors such as HTGR CAPEX levels, types of industrial loads (or the contribution of NG boilers in meeting optimization goals), and deployment scenarios. For example, the HTGR-TES-CHP system remains competitive when NG prices are 3.5–9.5× higher than HTGR variable O&M costs for single industrial processes, assuming a base HTGR CAPEX level of $3,250/kWth. In contrast, the combined industrial process scenario, which has a more electricity-intensive profile, is generally less sensitive to changes in NG prices. This results in a crossover point at NG prices 8.5–9.5× higher, with a gentler slope compared to single industrial process scenarios. Similarly, NG price increases have little impact on self-sufficient and oversized cases, as well as on NPVs in operational goals where both heat and NG boilers are minimally used (low NGCF), as shown by the green lines in Figure 37 and Figure 38.

In summary, depending on the electrical load share in the total industrial thermal equivalent loads, we observe that the NG price level has a different impact on NPV in cases where the internal electricity supply is prioritized (blue lines in Figure 37 and Figure 38). For instance, in a single industrial process scenario, undersized and mean-sized cases show that the NG boiler is actively used to increase internal electricity supply. As a result, nuclear heat is primarily used for internal electricity demands, leading to a worsening NPV as NG prices increase. In contrast, for self-sufficient and oversized cases, excess nuclear heat reduces the NG boiler's contribution, making the impact of NG price less evident. These trends are consistent with the results from moderate (Figure 73 and Figure 75) and low HTGR CAPEX estimates (Figure 74 and Figure 76).

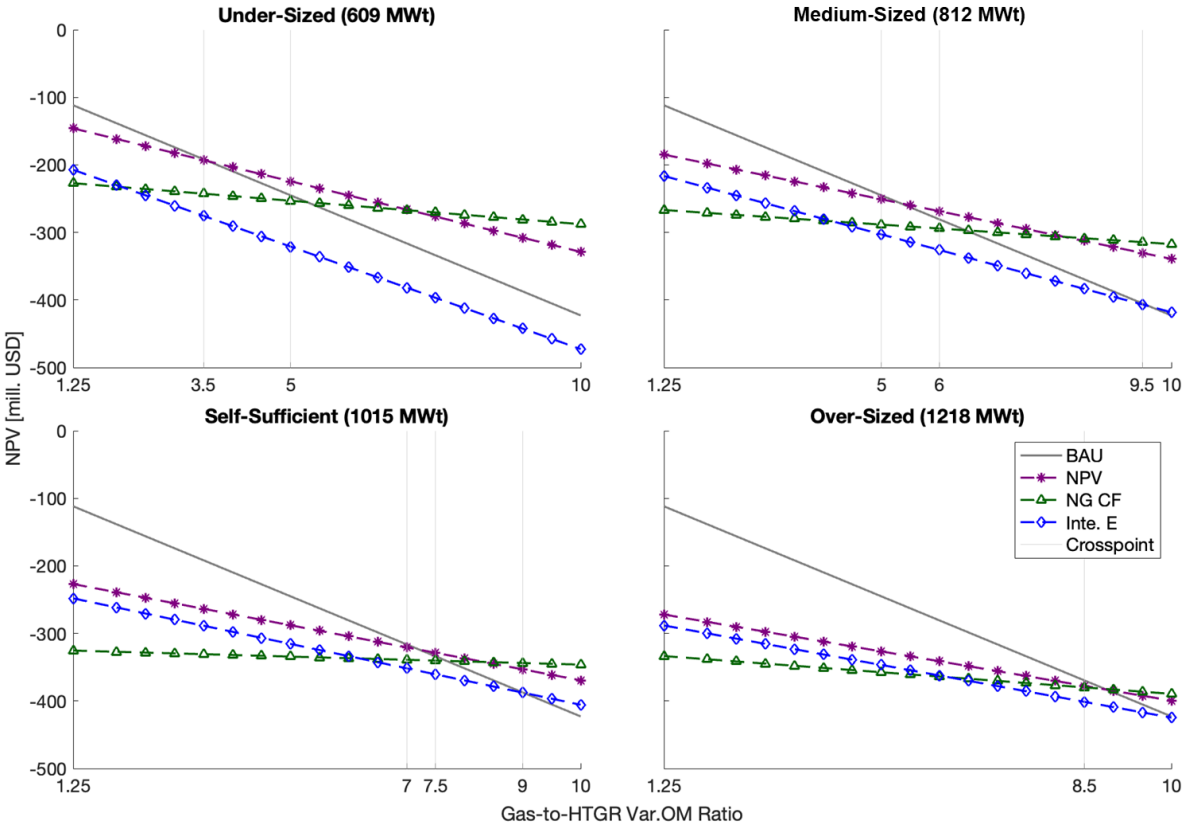

Figure 36. Crossover points where the HTGR-TES system outperforms standalone NG boilers in cost-effectiveness (NPV) for a single industrial process. Starting from a base cost ratio of 1.25 between NG boiler variable O&M ($15/MWht) and HTGR variable O&M ($12/MWht), crossover points are explored in increments of 0.5 up to a ratio of 10. Any NPV from individual operation goals that outperforms the BAU operation is marked on the x-axis. Due to data point resolution, these points may not match exactly with those derived from interpolation.

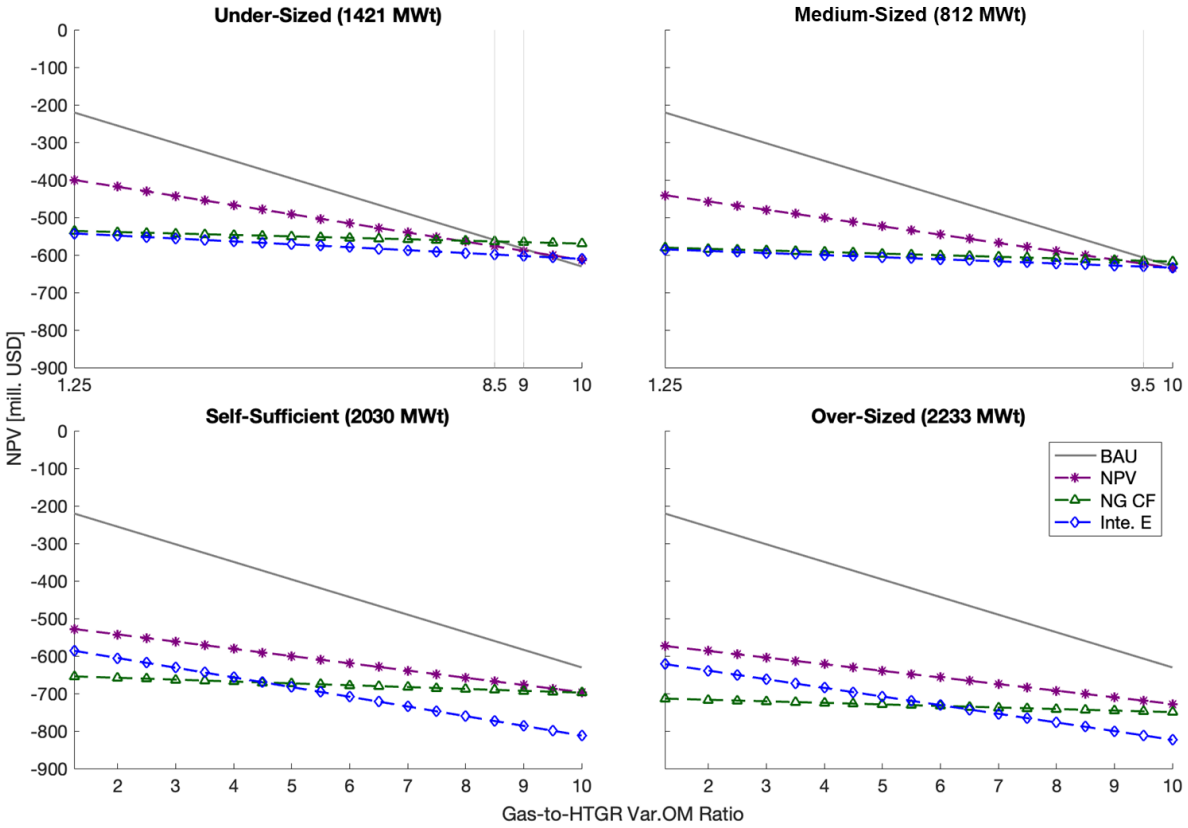

Figure 37. Crossover points where the HTGR-TES system outperforms standalone NG boilers in cost-effectiveness (NPV) for combined industrial processes. Starting from a base cost ratio of 1.25 between NG boiler variable O&M ($15/MWht) and HTGR variable O&M ($12/MWht), crossover points are explored in increments of 0.5 up to a ratio of 10. Any NPV from individual operation goals that outperforms the BAU operation is marked on the x-axis. Due to data point resolution, these points may not match exactly with those derived from interpolation.

7.3 Impacts of External Grid Access Availability

This section explores how two modeling settings, external export, and import capacities, shape the overall system economics and performance parameters. As noted in the previous section, the level of external grid access is a key driver in achieving the target goals in our modeling. The observed export and import capacities under the individual goals are posterior outcomes. In other words, these values result from exploring the industrial energy park configurations that meet either the maximum NPV, minimum NGCF, or maximum internal electricity supply. The set of export and import capacities does not necessarily ensure solutions for each goal, as their determination is tied to the relationships within the specifications of the HTGR-TES system, input price signals and industrial profiles. Thus, our investigation extends to possible combinations of export and import capacities to identify a feasible design space that achieves the parameters of interest. Additionally, decision makers may utilize this approach to estimate the impact of varying transmission constraints on the system by matching the expected export and import capacities of the site of interest. In this evaluation, we focus on NPV and NGCF; however, the evaluation framework presented remains transferrable for net electricity sales revenue and internal electricity supply.

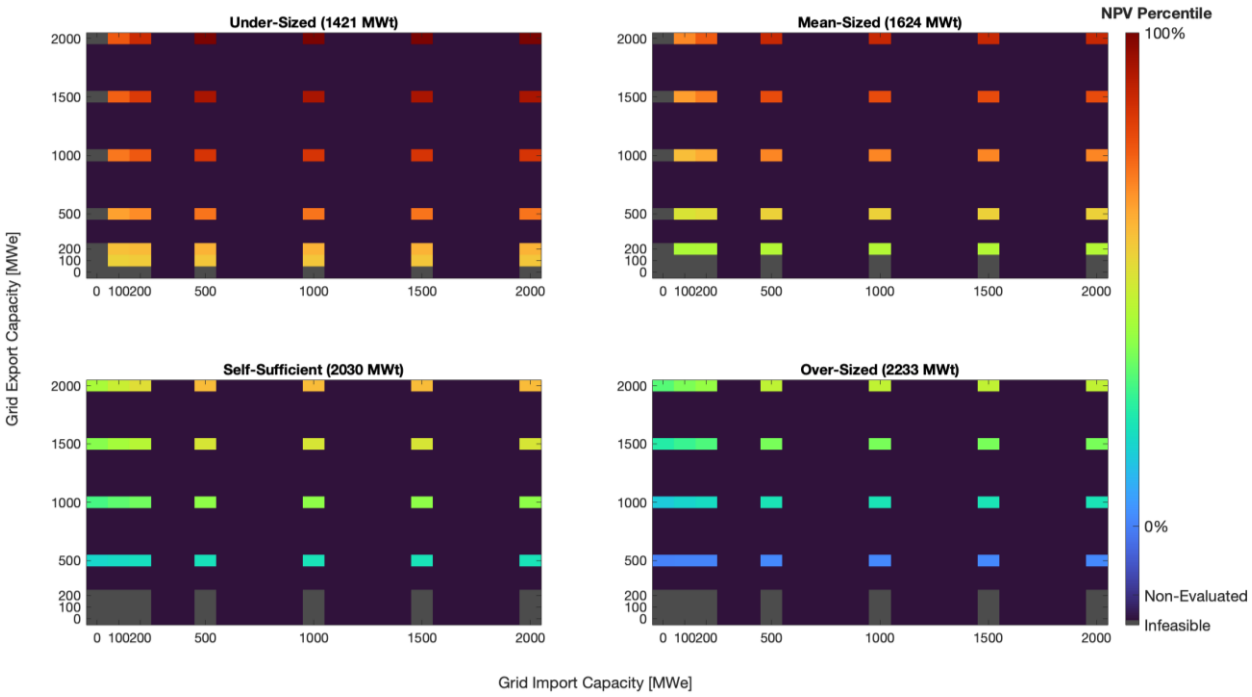

Figure 38. NPV percentile distribution with varying external grid access availability under different deployments (combined industrial processes). At seven-, eight-, 10-, and 11-units deployment, NPVs are optimized for given export-import capacities. NPV percentiles are evaluated within four categories: undersized, medium-sized, self-sufficient, and oversized. The dark blue area represents optimization steps not explored area in HERON; dark grey represents areas infeasible in solving the optimization problem.

Figure 38 and Figure 39 summarize the NPV percentile and NGCF distribution with varying levels of external grid access availability for combined industrial processes. The results are categorized with respect to deployment cases (in terms of total reactor capacities) are categorized. For NPV, the highest values occur with a high level of export capacity, which leads to increased electricity sales and a subsequent rise in NPV. Interestingly, we find that, beyond an import capacity level of 500–1000 MWe, the NPV level does not vary. This is due to the required import capacity being limited by the internal electricity demand. If this internal demand is reduced, this import insensitivity will be observed at a smaller import capacity, as shown in Figure 45. As there is no compensation for providing energy to the industrial processes from the HTGR, oversized cases show a lower NPV compared to undersized cases. However, if we explore beyond 2,000 MWe of export capacities, the oversized case should present the highest NPV under a price-taker assumption.

As expected, the highest NGCF is observed in the case where the HTGR is undersized. We also find that the import capacity becomes insensitive starting from 500–1,000 MWe. Our framework highlights the multifaceted aspects of recovering capital investment in a coordinated manner, which can provide reasonable outcomes depending on the specific deployment cases. Overall, undersized cases show a more granular distribution with minimal infeasible solutions in 0–2,000 MWe capacities. This is the case for the single industrial process scenario (Figure 38 and Figure 39), which suggests that an undersized deployment strategy may be suitable in regions with limited external grid access availability. To make medium- to oversized cases feasible under such external grid access conditions, higher TES capacities, specifically beyond 9× reactor capacities, will be required.

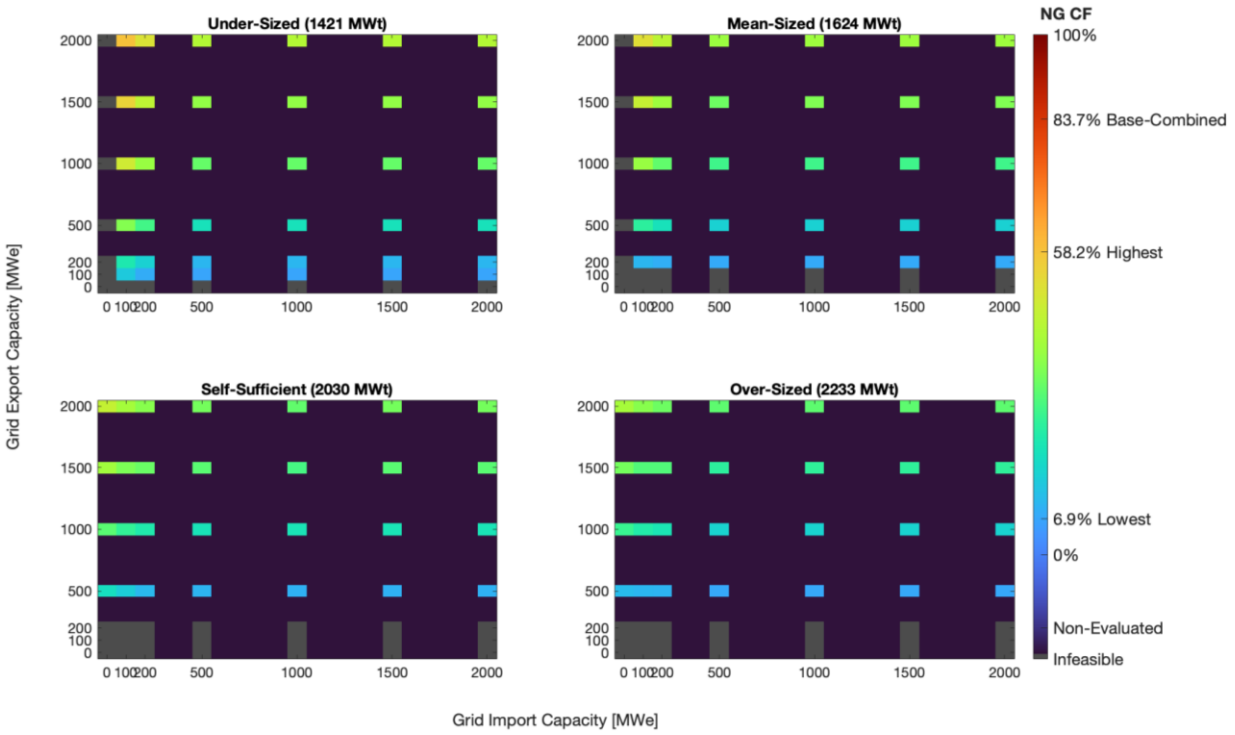

Figure 39. NGCF distribution with varying external grid access availability under different deployments (combined industrial processes). At seven-, eight-, 10-, and 11-units deployment, NGCF values are evaluated within four categories: undersized, medium-sized, self-sufficient, and oversized. The optimal sizing of TES and BOP capacity is identical to that listed in Figure 38. The dark blue area represents optimization steps not explored in HERON, while the dark grey area represents regions infeasible for solving the optimization problem.

The changes in optimal sizing of TES and BOP at different export and import capacities are presented in Appendix H, Core HERON Optimization Results. This is also reflected in the single industrial process scenario (Figure 79). With differing levels of export and import capacities, the design space of TES and BOP is significantly varied even with a fixed HTGR capacity. Since real-world siting is likely constrained by these factors, identifying expected export and import capacities can be profoundly important in relation to transmission congestion and the availability of VRE in the considered region.

7.4 HTGR Energy Delivery Requirements

In planning capital-intensive engineering projects, it is essential to identify technical requirements and price (or cost) targets to realize the estimated economic potentials. To this end, we trace detailed energy delivery focusing on TES operation for both single and combined industrial profile(s) scenarios (Table 6 and Table 20). We notice significant variations in TES operation in terms of the frequency and amplitude of charge and discharge cycles. For instance, when the system is operated to maximize NPV (or maximizing net electricity revenue), we observe frequent deep discharges of TES, as price peaks in ERCOT are concentrated at limited times of the day. In contrast, for minimizing the NGCF goal, we observe more frequent deep charges to accommodate periods of low internal thermal demand, whereas during periods of high demand, most of the reactor output is diverted to the process along with the discharged heat from the TES. For maximizing internal electricity supply, we find differing charge and discharge amplitudes depending on reactor capacities due to export capacities (Table 4). In the single process scenario, where static internal load is excluded, we observe the impact of export capacities even in an undersized case (Table 20).

In fact, the goal of maximizing NPV presents the most extreme environment for a TES, as electricity price signals are more volatile than those of industrial loads. In examining the integrity of TES under nuclear TES integrated energy system operation, previous studies have identified that TES is well poised to accommodate these frequencies and amplitudes of charge and discharge without the degradation issues that may arise with a battery-type storage [72].

Table 6. Breakdown of the HTGR-TES system operation for combined industrial processes under varying operational goals: maximizing NPV and minimizing the NGCF.

HTGR		TES Capacity [MWht]	BOP Capacity [MWt]	Charge Event	Discharge Event	Avg. Charge Power [MWt]	Avg. Discharge Power [MWt]	Target Goal
Units	Capacity [MWt]							
7	1,421	6,217	12,789	2,478	703	2,786	8,838	NPV
		1,776	1,421	1,097	1,923	1,315	675	NG CF
		1,599	1,421	1,480	1,371	339	329	Inte. E
8	1,624	6,496	12,992	2,393	765	3,190	8,981	NPV
		2,030	1,624	1,074	1,938	1,580	788	NG CF
		2,030	1,624	1,494	1,451	733	679	Inte. E
10	2,030	6,598	18,270	2,208	916	4,102	8,899	NPV
		3,045	4,060	1,236	1,962	2,809	1,592	NG CF
		7,105	10,150	2,673	581	1,728	7,154	Inte. E
11	2,233	6,699	17,864	2,117	1,008	4,526	8,554	NPV
		2,791	4,466	1,180	2,254	2,429	1,144	NG CF
		6,420	11,165	2,552	662	2,131	7,394	Inte. E

NPV, maximizing NPV; NGCF, minimizing the natural gas boiler capacity factor; Inte. E, maximizing internal electricity demand.

The charge and discharge events reflect one year of operation.

The ITC serves as a mechanism to promote nascent clean energy technologies with high CAPEX by reducing the upfront costs. Toward this end, we compute a minimum allowable HTGR heat price under different ITC levels (Table 7). Detailed steps for the calculations can be found in the annotation [C] in Table 21 (Appendix H). Additionally, we investigate the impacts of the ITC on the minimum allowable HTGR heat price for moderate ($2,500/kWt) and low estimates ($1,750/kWt) of HTGR CAPEX (Table 24 and Table 8, respectively). This comprehensive investigation enables decision makers to match economically viable industrial customers based on their expected HTGR CAPEX. Details regarding the representation of ITC in this calculation are available in Table 21.

The ITC significantly lowers the threshold for the price level needed to break even in terms of NPV. In other words, the HTGR-TES project can be profitable (NPV > 0) even when selling their energy (heat and electricity) at a lower price. This effect varies depending on the operational target. We observe a reduction of 41%, 30%, and 32% in the threshold for maximizing NPV, minimizing NGCF, and maximizing internal electricity supply goals, respectively, at an HTGR CAPEX of $3,250/kWe. For a single load, the respective reductions are 48%, 30%, and 39% at the same CAPEX level. While these reductions are notable, it is important to note that the heat and electricity from the HTGR-TES are competitive with NG boilers only in limited cases as well as under specific ITC levels and operational goals (Table 8, Table 22, and Table 23). To achieve economic viability for the system in industrial processes, it is crucial to carefully coordinate the ITC level, deployment case, and target goals comprehensively.

As mentioned earlier, the industrial energy park configurations under the goal of maximizing NPV show the best economics in terms of total NPV before monetizing the HTGR energy provided for internal demands. In this setting, the HTGR energy is primarily used for electricity sales, with the NG boiler covering internal thermal demands. However, the electricity levels used in our modeling are not sufficient to recover the CAPEX of the HTGR, and the total amount of HTGR heat energy (MWht) supplied for internal demands is low (due to the electricity exported), leading to a higher minimum allowable HTGR heat price ($/MWht).

Table 7. Change in minimum allowable HTGR heat price under varying ITC levels for combined industrial processes. (HTGR CAPEX: $3250/kWt, $8228/kWe)

HTGR		Minimum Allowable HTGR Heat Cost [a] [$/MWth]					
Units	Capacity [MWt]	ITC 0	ITC 6	ITC 30	ITC 40	ITC 50	Target Goal
7	1,421	73.2	70.0	57.3	49.7	44.0	NPV
		45.5	44.0	38.1	34.6	31.9	NG CF
		44.5	43.0	37.4	34.0	31.4	Inte. E
8	1,624	72.5	69.2	56.2	48.4	42.5	NPV
		47.8	46.2	39.7	35.7	32.8	NG CF
		46.0	44.5	38.3	34.5	31.7	Inte. E
10	2,030	76.9	73.3	58.9	50.3	43.8	NPV
		57.2	55.0	46.4	41.2	37.3	NG CF
		49.8	47.7	39.3	34.2	30.5	Inte. E
11	2,233	79.1	75.4	60.4	51.3	44.6	NPV
		58.7	56.4	47.5	42.1	38.1	NG CF
		51.7	49.5	40.4	35.0	30.9	Inte. E

NPV, maximizing NPV; NGCF, minimizing the natural gas boiler capacity factor; Inte. E, maximizing internal electricity demand. The optimal sizing of TES and BOP capacity is identical to that listed in Table 5.

[a] The minimum allowable HTGR heat cost is the price at which the selling price must be set to break even on the investment. If the goal is to achieve a market rate of return, these values need to be higher.

In light of this, having operational goals that direct HTGR heat energy primarily for internal demands can increase the denominator (HTGR heat used for internal demands). We observe that the thresholds are sensitive to the deployment cases. While under- and medium-sized cases may be cost-effective in operating with an NG boiler, the most affordable HTGR can be achieved under self-sufficient or oversized cases as they maximize nuclear utilization for internal demands and lower the unit HTGR heat price needed to break even on the investment. These threshold values are also influenced by the composition of internal electrical loads. When electrical loads dominate the total internal loads, restricting imported electricity further increases HTGR heat utilization for internal demands. This trend intensifies under self-sufficient and oversized cases. Our findings highlight that to penetrate markets, it is essential to understand not only nuclear capacity factors but also its share of utilization for internal demands.

Table 8. Change in minimum allowable HTGR heat price under varying ITC levels for combined industrial processes. (HTGR CAPEX: $1750/kWt, $4430/kWe)

HTGR		Minimum Allowable HTGR Heat Cost [a] [$/MWth]					
Units	Capacity [MWt]	ITC 0	ITC 6	ITC 30	ITC 40	ITC 50	Target Goal
7	1,421	43.9	42.2	35.4	31.3	28.2	NPV
		31.9	31.1	27.9	26.1	24.6	NG CF
		31.4	30.6	27.5	25.7	24.3	Inte. E
8	1,624	42.4	40.7	33.7	29.5	26.3	NPV
		32.8	31.9	28.4	26.3	24.7	NG CF
		31.7	30.8	27.5	25.5	24.0	Inte. E
10	2,030	43.7	41.7	34.0	29.3	25.8	NPV
		37.2	36.1	31.4	28.6	26.5	NG CF
		30.4	29.3	24.7	22.0	20.0	Inte. E
11	2,233	44.5	42.4	34.4	29.5	25.9	NPV
		38.0	36.8	32.0	29.1	26.9	NG CF
		30.8	29.6	24.7	21.8	19.6	Inte. E
					Historical NG price range of mean ± 2σ [b]		

NPV, maximizing NPV; NGCF, minimizing the natural gas boiler capacity factor; Inte. E, maximizing internal electricity demand. The optimal sizing of TES and BOP capacity is identical to that listed in Table 5.

[a] The minimum allowable HTGR heat cost is the price at which the selling price must be set to break even on the investment. If the goal is to achieve a market rate of return, these values need to be higher.

[b] Estimated minimum allowable HTGR heat price that falls into historical NG price ranges is colored in green. The past 5 years' price data (07/22/2019–07/19/2024) from the Henry Hub NG spot prices are used [45].

8. CONCLUSIONS

This study proposed and assessed approaches for integrating nuclear power into industrial systems that require both electricity and heat, with specific cases being considered for TES implementation (i.e., chemical plants, petroleum refineries, and iron and steel production involving an EAF facility).

Chemical plants, characterized by their batch operations and transient nature, could potentially benefit from integrating TES to stabilize fluctuating energy demands. Petroleum refineries were chosen to represent industries with consistent energy demand profiles. Although iron and steel production poses challenges for nuclear integration, due to limited opportunities and the complexities of traditional processes, integrating TES could aid in managing the variable electricity demands of EAFs. Additionally, this study identified food processing plants, pulp and paper mills, and methanol plants as being unsuitable for TES. Food processing is unsuitable due to its low energy requirements. Methanol plants and pulp and paper mills restrict opportunities for nuclear integration because they are mostly self-sufficient from internal energy production.

Various power conversion system layouts were investigated, focusing on providing electricity and heat to meet industrial demand, while also incorporating TES for load flexibility. The present study is based on the use of an HTGR (i.e., the Xe-100), with system parameters allowing for a high-temperature steam supply. While the steam or extracted steam can be considered as a point for TES integration, the best solution was to locate the TES between the nuclear primary loop and the steam cycle conversion system. These decoupled systems also afford flexibility in terms of steam cycle parameters and configuration, raising efficiency compared to the baseline system.

This study considered configurations of integrated industrial parks that incorporate nuclear energy alongside conversion systems for heat and power delivery. Various scenarios—chemical plants with diverse heat-to-electricity demands, a petroleum refinery, and an EAF—were explored. These investigations revealed that, by connecting a TES unit to a single reactor unit, CHP systems with multiple reactor units can offer sufficient flexibility for the entire integrated system. Simple dispatch algorithms and preliminary sizing of TES are presented to highlight the different roles, objectives, and dispatch strategies of TES systems. The findings showcased that TES could enhance energy system efficiency, balancing the energy import and export, minimizing reliance on backup fossil-fuel-based heating systems, and ensuring a consistent electricity export post-heat-demand fulfillment. Nonetheless, challenges persist, especially for system sizing, robust dispatch optimization, and technoeconomic feasibility of heat-to-power systems for highly fluctuating energy markets. These challenges will be discussed in future works.

We examined configurations of integrated industrial parks that incorporate nuclear energy alongside conversion systems for heat and power delivery. Various scenarios—chemical plants with diverse heat-to-electricity demands, a petroleum refinery, and an EAF—were explored. These investigations revealed that, by connecting a TES unit to a single reactor unit, CHP systems with multiple reactor units can offer sufficient flexibility for the entire integrated system. Simple dispatch algorithms and a preliminary sizing of TES are presented to highlight the different roles, objectives, and dispatch strategies of TES systems. The findings showcased that TES could enhance energy system efficiency, balancing the energy import and export, minimizing reliance on backup fossil-fuel-based heating systems, and ensuring a consistent electricity export post-heat-demand fulfillment. Nonetheless, challenges persist, especially for system sizing, robust dispatch optimization, and technoeconomic feasibility of heat-to-power systems for highly fluctuating energy markets. These challenges will be discussed in future works.

Finally, we evaluated the potential of the HTGR-TES system and compared its economic competitiveness to the respective BAU operation with NG boilers. Our findings particularly emphasize the number and types of industrial profiles, HTGR CAPEX levels, deployment strategies, operational goals, and tax credit levels. Each uncertainty is explored in terms of NPV, TES, and BOP sizing, as well as the degree to which the system substitutes for NG boilers and dependence on the external grid. We find that introducing the HTGR-TES system significantly lowers the contribution of NG boilers and grid imports to internal thermal and electricity demands. Our modeling also highlights that the optimal TES and BOP depends on the target operational goals. Exploring the sensitivity of the findings to external grid access availability points to the importance of identifying expected export and import capacities, particularly in relation to transmission congestion and the availability of VRE in the considered region. Detailed tracing of TES operations reveals that, across all operational goals, the frequencies and amplitudes of charge and discharge cycles are within the previously identified design limits. Our tax credit modeling shows that the ITC significantly lowers the threshold for the price level needed to break even, and in certain cases, it is even comparable to NG boilers.

9. REFERENCES

1. U.S. DOE. 2022. “Industrial Decarbonization Roadmap (DOE/EE-2635).” United States Department of Energy, Washington D.C. https://www.energy.gov/sites/default/files/2022-09/Industrial%20Decarbonization%20Roadmap.pdf.
2. International Energy Agency. 2021. “Net Zero By 2050 - A Roadmap for the Global Energy Sector.” International Energy Agency, Paris, France. https://iea.blob.core.windows.net/assets/deebef5d-0c34-4539-9d0c-10b13d840027/NetZeroby2050-ARoadmapfortheGlobalEnergySector_CORR.pdf.
3. Federal Register. 2021. “Tackling the Climate Crisis at Home and Abroad – A Presidential Document by the Executive Office of the President on 02/01/2021.” Executive Order 14008, January 27, 2021. Accessed August 11, 2024. https://www.federalregister.gov/documents/2021/02/01/2021-02177/tackling-the-climate-crisis-at-home-and-abroad.
4. United States Department of State and the United States Executive Office of the President. 2021. “The Long-Term Strategy of the United States: Pathways to Net-Zero Greenhouse Gas Emissions by 2050.” Accessed August 15, 2024. https://www.whitehouse.gov/wp-content/uploads/2021/10/US-Long-Term-Strategy.pdf.
5. U.S. Department of Energy. 2022. “Industrial Decarbonization Roadmap.” U.S. Department of Energy, DOE/EE-2635, Washington D.C. https://www.energy.gov/sites/default/files/2022-09/Industrial%20Decarbonization%20Roadmap.pdf.
6. U.S. Department of Energy. 2019. “Manufacturing Energy and Carbon Footprints (2018 MECS).” U.S. Department of Energy. Accessed February 28, 2024. https://www.energy.gov/eere/iedo/manufacturing-energy-and-carbon-footprints-2018-mecs.
7. McMillan, C. 2024. “Manufacturing Thermal Energy Use in 2014.” National Renewable Energy Laboratory Data Catalog. Golden, CO. Accessed February 28, 2024. https://data.nrel.gov/submissions/118.
8. Naegler, T., S. Simon, M. Klein, and H. C. Gils. 2015. “Quantification of the European industrial heat demand by branch and temperature level.” *International Journal of Energy Research* 39(15): 2019–2030. https://doi.org/10.1002/er.3436.
9. Rehfeldt, M., T. Fleiter, and F. Toro. 2018. “A bottom-up estimation of the heating and cooling demand in European industry.” *Energy Efficiency* 11: 1057–1082. https://doi.org/10.1007/s12053-017-9571-y.
10. OECD-NEA. 2022. “Beyond Electricity: The Economics of Nuclear Cogeneration.” OECD Publishing, Paris, France. https://www.oecd-nea.org/upload/docs/application/pdf/2022-07/7363_cogen.pdf.
11. Moniz, E. J., H. D. Jacoby, A. J. Meggs, et al. 2011. “The Future of Natural Gas - An Interdisciplinary MIT Study.” Cambridge, MA: Massachusetts Institute of Technology. https://energy.mit.edu/wp-content/uploads/2011/06/MITEI-The-Future-of-Natural-Gas.pdf.
12. U.S. Energy Information Administration. 2023. “Use of energy explained - Energy use in industry.” Accessed August 7, 2024. https://www.eia.gov/energyexplained/use-of-energy/industry.php.
13. International Atomic Energy Agency. 2000. “Introduction of Nuclear Desalination.” Technical Reports Series No. 400, IAEA, Vienna, Austria. https://www.iaea.org/publications/5925/introduction-of-nuclear-desalination.
14. International Atomic Energy Agency. 2017. “Opportunities for Cogeneration with Nuclear Energy.” No. NP-T-4.1. IAEA, Vienna, Austria. https://www.iaea.org/publications/10877/opportunities-for-cogeneration-with-nuclear-energy.

15. Shah, Y. T. 2020. “Modular systems for energy usage management (1st ed.).” CRC Press, Boca Raton. https://doi.org/10.1201/9780367822392.

16. IAEA. 2019. “Guidance on Nuclear Energy Cogeneration.” IAEA Nuclear Energy Series No. NP-T-1.17, Vienna, Austria. https://www.iaea.org/publications/13385/guidance-on-nuclear-energy-cogeneration.

17. Losev, V. L., M. V. Sigal, and G. E. Soldatov. 1989. “Nuclear district heating in CMEA countries.” *International Atomic Energy Agency Bulletin* 31(3): 46–49. https://www.iaea.org/sites/default/files/31304794649.pdf.

18. X-Energy. 2024. “Xe-100: The Most Advanced Small Modular Reactor.” Accessed March 14, 2024. https://x-energy.com/reactors/xe-100.

19. Hilborn, J. S., J. S. Glen, W. A. Seddon, and A. G. Barnstaple. 1980. “Industrial Process Heat from CANDU Reactors.” No. AECL-7066, Atomic Energy of Canada Ltd., Chalk River, Ontario, Canada. https://inis.iaea.org/collection/NCLCollectionStore/_Public/12/578/12578230.pdf.

20. Seddon, W. A. 1981. “Nuclear Process Steam for Industry Potential for the Development of an Industrial Energy Park Adjacent to the Bruce Nuclear Power Development.” No. AECL-7426, Atomic Energy of Canada Ltd., Chalk River, Ontario, Canada. https://inis.iaea.org/collection/NCLCollectionStore/_Public/13/706/13706369.pdf.

21. Suhr, M., G. Klein, I. Kourti, et al. 2015. “Best Available Techniques (BAT) Reference Document for the Production of Pulp, Paper and Board.” European Commission, Brussels, Belgium. https://eippcb.jrc.ec.europa.eu/sites/default/files/2019-11/PP_revised_BREF_2015.pdf.

22. Fernandez, A. G., H. Galleguillos, E. Fuentealba, and F. J. Perez. 2015. “Thermal characterization of HITEC molten salt for energy storage in solar linear concentrated technology.” *Journal of Thermal Analysis and Calorimetry* 122: 3–9. https://doi.org/10.1007/s10973-015-4715-9.

23. Kraemer, S. 2023. “Oxygen fix for high-temperature molten-salt degradation (and corrosion) at 620°C.” SolarPACES. Accessed February 28, 2024. https://www.solarpaces.org/high-temperature-molten-salt-degradation-gets-oxygen-fix/.

24. Novotný, V., V. Basta, P. Smola, and J. Spale. 2022. “Review of Carnot Battery Technology Commercial Development.” *Energies* 15(2): 647. https://doi.org/10.3390/en15020647.

25. Saeed, R. M., V. Novotný, S.-B. Cho, et al. 2023. “A Multidisciplinary Approach to Integrated Energy Systems: Advanced Nuclear Plants with Thermal Storage for Dynamic and Flexible Operation in Diverse Markets.” INL/RPT-23-74725 (unpublished), Idaho National Laboratory, Idaho Falls, ID.

26. Greenwood, M. S., A. G. Yigitoglu, J. D. Rader, et al. 2020. “Integrated Energy System Investigation for the Eastman Chemical Company, Kingsport, TN Facility.” Oak Ridge National Laboratory, Oak Ridge, TN. https://doi.org/10.2172/1643929. https://www.osti.gov/servlets/purl/1643929.

27. Joseck, F., V. Novotný, E. A. R. Molina, et al. 2023. “Thermal Integration of Advanced Nuclear Reactors with a Reference Refinery, Methanol Synthesis, and Wood Pulp Plant.” INL/RPT-24-76435 Rev:001 (unpublished), Idaho National Laboratory, Idaho Falls, ID.

28. Dock, J., D. Janz, J. Weiss, A. Marschnig. and T. Kienberger. 2021. “Time- and component-resolved energy system model of an electric steel mill.” *Cleaner Engineering and Technology* 4: 100223. https://doi.org/10.1016/j.clet.2021.100223.

29. Nurin, T. 2023. “Small Changes, Big Impact: Reducing Energy Expenses in Breweries.” Precision Fermentation. Accessed February 28, 2024. https://www.precisionfermentation.com/blog/small-changes-big-impact-economizing-energy-expenses/.

30. Brewers Association. 2005. “Energy Usage, GHG Reduction, Efficiency and Load Management Manual.” Accessed February 28, 2024. https://www.brewersassociation.org/attachments/0001/1530/Sustainability_Energy_Manual.pdf.
31. Le-bail, A., T. Dessev, V. Jury, et al. “Energy demand for selected bread making processes: Conventional versus part baked frozen technologies.” *Journal of Food Engineering* 96(4): 510–519. https://doi.org/10.1016/j.jfoodeng.2009.08.039.
32. Hasanbeigi, A. 2021. “Industrial Heating Profile and Electrification.” Global Efficiency Intelligence. Accessed February 28, 2024. https://www.globalefficiencyintel.com/new-blog/2021/3/22/industrial-heating-profile-and-electrification.
33. Office of Energy Efficiency & Renewable Energy, US Department of Energy. 2018. “Manufacturing Energy and Carbon Footprints (2018 MECS).” Office of Energy Efficiency & Renewable Energy, US Department of Energy. Accessed August 8, 2024. https://www.energy.gov/eere/iedo/manufacturing-energy-and-carbon-footprints-2018-mecs.
34. Garvey, S. 2020. “FEATURE: Why medium-duration energy storage is vital for a ‘net zero’ UK.” Institute of Mechanical Engineers. Accessed August 22, 2024. https://www.imeche.org/news/news-article/feature-why-medium-duration-energy-storage-is-vital-for-a-net-zero-uk.
35. Kawasaki. 2020. “Kawasaki Completes Basic Design for World’s Largest Class (11,200-cubic-meter) Spherical Liquefied Hydrogen Storage Tank.” Kawasaki. Accessed August 22, 2024. https://global.kawasaki.com/en/corp/newsroom/news/detail/?f=20201224_8018.
36. Dvorsky, G. 2023. “World’s Largest Hydrogen Tank Will Make It Easier for NASA to Launch SLS Megarocket.” Gizmodo. Accessed August 22, 2024. https://gizmodo.com/largest-hydrogen-tank-nasa-sls-rocket-artemis-1850059559.
37. Fesmire, J. E. and A. Swanger. 2021. “DOE/NASA Advances in Liquid Hydrogen Storage Workshop.” Accessed August 22, 2024. https://www.energy.gov/sites/default/files/2021-10/new-lh2-sphere.pdf.
38. Talbot, P. W. et al. 2020. “Evaluation of Hybrid FPOG Applications in Regulated and Deregulated Markets Using HERON.” INL/EXT-20-60968. Idaho National Laboratory, Idaho Falls, ID. https://doi.org/10.2172/1755894.
39. ERCOT. 2024. LMPs by Resource Nodes, Load Zones and Trading Hubs.” https://www.ercot.com/mp/data-products/data-product-details?id=NP6-788-CD.
40. U. S. Congress. 2022. “Inflation Reduction Act of 2022.” 117th Congress.
41. Steinberg, D. C., M. Brown, R. Wiser, et al. 2023. “Evaluating Impacts of the Inflation Reduction Act and Bipartisan Infrastructure Law on the U.S. Power System.” MREL/TP-6A20-85242. National Renewable Energy Laboratory, Golden, CO.
42. Guaita, N. and J. K. Hansen. 2024. “Analyzing the Inflation Reduction Act and the Bipartisan Infrastructure Law for Their Effects on Nuclear Cost Data.” INL/RPT-23-72925. Idaho National Laboratory, Idaho Falls, ID. https://doi.org/10.2172/2335485.
43. So-Bin Cho, Sam J. Root, Rami M. Saeed, Tyler L. Westover. 2024. "Microreactor-Liquid Metal Battery System Potential in Energy Markets: An Ex Ante Evaluation of Costs, Technology, and Policy Impacts", INL/RPT-24-80420 Idaho National Laboratory, Idaho Falls, ID.
44. Armstrong, R. et al. 2022. “The Future of Energy Storage: An Interdisciplinary MIT Study.” https://energy.mit.edu/wp-content/uploads/2022/05/The-Future-of-Energy-Storage.pdf.
45. U.S. Energy Information Administration. 2024. “Natural Gas Weekly Update.” https://www.eia.gov/naturalgas/weekly/.

46. Barnert, H., V. Krett, and J. Kupitz. 1991. “Nuclear energy for heat applications.” *IAEA Bulletin* 33(1): 21–24. https://www.iaea.org/sites/default/files/publications/magazines/bulletin/bull33-1/33104782124.pdf.

47. Sadhankar, R. 2020. “Potential of Advanced Reactors/SMRs for Decarbonization - beyond Electricity in Canadian Context.” NEA Workshop Electricity System (R)Evolution. Accessed March 28, 2024. https://www.oecd-nea.org/upload/docs/application/pdf/2020-07/workshop_esr_11._potential_of_advanced_reactors_smrs_for_decarbonization.pdf.

48. Muhlhauser, H. J. 1978. “Steam Turbines for District Heating in Nuclear Power Plants.” *Nuclear Technology* 38(1): 113–119. https://doi.org/10.13182/NT78-A16163.

49. Wright, J. S. 1996. “Steam Turbine Cycle Optimization, Evaluation, and Performance Testing Considerations.” GER-3642E. GE Power Systems, Schenectady, NY. https://www.gevernova.com/content/dam/gepower-new/global/en_US/downloads/gas-new-site/resources/reference/ger-3642e-st-cycle-opt-eval-perf-testing-considerations.pdf.

50. Lipka, M. and A. Rajewski. 2020. “Regress in nuclear district heating. The need for rethinking cogeneration.” *Progress in Nuclear Energy* 130: 103518. https://doi.org/10.1016/j.pnucene.2020.103518.

51. International Atomic Energy Agency. 2002. “Status of design concepts of nuclear desalination plants.” IAEA-TECDOC-1326. IAEA, Vienna, Austria. https://www-pub.iaea.org/mtcd/publications/pdf/te_1326_web.pdf.

52. Handl, K. H. 1998. “75 MW Heat Extraction from Beznau Nuclear Power Plant (Switzerland).” Accessed August 4, 2024. https://inis.iaea.org/collection/NCLCollectionStore/_Public/29/067/29067739.pdf.

53. Paley, I. 1998. “Heat Delivery from Bohunice NPP, Slovakia.” Accessed August 4, 2024. https://inis.iaea.org/collection/NCLCollectionStore/_Public/29/067/29067740.pdf?r=1.

54. Panov, Y. and V. Polunichev. 1998. “Nuclear heat applications: Design aspects and operating experience.” IAEA-TECDOC-1056. IAEA, Vienna. https://www-pub.iaea.org/mtcd/publications/pdf/te_1056_prn.pdf.

55. Leurent, M., F. Jasserand, G. Locatelli, J. Palm, M. Rama, and A. Trianni. 2017. “Driving forces and obstacles to nuclear cogeneration in Europe: Lessons learnt from Finland.” *Energy Policy* 107: 138–150. https://doi.org/10.1016/j.enpol.2017.04.025.

56. World Nuclear Association. n.d. “Nuclear Reactor Database.” World Nuclear Association. Accessed March 28, 2024. https://world-nuclear.org/nuclear-reactor-database.

57. O Energetice. 2023. “The heat pipeline from Temelín to Budějovice will supply 750 TJ of heat annually, it cost 1.69 billion CZK.” O Energetice. Accessed August 7, 2024. https://oenergetice.cz/teplarenstvi/horkovod-z-temelina-do-budejovic-doda-rocne-750-tj-tepla-stal-169-mld-kc.

58. Martin Leurent, Pascal Da Costa, Sébastien Sylvestre, Michel Berthélemy. 2018. “Feasibility assessment of the use of steam sourced from nuclear plants for French factories considering spatial configuration.” *Journal of Cleaner Production* 189: 529-538. https://doi.org/10.1016/j.jclepro.2018.04.079.

59. Verfondern, K. 2013. “Overview of Nuclear Cogeneration in High-Temperature Industrial Process Heat Applications.” JÜLICH. Accessed August 7, 2024. https://www.oecd-nea.org/ndd/workshops/nucogen/presentations/15_Verfondern_2013-OECD-IAEA-Workshop.pdf.

60. World Nuclear News. 2024. “Start up of Chinese industrial nuclear steam project begins.” World Nuclear News. Accessed August 7, 2024. https://www.world-nuclear-news.org/Articles/Start-up-of-Chinese-industrial-nuclear-steam-proje.

61. Seddon, W. A. 1981. “Nuclear process steam for industry: potential for the development of an Industrial Energy Park adjacent to the Bruce Nuclear Power Development.” AECL-7426. Atomic Energy of Canada, Chalk River, Ontario, Canada. https://www.osti.gov/etdeweb/biblio/8140770.

62. Vibhag, P.O. and B. Sarkar. 1976. “Annual Report of the Department of Atomic Energy 1975–76.” Government of India. Accessed August 7, 2024. https://inis.iaea.org/collection/NCLCollectionStore/_Public/08/291/8291153.pdf.

63. OECD-NEA. 2008. “50 Years of Safety-Related Research - The Halden Project 1958–2008.” Accessed August 11, 2024. https://www.oecd-nea.org/jointproj/docs/halden/the-halden-project-1958-2008.pdf.

64. J. Kupitz. 2000. “Small and medium reactors: Development status and application aspects.” in Workshop on nuclear reaction data and nuclear reactors: Physics, design and safety, Trieste, Italy. https://www.osti.gov/etdeweb/biblio/20854884.

65. NEA. 2022. “High-temperature Gas-cooled Reactors and Industrial Heat Applications.” OECD Publishing, Paris, France. https://www.oecd-nea.org/jcms/pl_70442/high-temperature-gas-cooled-reactors-and-industrial-heat-applications.

66. Hancock, S. and T. Westover. 2022. “Simulation of 15% and 50% Thermal Power Dispatch to an Industrial Facility Using a Flexible Generic Full-Scope Pressurized Water Reactor Plant Simulator.” *Energies* 15(3): 1151. https://dx.doi.org/10.3390/en15031151.

67. Arent, D. J., S. M. Bragg-Sitton, D. C. Miller, et al. 2021. “Multi-input, Multi-output Hybrid Energy Systems.” *Joule* 5(1): 47–58. https://doi.org/10.1016/j.joule.2020.11.004.

68. Bistline, J., S. Bragg-Sitton, W. Cole, et al. 2023. “Modeling nuclear energy’s future role in decarbonized energy systems.” *iScience* 26(2): 105952. https://doi.org/10.1016/j.isci.2023.105952.

69. Davis, S. J., N. S. Lewis, M. Shaner, et al. “Net-Zero Emissions Energy Systems.” *Science* 360: 6396. https://doi.org/10.1126/science.aas9793.

70. Boardman, R. D., M. G. McKellar, B. D. Dold, A. W. Foss, and H. C. Bryan. 2021. “Process Heat for Chemical Industry.” *Encyclopedia of Nuclear Energy* 49–60. https://doi.org/10.1016/B978-0-12-819725-7.00198-7.

71. Saeed, R. M., E. K. Worsham, B.-H. Choi, et al. 2023. “Industrial Requirements Status Report and Down-Select of Candidate Technologies.” INL/RPT-23-73026. Idaho National Laboratory, Idaho Falls, ID. https://inldigitallibrary.inl.gov/sites/sti/sti/Sort_66464.pdf.

72. Verfondern, K., X. Yan, T. Nishihara, and H. J. Allelein. 2017. “Safety concept of nuclear cogeneration of hydrogen and electricity.” *International Journal of Hydrogen Energy* 42(11): 7551–7559. https://doi.org/10.1016/j.ijhydene.2016.04.239.

73. Kowalczyk, T., J. Badur, and M. Bryk. 2019. “Energy and exergy analysis of hydrogen production combined with electric energy generation in a nuclear cogeneration cycle.” *Energy Conversion and Management* 198: 111805. https://doi.org/10.1016/j.enconman.2019.111805.

74. Bartnik, R., Z. Buryn, and A. Hnydiuk-Stefan. 2023. “Comparative thermodynamic and economic analysis of a conventional gas-steam power plant with a modified gas-steam power plant.” *Energy Conversion and Management* 293: 117502. https://doi.org/10.1016/j.enconman.2023.117502.

75. Bartnik, R., A. Hnydiuk-Stefan, and W. Skomudek. 2023. “Methodology for thermodynamic and economic analysis of hierarchical dual-cycle gas-gas nuclear power and CHP plants with high-temperature reactors and helium as the circulating medium.” *Progress in Nuclear Energy* 158: 104625. https://doi.org/10.1016/j.pnucene.2023.104625.

76. Sadhankar, R. 2019. “Gen IV - International Forum: Position Paper on Flexibility of Gen IV Systems.” Gen IV International Forum. Accessed August 4, 2024. https://www.gen-4.org/gif/upload/docs/application/pdf/2021-06/position_paper_on_flexibility_of_gen_iv_systems_r._sadhankar_final.pdf.

77. Ohashi, H., Y. Inaba, T. Nishihara, et al. 2006. “Current Status of Research and Development on System Integration Technology for Connection between HTGR and Hydrogen Production System at JAEA.” Japan Atomic Energy Agency. https://www.oecd-ilibrary.org/current-status-of-research-and-development-on-system-integration-technology-for-connection-between-htgr-and-hydrogen-production-system-at-jaea_5l9k8lk2zr6g.pdf.

78. Global First Power. 2019. “Project Description for the Micro Modular Reactor Project at Chalk River.” CRP-LIC-01-001. Global First Power. https://iaac-aeic.gc.ca/050/documents/p80182/130911E.pdf.

79. Roe, K. K. and I. Oliker. 1988. “Economic feasibility of heat supply from nuclear power plants in the United States.” in Pacific Basin Nuclear Conference, Beijing, China. https://inis.iaea.org/collection/NCLCollectionStore/_Public/20/013/20013262.pdf.

80. Saeed, R. M., A. Shigrekar, D. M. Mikkelson, et al. “Multilevel Analysis, Design, and Modeling of Coupling Advanced Nuclear Reactors and Thermal Energy Storage in an Integrated Energy System.” INL/RPT-22-69214, Idaho National Laboratory, Idaho Falls, ID. https://doi.org/10.2172/1890160.

81. Saeed, R. M., K. L. Frick, A. Shigrekar, D. Mikkelson, and S. Bragg-Sitton. 2022. “Mapping thermal energy storage technologies with advanced nuclear reactors.” *Energy Conversion and Management* 267: 115872. https://doi.org/10.1016/j.enconman.2022.115872.

82. Cho, S.-B. and R. M. Saeed. 2024. “Evaluating Energy Storage Options and Costs for Consistent Energy Supply to Non-Electric Sectors.” INL/RPT-24-76179. Idaho National Laboratory, Idaho Falls, ID.

83. Balliet, H., L. McLaughlin, Z. Ma, and K. Glusenkamp. 2023. “Technology Strategy Assessment: Findings from Storage Innovations 2030 Thermal Energy Storage.” INL/RPT-23-72978. Idaho National Laboratory, Idaho Falls, ID. https://doi.org/10.2172/1998552.

84. Westover, T., H. R. Fidlow, H. Gaudin, J. Miller, G. Neimark, and N. Richards. 2023. “Impacts of Extracting 30% of Reactor Power from a Pressurized Water Reactor.” INL/RPT-23-74666 (unpublished). Idaho National Laboratory, Idaho Falls, ID.

85. Kosman, W., A. Rusin, and P. Reichel. 2023. “Application of an energy storage system with molten salt to a steam turbine cycle to decrease the minimal acceptable load.” *Energy* 266: 126480. https://doi.org/10.1016/j.energy.2022.126480.

86. Dong, Z., B. Li, J. Li, et al. 2021. “Flexible control of nuclear cogeneration plants for balancing intermittent renewables.” *Energy* 221: 119906. https://doi.org/10.1016/j.energy.2021.119906.

87. Carlson, F. and J. H. Davidson. 2021. “Parametric study of thermodynamic and cost performance of thermal energy storage coupled with nuclear power.” *Energy Conversion and Management* 236: 114054. https://doi.org/10.1016/j.enconman.2021.114054.

88. Forsberg, C. 2022. “Separating nuclear reactors from the power block with heat storage to improve economics with dispatchable heat and electricity.” *Nuclear Technology* 208: 668–710. https://doi.org/10.1080/00295450.2021.1947121.

89. Al Kindi, A. A., M. Aunedi, A. M. Pantaleo, G. Strbac, and C. N. Markides. 2022. "Thermo-economic assessment of flexible nuclear power plants in future low-carbon electricity systems: Role of thermal energy storage." *Energy Conversion and Management* 258: 115484. https://doi.org/10.1016/j.enconman.2022.115484.

90. Heo, J. Y., J. H. Park, Y. J. Chae, et al. 2021. "Evaluation of various large-scale energy storage technologies for flexible operation of existing pressurized water reactors." *Nuclear Engineering and Technology* 53(8): 2427–2444. https://doi.org/10.1016/j.net.2021.02.023.

91. Lou, J., J. Wang, J. Xia, Y. Du, P. Zhao, and S. Wang. 2022. "Thermodynamic analysis and performance evaluation of a novel energy storage-based supercritical CO_2 power system with ejector driven by nuclear energy." *Energy Conversion and Management* 272: 116368. https://doi.org/10.1016/j.enconman.2022.116368.

92. Edwards, J. and H. Bindra. 2017. "An experimental study on storing thermal energy in packed beds with saturated steam as heat transfer fluid." *Solar Energy* 157: 456–461. https://doi.org/10.1016/j.solener.2017.08.065.

93. Bruch, A., J. F. Fourmigue, and R. Couturier. "Experimental and numerical investigation of a pilot-scale thermal oil packed bed thermal storage system for CSP power plant." *Solar Energy* 105: 116–125. https://doi.org/10.1016/j.solener.2014.03.019.

94. Elsihy, E. S., Z. Liao, C. Xu, and X. Du. 2021. "Dynamic characteristics of solid packed-bed thermocline tank using molten-salt as a heat transfer fluid." *International Journal of Heat and Mass Transfer* 165: 120677. https://doi.org/10.1016/j.ijheatmasstransfer.2020.120677.

95. Morton, T. J. 2021. "Thermal Energy Distribution System (TEDS) Startup and Commissioning." INL/EXT-21-64160. Idaho National Laboratory, Idaho Falls, ID. https://inldigitallibrary.inl.gov/sites/sti/sti/Sort_52960.pdf.

96. Knobloch, K., Y. Muhammad, M. S. Costa, et al. 2022. "A partially underground rock bed thermal energy storage with a novel air flow configuration." *Applied Energy* 315: 118931. https://doi.org/10.1016/j.apenergy.2022.118931.

97. Siemens Gamesa. 2019. "ETES: Electric Thermal Energy Storage - How thermal power plants can benefit from the energy transition." Accessed February 28, 2024. https://assets.new.siemens.com/siemens/assets/api/uuid:6f83e987-b0b8-4663-8a19-cd011682f9a0/3-schumacher-benefits-of-energy-transition-for-thermal-power-pla.pdf.

98. Sciacovelli, A., A. Vecchi, and Y. Ding. 2017. "Liquid air energy storage (LAES) with packed bed cold thermal storage - From component to system level performance through dynamic modelling." *Applied Energy* 190: 84–98. https://doi.org/10.1016/j.apenergy.2016.12.118.

99. Knobloch, K., T. Ulrich, C. Bahl, and K. Engelbrecht. 2022. "Degradation of a rock bed thermal energy storage system." *Applied Thermal Engineering* 214: 118823. https://doi.org/10.1016/j.applthermaleng.2022.118823.

100. Ma, Z., X. Wang, P. Davenport, J. Gifford, and J. Martinek. 2021. "Economic Analysis of a Novel Thermal Energy Storage System Using Solid Particles for Grid Electricity Storage." NREL/CP-5700-79014. National Renewable Energy Laboratory, Golden, CO. https://www.nrel.gov/docs/fy21osti/79014.pdf.

101. Calderon, A., C. Barreneche, A. Palacios, et al. 2019. "Review of solid particle materials for heat transfer fluid and thermal energy storage in solar thermal power plants." *Energy Storage* 1(4): e63. https://doi.org/10.1002/est2.63.

102. Ho, C. K. 2019. “High-Temperature Particle-Based CSP with Thermal Storage.” SAND2019-8509PE presented in The Heat Storage for Gen IV Reactors for Variable Electricity from Base-Load Reactors Workshop, Idaho Falls, ID. https://art.inl.gov/Meetings/Heat%20Storage%20for%20Gen%20IV%20Reactors%20Workshop%20July%2023-24/Presentations/11_Ho_Particle_Thermal_Storage.pdf.

103. Gulfam, R., P. Zhang, and Z. Meng. 2019. “Advanced thermal systems driven by paraffin-based phase change materials - A review.” *Applied Energy* 238: 582–611. https://doi.org/10.1016/j.apenergy.2019.01.114.

104. Lin, Y., G. Alva, and G. Fang. 2018. “Review on thermal performances and applications of thermal energy storage systems with inorganic phase change materials.” *Energy* 165: 685–708. https://doi.org/10.1016/j.energy.2018.09.128.

105. Johnson, M. and M. Fiss. 2023. “Superheated steam production from a large-scale latent heat storage system within a cogeneration plant.” *Communications Engineering* 2(1): 68. https://doi.org/10.1038/s44172-023-00120-0.

106. Bauer, D., M. Johnson, F. Trebilcock, and S. Lecompte. 2022. “Design, build and operation of the CHESTER system.” Presented in 3rd International Workshop on Carnot Batteries, Stuttgart, Germany. https://elib.dlr.de/191256/.

107. U.S. Department of Energy, Office of Energy Efficiency and Renewable Energy. 2007. “Save Energy Now - Dow Chemical Company: Assessment Leads to Steam System Energy Savings in a Petrochemical Plant.” DOE/GO-102007-2467. https://cdn2.hubspot.net/hub/297110/file-300136228-pdf/docs/42009.pdf?t=1502892574327.

108. Laing, D., C. Bahl, M. Fiss, et al. “Combined storage system developments for direct steam generation in solar thermal power plants.” Presented in ISES Solar World Congress, Kassel, Germany. https://proceedings.ises.org/conference/swc2011/papers/swc2011-0073-Laing.pdf.

109. Soto, G. J. and P. Talbot. 2024. “Economic Parameter Uncertainty Quantification Demonstration.” INL/RPT-24-77193. Idaho National Laboratory, Idaho Falls, ID. https://inldigitallibrary.inl.gov/sites/STI/STI/Sort_98338.pdf.

110. Pirnay, H., R. López-Negrete, and L. T. Biegler. 2012. “Optimal sensitivity based on IPOPT.” *Mathematical Programming Computation* 4: 307–331. https://doi.org/10.1007/s12532-012-0043-2.

111. Forrest, J. 2012. “CBC User Guide.” Computational Infrastructure for Operations Research. https://github.com/coin-or/Cbc.

112. Abou-Jaoude, A. et al. 2024. “Meta-Analysis of Advanced Nuclear Reactor Cost Estimations.” INL/RPT-24-77048. Idaho National Laboratory, Idaho Falls, ID. https://inldigitallibrary.inl.gov/sites/sti/sti/Sort_107010.pdf.

Appendix A

Review of CHP Applications in Nuclear Power Plants

Nuclear cogeneration has traditionally been applied to desalination and DH, and it has a rich history dating back to the early 1970s with upwards of 750 reactor-years of global experience. [14] This trend arises from the fact that these applications usually require only a small fraction of the reactor's total thermal output, with temperatures not exceeding 200ºC. Moreover, the byproducts, potable water and heat, can be easily stored as part of the production process, as the plants may be equipped with a hot water network itself acting as storage. These features provide flexibility to accommodate load changes and fluctuations that are expected during normal process operations. [10] For instance, aside from the Kazakhstan case, all nuclear desalination plants account for less than 1% of the coupled reactor's electrical output (see Table 9). Of the 21 sites with past and ongoing DH services, more than 16 sites were engineered to allocate less than 10% of their heat production for DH services (see Table 10).

In nuclear CHP operations, the system can be configured either in parallel or series modes. [46] Parallel cogeneration is managed by diverting a portion of steam from the secondary side of the steam generator before it enters the turbine. This configuration offers enhanced flexibility in energy utilization, making it particularly suitable for applications where nuclear heat—approximately 30% or more of the output from a single reactor [47]—is primarily dedicated for process heat rather than electricity generation. A prime example of this parallel cogeneration approach is the Bruce A power station in Canada. [12] In this plant, steam is diverted from the secondary sides of the four Bruce A reactors, in parallel with the delivery of steam to the turbines. The rerouted steam is then fed into the Bruce Bulk Steam System plant, the largest nuclear process heat system in the world (see Table 11). [14] Since the rerouted steam at Bruce A does not serve in electricity generation, its turbines are small compared to those at the Bruce B station where a greater steam flow is converted to power. [14] This approach does not, however, bring primary energy savings as a result of cogeneration operation.

In contrast, series cogeneration involves extracting either a fraction (e.g., steam bleeding) or all of the steam (e.g., backpressure turbine) at suitable points during its expansion in the high-pressure turbine and low-pressure turbine (LPT), when the steam reaches the thermal requirements (temperature and pressure) for the desired application. [48] Uncontrolled steam bleed from the LPT typically provides sufficient heat for consistent thermal load and modest thermal demand (up to approximately 5%–10% of the reactor thermal output). [49] Many nuclear CHP plants have adopted this technique, extracting steam at temperatures ranging from 60°C to 150°C, commonly used for desalination and DH. [14] In nuclear CHP plants with a high thermal demand, the backpressure system is a feasible option, whereby all steam is used for heating after expanding in the turbine to a backpressure based on the process heat demand. However, this backpressure approach has limited flexibility in modifying the ratio of process heat to electricity generation. [50] It is preferentially used for applications with a constant thermal baseload, as well-exemplified by the BN-350 plant integrated with the Aktau power and desalination complex (see Table 9). [51] For nuclear DH plants with seasonal load variations, a multistage approach involving steam extraction from several turbine stages is applied, as observed in facilities such as the Beznau (Switzerland) [52] and Bohunice (Slovakia) plants. [53] Under this approach, steam from lower pressure bleed serves the base heating demand, while additional steam from higher pressure bleed is utilized to address peak heat demands, as they occur. [54]

Table 9. Existing and past operating nuclear CHP plants for desalination. [14]

Country and Plant	Reactor Type	Net Capacity [MWe]	Water Capacity [m^3/d]	Total Equivalent Energy Consumption (desali.) [MWe]	Remarks
Japan					
Ohi-1,2	PWR	2 × 1,175	3,900	1.73	MSF (1 × 1,300 m^3/d) MED (2 × 1,300 m^3/d)
Ohi-3,4	PWR	2 × 1,180	2,600	0.54	RO (1 × 1,300 m^3/d)
Ikata-1,2	PWR	2 × 566	2,000	1.25	MSF (2 × 1,000 m^3/d)
Ikata-3,4	PWR	890	2,000	0.42	RO (2 × 1,000 m^3/d)
Genkai-3,4	PWR	2 × 1,180	2,000	0.56	MED (1 × 1,000 m^3/d) RO (1 × 1,000 m^3/d)
Takahsama-3,4	PWR	2 × 870	2,000	0.67	MED/VC (2 × 1,000 m^3/d)
Kashiwazaki	BWR	1,100	1,000	0.63	MSF
Kazakhstan					
BN-350	LFMR	150	80,000	39.17	MED, MSF
USA					
Diablo Canyon-1,2	PWR	2 × 1,100	2,200	0.46	Two-stage RO
India					
Kalapakkam-1,2	HWR	235	6,300	1.31	Hybrid MSF/RO
Pakistan					
Karachi	HWR/ CANDU	125	1,600	0.57	MED

NOTE: BWR—boiling-water reactor; CANDU—Canada deuterium-uranium; HWR—heavy-water reactor; LFMR—liquid-metal fast reactor; MED—multi-effect distillation; MSF—multistage flash; PWR—pressurized-water reactor; RO—reverse osmosis; VC—vapor compression. Total energy consumption [MWe] is calculated using the average of the energy consumption range for each technology (kWhe/m^3, with energy recovery) [13] multiplied by the plant's daily water production capacity [m^3/d].

Table 10. Existing and past operating nuclear CHP plants for DH. [55]

Country and Plant	Reactor Type	Net Capacity [MWe]	Thermal Capacity [MWth]	Heat Output [MWth]/ Share of Thermal Output [%]	Length of Main Pipe [km]	Temp. at Interface (feed/return) [°C]
Bulgaria						
Kozloduy-5,6	PWR/ WWER	2 × 953	2 × 3120	2 × 20/0.6	5	150/70
Czech Republic						
Temelín-1,2	PWR/ WWER	2 × 1,086	2 × 3,120	2 × 180/5.8	5 and 26*	90–140/70
Hungary						
Paks-2,3,4	PWR/ WWER	3 × 433	3 × 1485	3 × 30/2	6	130/70
Russia						

Country and Plant	Reactor Type	Net Capacity [MWe]	Thermal Capacity [MWth]	Heat Output [MWth]/ Share of Thermal Output [%]	Length of Main Pipe [km]	Temp. at Interface (feed/return) [°C]
Bilibino-1–4	RBMK/ EGP	4 × 12	4 × 62	4 × 19/30.6	3.5	150/70
Novovoronezh-3,4	PWR/ WWER	2 × 385	2 × 1,375	2 × 33/2.4	50	130/70
Balakovo-1–4	PWR/ WWER	4 × 950	3,000, 3,200	4 × 200/12.9	12	130/70
Kalinin-1,2	PWR/ WWER	2 × 950	2 × 3,000	2 × 80/2.7	4	130/70
Kola-1–4	PWR/ WWER	4 × 410	4 × 1,375	4 × 25/1.8	64	130/70
Beloyarsk-3	LMFR/ BN-600	560	1,470	170/11.6	—	130/70
Leningrad-1–4	RBMK	4 × 925	4 × 3,200	4 × 25/0.8	5	130/70
Kursk-1	RBMK	3 × 925	3,200	128/4.0	3	130/70
Kursk-2–4	RBMK	3 × 925	3 × 3,200	3 × 175/5.5	3	130/70
Smolensk-1,2	RBMK	2 × 410	2 × 3,200	2 × 173/5.4	5	130/70
Slovakia						
Bohunice-3,4	PWR/ WWER	2 × 365	2 × 1,471	2 × 240/16.3	18	150/70
Switzerland						
Beznau-1,2	PWR	365, 357	2 × 1,130	2 × 80/7.1	35	128/70
Ukraine						
Rovno-1,2	PWR/ WWER	376, 381	2 × 1,375	2 × 58/4.2	4	130/70
Rovno-3	PWR/ WWER	950	3,000	233/7.8	4	130/70
South Ukraine-1,2	PWR/ WWER	2 × 950	2 × 3,000	2 × 151/5.0	3	150/70
South Ukraine-3	PWR/ WWER	950	3,000	2 × 232/7.7	3	150/70
Zaporozhye-1–6	PWR/ WWER	6 × 950	6 × 3,000	6 × 232/31.7	5	—
Romania						
Cernavoda-1	HWR/ CANDU-6	660	2,180	47/2.2	2	150/70

NOTE: CANDU—Canada deuterium-uranium; EGP—graphite steam power reactor; HWR—heavy-water reactor; LFMR—liquid-metal fast reactor; PWR—pressurized-water reactor; RBMK—high-power channel-type reactor; WWER—water-cooled, water-moderated reactor. To calculate the share of thermal output [%], thermal capacity values are acquired from the World Nuclear Association's reactor database. [56] Czech Republic Temelín-1,2 data is updated. [57]

Table 11. Existing and past operating nuclear CHP plants for process heat. [10,14,15,46,58–63]

Country and Plant	Reactor Type	Net Capacity [MWe]	Thermal Capacity [MWth]	Heat Output [MWth]	Length of Main Pipe [km]	Process Heat Temp. and Pressure [°C]/[MPa]	Remarks
Canada Bruce A	HWR/ CANDU	811, 777 770, 769	2 × 2,620 2 × 2,550	5,350 (or 793 [46])	6	—	Heavy-water production, building heating, Bruce Energy Centre
Germany Stade	PWR	640	1,900	30	1.5	190/1.5	Salt refinery
Switzerland Gösgen	PWR	2 × 1,180	2 × 1,501	25	1.75	220/1.37	Cardboard factory
Norway Halden	BWR (exper.)	0 (only heat)	35	35	—	240/3.4	Pulp and paper plant, intermittent operation
India Kota	HWR	160	—	85	Onsite	250°C	Heavy-water production
China Tianwan	PWR	6,100	17,810	340	23	248/1.8	Refinery and chemical plants

NOTE: CANDU—Canada deuterium-uranium; HWR—heavy-water reactor; PWR—pressurized-water reactor.

From previous experiences with nuclear CHP applications, it is clear that the foremost priority is to ensure the ability to responsively meet variations in customer demand for heat and electricity. For instance, if the reactor's thermal output is primarily allocated for supplying process heat, any fluctuations in the thermal demand of the process heat plants due to the startup, shutdown, or scheduled change of processes could propagate to the reactor system's primary coolant loop [64] and subsequent power conversion system. [66] Hence, recent advancements in nuclear CHP research have concentrated on enhancing the management and adaptation to thermal load transients. [67,68] This is essential as nuclear heat seeks to expand to sectors that are historically difficult to decarbonize, such as chemical production, oil refinery, and steel making. [69]. In these sectors, the requirements for high temperature (HT) heat and fluctuating thermal demand are currently met by fossil-fuel-based CHP installations or boilers. [70,71] To harness the prospective benefits of nuclear CHP systems, recent research has proposed high-temperature gas-cooled reactors (HTGRs). [72–75] Capable of consistently supplying large-scale heat at approximately 550°C or higher, HTGRs could be integrated into hydrogen production plants [72,73] as well as existing gas-steam power plants [74] or gas CHP facilities for DH. [75] While recognizing the higher capital costs for establishing HTGRs, infrastructure studies indicate that the benefits, such as reduced machinery and equipment size (e.g., helium turboexpanders) and improved efficiency, can compensate for the additional investment. [74]

In parallel, several mitigation strategies have been proposed to address such thermal disturbances within a nuclear CHP system: regulating the primary coolant flow, [76] enhancing the secondary circuit's thermal capacity (e.g., steam generator or heat distribution network), [77] integrating thermal fluctuation absorption mechanisms, such as TES, [78] and adjusting the allocation of heat supply and electricity generation. [10] Moreover, as advanced reactor designs develop, inherent mitigation strategies are being proposed. For instance, an HTGR, with its high thermal inertia, is capable of partially damping thermal disturbances. Additionally, the deployment of several microreactors or small modular nuclear reactors

(SMNRs), each mainly dedicated to the production of electricity and the supply of heat, can further mitigate the impact of load fluctuations. [79] These units act as mutual backups, compensating for each other when there are changes in either thermal or electrical demands. While each of the strategies can enhance the flexibility of nuclear cogeneration, recent literature has shown a distinct preference for integrating TES in nuclear CHP applications. [80–82] This inclination is backed by the versatility of TES applications across various nuclear reactor designs [81] and the proven trajectory of TES commercialization. [83]

In a nuclear-TES-CHP configuration, the nuclear reactor is maintained at its full power level with flexibility provided by both TES and cogeneration. This configuration offers improved operational versatility, both in terms of the heat-supply-to-electricity generation ratio [80,84] and its range [85], while minimizing the potential for thermal stress and mechanical wear associated with load-following operations. [86] Earlier research on the layout and thermal modeling of nuclear-TES systems has mainly been geared toward electricity market applications, with limited discussion on the utilization within industrial park settings. [85,87–90] Studies suggest that the most efficient configuration for PWR systems is to extract steam before the turbine for a TES charge, which later feeds into secondary power cycles dedicated to TES, though there is associated major efficiency drop. [87–89] This approach could also result in fluctuations in the feedwater temperature, potentially affecting the reactor coolant temperature and, by extension, the overall reactor stability. [90] Seeking a solution with minimal impact on the reactor system during off-design operations, Heo et al. [90] proposed a steam extraction branch placed between a high-pressure turbine and the LPT. Despite its benefits in terms of reactor system stability, this configuration comes with a further decrease in exergy efficiency, highlighting a trade-off between operational stability and system efficiency. An additional study examined the use of a steam-heated two-tank molten-salt TES for three different advanced reactor designs. [80] The key benefit of this design is that it obviates the need for extensive modifications to the existing nuclear island, thus simplifying the licensing procedures. A similar thermal bypass architecture, a recompression supercritical CO_2 (sCO_2) cycle operating at 550°C, was analyzed; though not explicitly detailed, it implies conditions characteristic of a sodium fast reactor. [91] While the sCO_2 cycle enhances the system's thermal efficiency under normal operating conditions, notable efficiency reductions are observed when steam is released from the energy storage system.

Notwithstanding this research, the literature reveals a gap concerning industry-specific, nuclear-TES-CHP applications that serve the specific needs for mid-temperature process heat in industrial parks—which may extend into even higher ranges. Addressing this oversight, the focus of this research has been set on the application of HTGR-TES-CHP systems in industrial parks. Through an extensive examination of power conversion and heat delivery configurations, we aim to improve energy efficiency and to optimize overall system performance, thus effectively meeting tailored needs of industrial applications.

Appendix B

Thermal Energy Storage Systems

B-1. Packed-Bed Sensible Heat Storage

Packed-bed storage systems are the second-most common and fully developed form of TES and may utilize either liquid or gas as the HTF; however, this technology is not widely adopted for steam generating or condensing heat transfer applications. [92] When using liquid, the HTFs can also function as storage materials but are typically more expensive than the bed filler material. Thermal oils and molten salts are common liquid HTFs, whereas the filler can be natural materials like rocks and sand or engineered ceramic particles. [93–95] Gaseous HTF and natural filler materials in the system significantly decrease capital costs compared to other material combinations.

Efficient operation of a packed-bed TES requires that the cold and hot outlets remain constant during charging and discharging, respectively, and this is achieved via a well-defined thermal stratification profile. The packed-bed concept is commonly associated with pumped TES systems and is suitable for Carnot battery systems. [24,96,97] The scope of applicability for packed-bed systems ranges from subzero temperatures [98] to the upper thermal limits of its materials' structural integrity (600°C–700°C [99] for natural rocks such as basalt and potentially higher for ceramics). However, these systems are more likely constrained by the lower temperature limit, which must remain within the operating range of the blower (or pump for liquid HTF).

Theoretically, a packed-bed TES could be integrated into the primary helium loop of an HTGR and its heat delivery systems, as shown in Figure 40a. However, this method could considerably increase costs due to the very high pressure requirements on the storage vessel. Consequently, an intermediate loop (shown in Figure 40b) is a more viable option, despite the need for large heat exchangers and blowers to counteract the accompanying pressure losses. These additions result in a higher parasitic load, decreasing the total energy that could be delivered to the application.

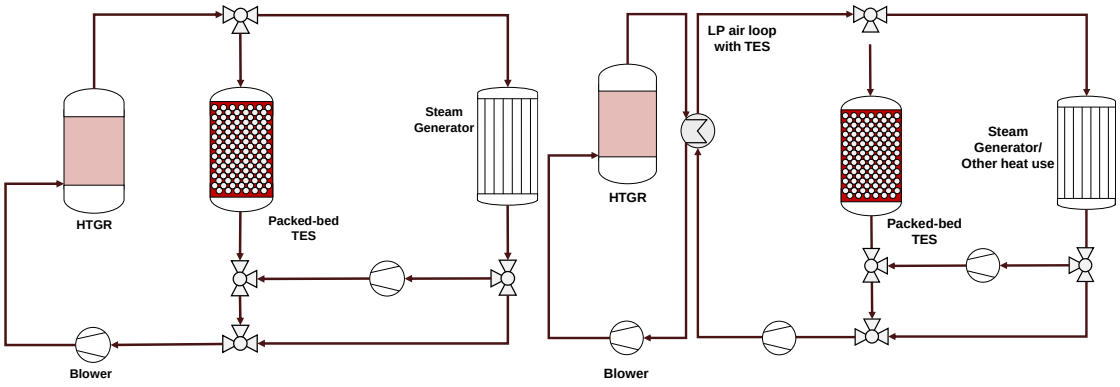

(a) (b)

Figure 40. Two conceptual integrated energy system layouts that integrate an HTGR with a packed-bed TES. (a) TES integrated into the primary helium loop, affording a simpler, less parasitic load but being less technically feasible in terms of the pressurized tanks and safety requirements. (b) TES with an intermediate low-pressure air loop, benefiting from very low-cost TES; the main safety features are limited to the helium loop, but the parasitic load is higher.

B-2. Solid Static Sensible Heat Storage

The conventional form of solid static sensible heat storage involves a monolithic section with integrated piping or external flow of HTF. These systems include modified concrete or ceramic blocks (e.g., Carboclean or EnergyNest systems) that can withstand HT cycling systems (upper limits of 400°C to over 1,000°C are reported). [24] In contrast to packed beds, solid materials do not always exhibit a clearly defined temperature stratification. Thus, the typical operating profile fluctuates between the delivery temperature and the highest structural temperature achievable. [24] Thermal stratification can be roughly achieved by segmenting the storage system into multiple sections. Given these features, solid static TES systems are better suited for scenarios in which excess electricity is available for charging or in which a significant temperature difference between charging and discharging is not a primary concern.

B-3. Particle Sensible Heat Storage

Particle storage systems are a promising technology for HT applications (i.e., concentrated solar power and electricity storage), utilizing materials such as silica sand. These systems were developed to capitalize on temperatures exceeding 1,000°C. Although developed for solar or electric heating with radiative heat exchangers, particle storage technology can be integrated with nuclear power systems using moving- and fluidized-bed heat exchangers. [100–102] This concept could, after sufficient design work, be suitable for primary heat due to its HT limits. At the system level, particle TES differs from two-tank or packed-bed TES primarily in terms of cost, the minimal temperature required for heat exchange, parasitic loads, and technology readiness level.

B-4. Latent Heat Storage

The constant temperature of phase change during both charging and discharging makes latent storage an attractive option for steam line integration, where condensation and evaporation are also constant-temperature-phase-change processes. Materials suitable for latent storage are available across wide temperature ranges—from paraffins at temperatures below 100°C, [103] to various molten salts, [104] to alumina and alumina alloys at around 600°C. [24] Despite the fact that each material poses different technical challenges, it is generally possible to find a suitable phase change material (PCM) that is well-suited to the given application, such as required process temperature.

Experiments have explored latent heat storage for process steam; [105] however, the challenges to this approach outweigh the benefits. For instance, one experiment involves a cascade of PCMs, with different melting temperatures, that can capture and provide the heat of subcooled and superheated fluids. For nuclear integration, a latent heat storage may require additional sensible heat storage [106] to heat subcooled source fluid to the required reactor inlet temperature. Some challenges to latent heat storage systems, such as thermohydraulic balancing of channels for HTFs, become more pronounced with increasing scale.

Appendix C

Power Conversion and Storage System

C-1. CHP System—Baseline

The “baseline” systems represent standard CHP configuration of steam cycles, which can be also used in the energy park without a TES system. This is because not all CHPs within the energy park need to be linked to the storage system; some can serve as baseload providers of heat and power, with an adjustable heat-to-power ratio. The resulting fluctuation between power production and demand can then be managed by a dedicated TES-integrated power-only producing unit. This strategy could be advantageous for larger systems with multiple generating units, as it streamlines the overall control of the energy system by separating the CHP and storage unit functionalities.

For steam extraction at 50 bar (allowing for pressure drop in delivery and for the temperature approach of heat exchangers delivering steam at about 42 bar [~ 600 psi], [107] which was a target steam pressure for industrial processes in this work), refer to the system shown in Figure 41. The maroon-colored box represents the nuclear island, where Components 16, 17, and 18 correspond to the economizer, boiler, and superheater within the steam generator, respectively. Steam is extracted from the high-pressure turbine (Component 30) and routed through the industrial process, indicated by the green-colored box. After 18,349 kW of energy is rejected, the condensate is returned to the feedwater line. This configuration represents a typical CHP system with an extraction-condensing turbine, commonly found in many CHP plants, particularly those powered by coal. The efficiency characteristics of the baseline CHP are shown in Figure 42.

Controlled extraction provides an operational flexibility of heat supply while the remaining thermal energy in steam is converted to power. Typically, at least 15% of nominal steam flowrate in the low-pressure section of the turbine needs to be maintained, primarily to provide cooling of turbine ventilation losses. Traditional industrial systems can then adjust the boiler’s output to match the demand of both heat and power. In the case of nuclear systems with limited (or economically undesired) maneuvering with reactor thermal output, TES systems are a prospective and cost-effective system to take over this capability.

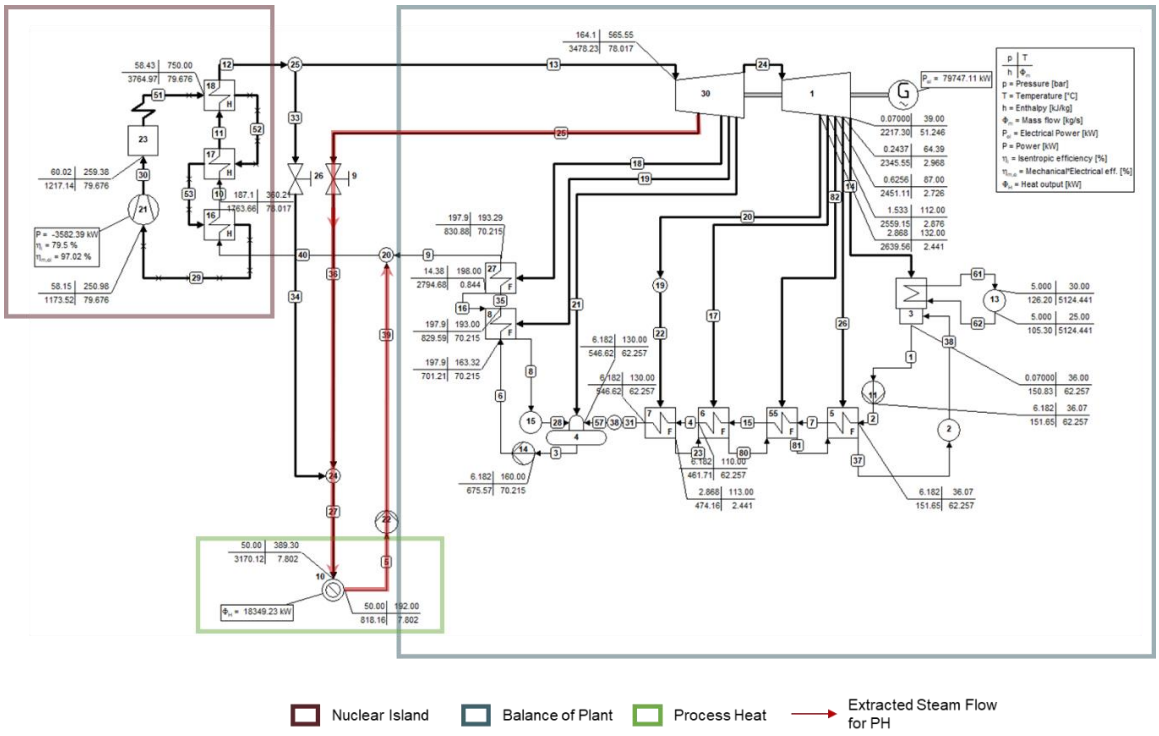

Figure 41. Baseline CHP system with extraction turbine (no integrated TES).

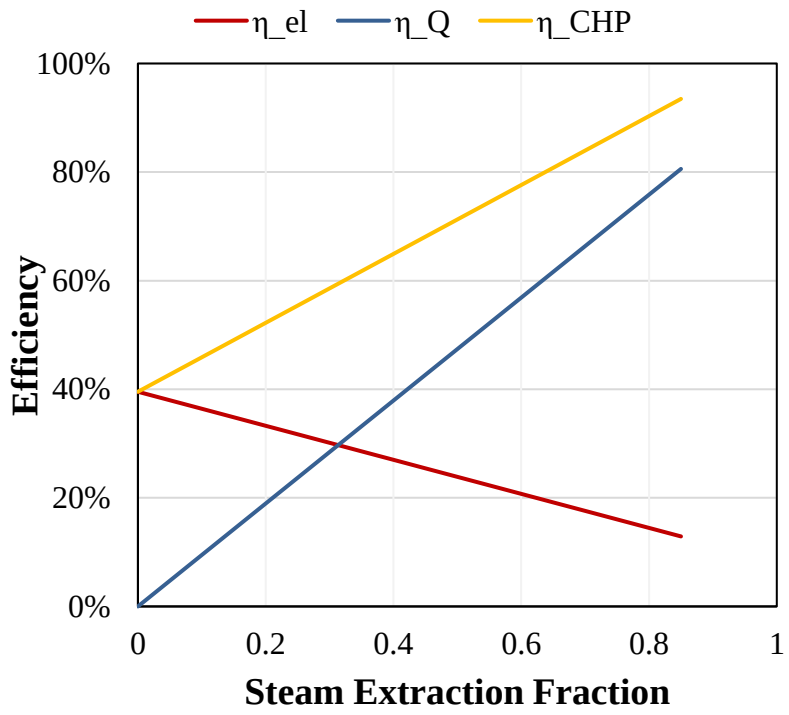

Figure 42. Efficiency characteristics of the baseline CHP system with extraction turbine (assuming ideal controlled extractions). η_{el} = Electrical Power / Reactor Design Thermal Power; η_{Q} = Thermal Output / Reactor Design Thermal Power; $\eta_{\mathrm{CHP}} = \eta_{\mathrm{el}} + \eta_{\mathrm{Q}}$.

The CHP system with a backpressure turbine is advantageous when the heat demand greatly exceeds the electricity demand. Backpressure turbines increase the system's thermal efficiency by utilizing all energy from the turbine exhaust. In addition, eliminating the low-pressure section of the turbine results in a significantly smaller and more affordable turbine, but it also reduces the flexibility of heat and power production. In a backpressure turbine system, flexibility could only be achieved by boosting the thermal output and limiting power production via the reduction valve and desuperheater bypassing the turbine. Figure 43 and Figure 44 present a process flow diagram (PFD) and CHP efficiency characteristics of this configuration, respectively. Note that parasitic loads can cause the electricity production efficiency to drop below zero. Heat production efficiency can also technically exceed 100% if an electric load is converted to heat.

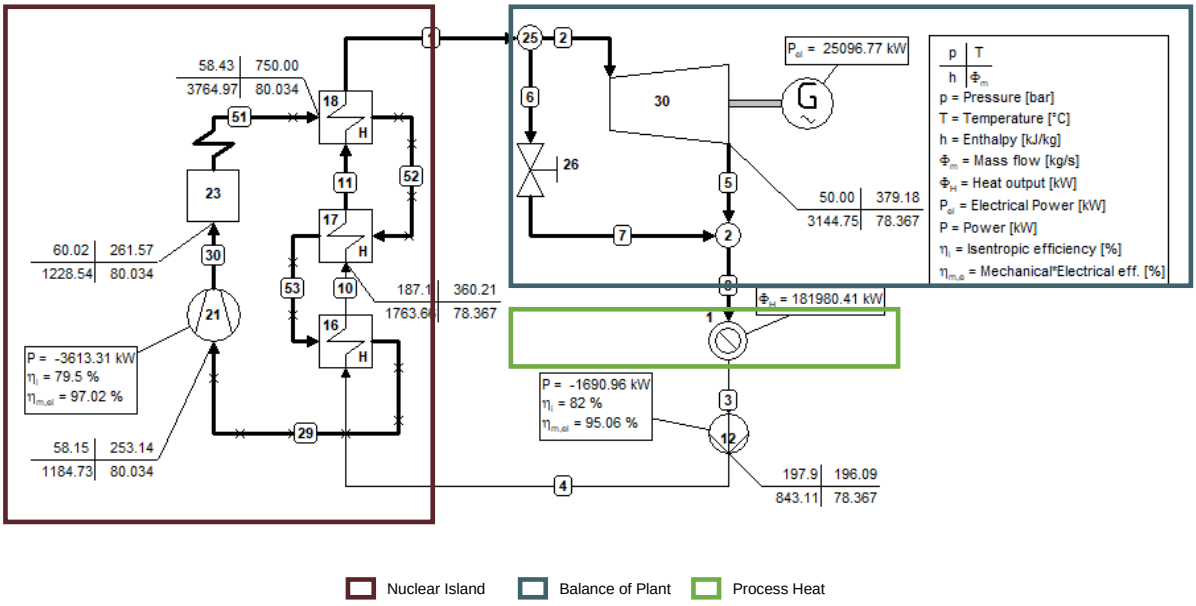

Figure 43. Baseline CHP system with backpressure turbine.

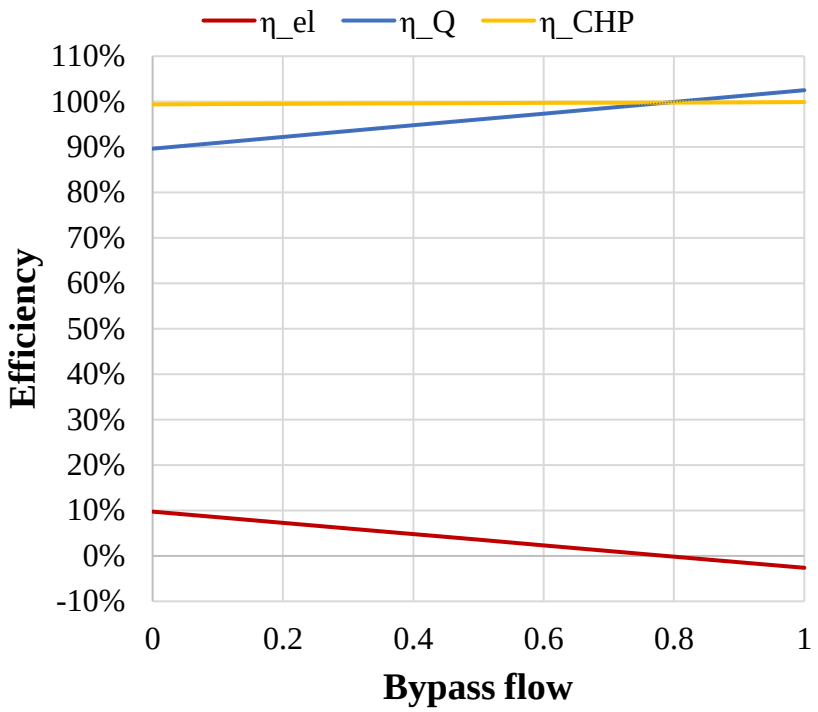

Figure 44. Efficiency characteristics of the baseline CHP system with a backpressure turbine. η_{el} = Electrical Power / Reactor Design Thermal Power; η_{Q} = Thermal Output / Reactor Design Thermal Power; $\eta_{\mathrm{CHP}} = \eta_{\mathrm{el}} + \eta_{\mathrm{Q}}$.

C-2. CHP Systems with TES Charged by Main Steam

The utilization of main steam as a charging fluid for TES was proposed in Reference [80]. Thermal energy discharged from the TES can be directed into a dedicated secondary steam cycle or used as process steam, as shown in Figure 45. This approach is suggested to leverage the nuclear primary circuit and steam generator in existing reactor designs, potentially streamlining the licensing and permitting process for TES integration. The system PFD is depicted in Figure 46(a), while the QT diagrams illustrating charging and discharging from TES are presented in Figure 46(b) and (c), respectively.

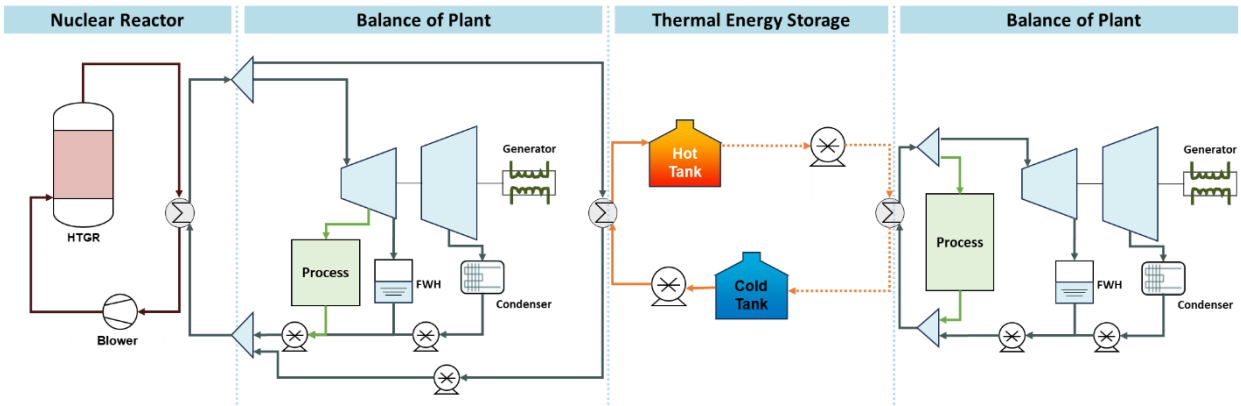

Figure 45. Nuclear-TES coupling approach using steam for charging, which features the option of routing a portion of the energy through the TES system and dedicated balance of plant.

There are several thermodynamic and technical limitations to this approach though. The sensible heat TES system, during both the charging and discharging phases, is limited by the pinch points between the phase-change fluid (e.g., steam) and salt. If steam is used as the primary heating source for TES, pinch point limits lead to significantly lower storage temperatures in the TES and therefore lower steam discharge temperatures and pressures from TES, resulting in exergy losses. For the HTGR Xe-100 reference design specifically, the feedwater inlet temperature limit of approximately 193°C affects the achievable efficiency and operating ranges. In addition, if the system is capable of diverting all steam into TES and discharges the TES to a dedicated steam cycle, the feasible discharge steam pressure at maximum is 25 bar. A pressure over 25 bar would not allow to adequately cool the TES fluid. Consequently, electricity production from the TES-dedicated steam cycle achieves only 28% efficiency[f] due to the lower steam pressure produced within the power cycle.

The deaerator's (Component 36 in Figure 46(a)) function as a feedwater heater becomes unnecessary here since only a small quantity of steam is utilized due to the requirement to cool the TES fluid. Additionally, a more complex heat exchanger configuration may be required to prevent salt crystallization in the HTF. Crystallization can occur if the wall temperature in the salt-steam heat exchanger drops below the salt melting point (142°C for HITEC). While it is possible to achieve higher efficiency by reducing the temperature difference between charging and discharging fluids in TES, efficiency is limited by the total heat diversion ratio, leading to a smaller percentage of reactor heat that can be stored in TES. [80] Given the current constraints on pinch points, the efficiency increase is minimal, around 1%, when raising the pressure to 42 from 25 bar, while achieving a maximum heat diversion ratio of only 50%. This would also necessitate more active control of the main steam cycle feedwater heating system, which adds complexity.

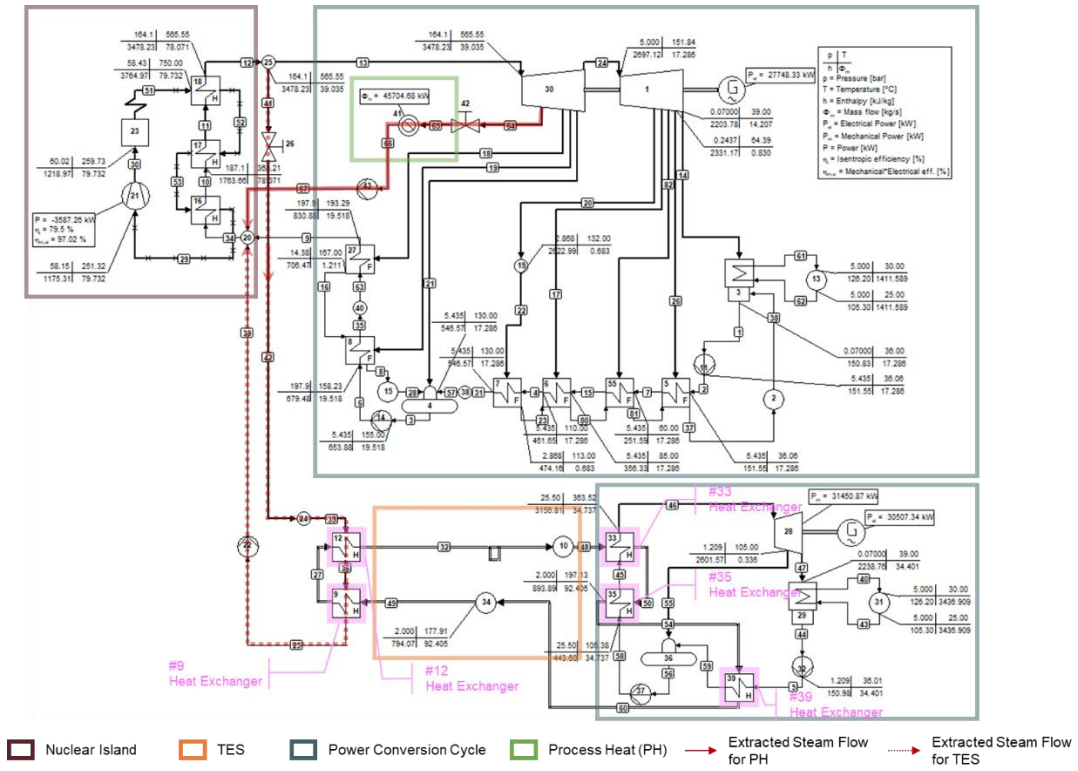

(a)

[f] In this setup, feedwater heating is omitted to minimize the return temperature of the cold TES fluid.

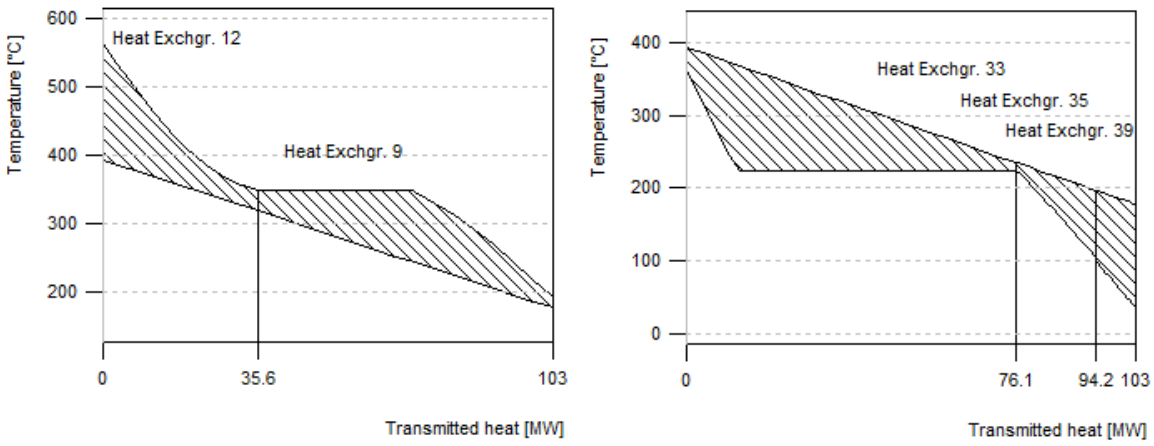

(b) (c)

Figure 46. Nuclear-TES coupling approach in which steam is used for charging the TES and a dedicated balance of plant is used for TES discharging: (a) PFD illustrating a nuclear-TES coupling and process heat extraction strategy, (b) QT diagrams of TES charging, and (c) QT diagrams of TES discharging.

As stated before, the steam pressure of 25 bar from TES discharging is below the considered process steam demand of 42 bar, and therefore no process heating stream from TES discharging is modeled in Figure 46(a). One potential solution to this involves implementing steam extraction for heat demand from the main cycle, then modulating the output by routing steam to extraction and to the TES. This would introduce limitations on operational flexibility. Combined steam extraction to TES and for process heating should not exceed about 85% of the main steam flow, as at least 15% of the nominal flowrate is typically required in the low-pressure section for turbine blade cooling. The efficiency characteristics of the main cycle are identical to those of the baseline CHP system. From a control and performance standpoint, the CHP and TES, along with the dedicated conversion system, operate independently so long as they remain within the operating range limits.

C-3. CHP Systems with TES Charged by Extracted Steam

The concept for charging the TES with extracted steam involves positioning the TES system on the heat delivery branch. For charging, steam is extracted at a high pressure, allowing for a higher margin in temperatures so that the discharged steam (or other HTF) meets the required process parameters. A conceptual layout of the charged-by-extracted-steam system is shown in Figure 47. Extraction controls are implemented in all cases given that the amount of extracted steam will need to vary over time.

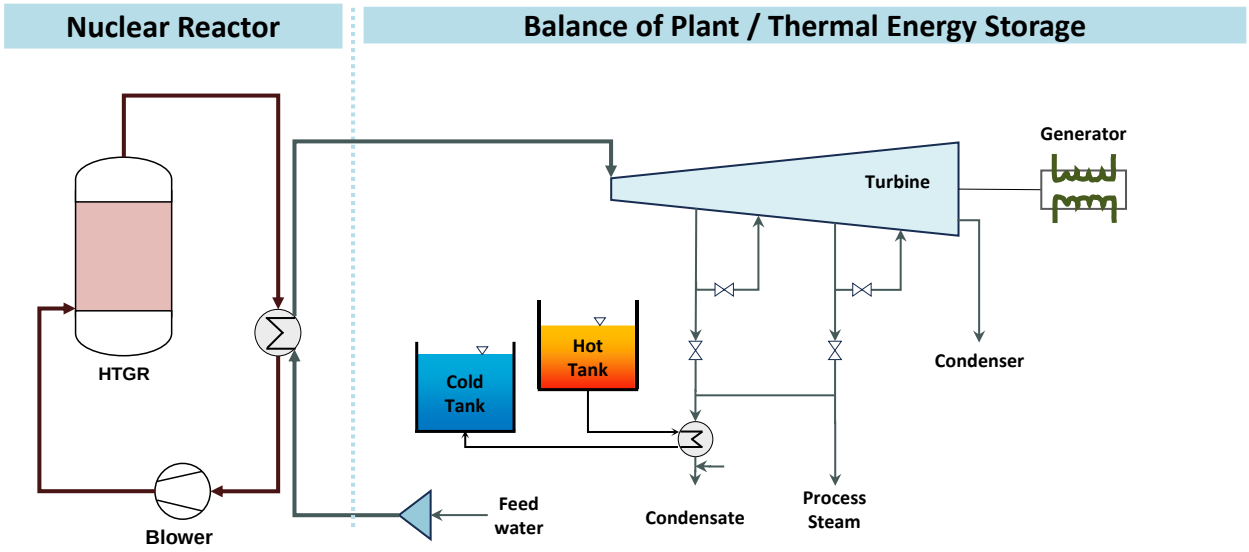

Figure 47. Conceptual layout of TES integration on the heat extraction branch.

As discussed in the previous section, the pinch point limitations restrict the feasibility of this system when using sensible heat storage systems. The PFD shown in Figure 48 illustrates a scenario in which steam is extracted at 110 bar, resulting in minimal power produced in the turbine by the extraction steam. To produce 42 bar of steam during discharging, the TES cold and hot temperatures must be 236°C and 320°C, respectively, resulting in a difference of less than 100°C. Additionally, the steam diversion ratio is restricted to approximately 30% because the return condensate temperature from TES (254°C) is significantly higher than the required steam generator nominal inlet temperature of 165°C.

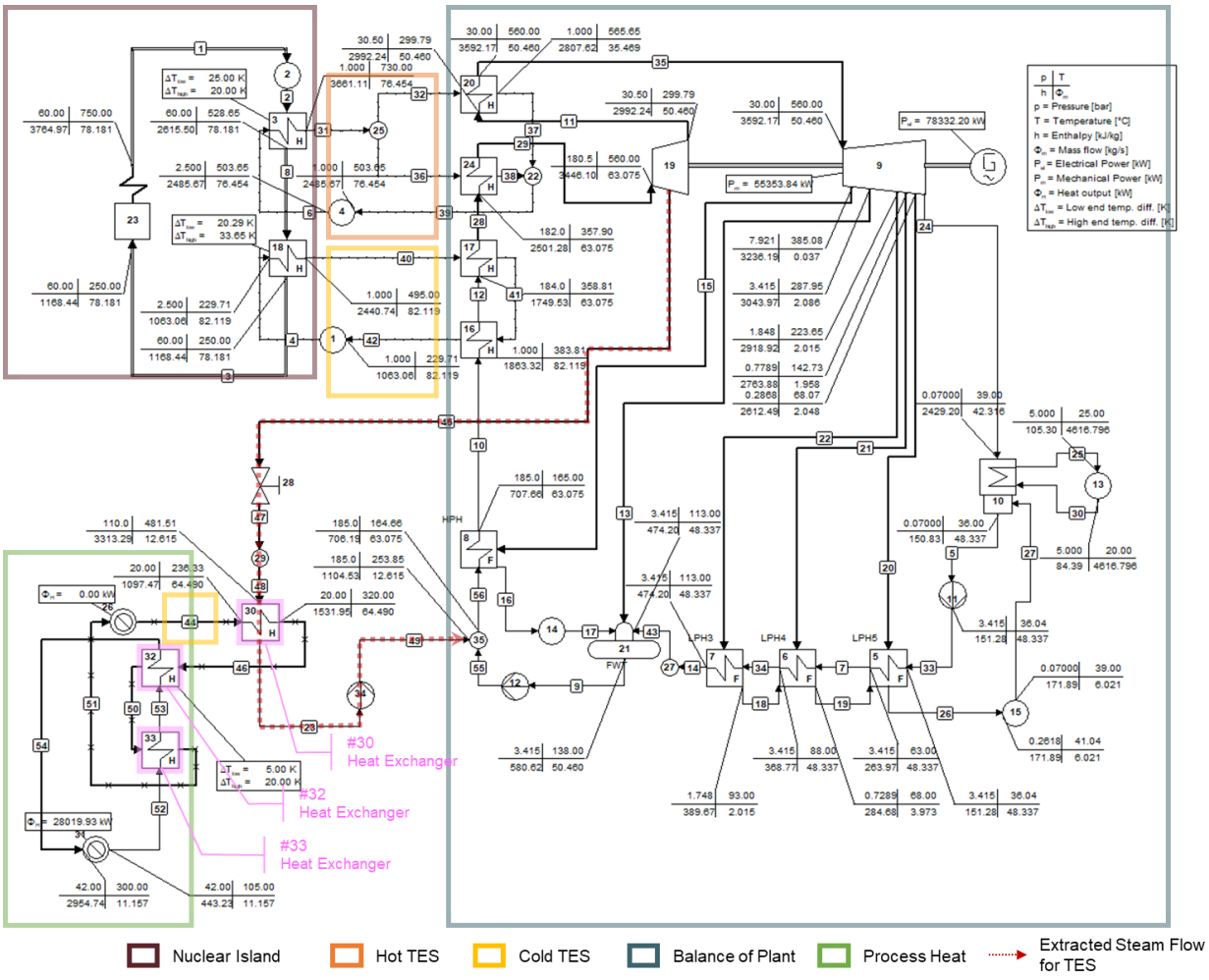

(a)

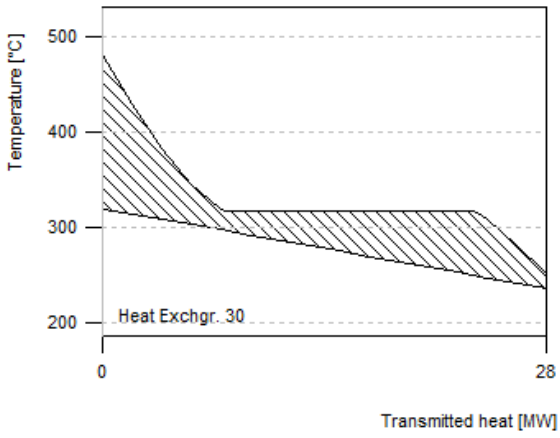

(b)

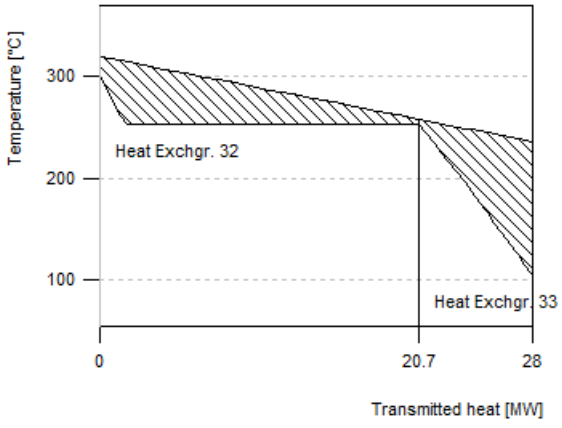

(c)

Figure 48. A nuclear-TES coupling approach with extraction-charged TES, which then discharges into a process steam line: (a) PFD illustrating a nuclear-TES coupling and process heat delivery strategy, (b) QT diagrams of TES charging: Heat Exchanger 30, and (c) QT diagrams of TES discharging: Heat Exchangers 32 and 33.

As latent heat storage systems progress in their development, the feasibility of this approach may improve. Systems designed to store heat at lower temperatures and pressures may be closer to commercial viability than those intended for use in the main steam cycle. Utilizing latent storage with a (near) constant phase change temperature facilitates a minimal temperature differential between the steam condensation during charging and the steam evaporation during discharging.

Even though latent heat storage systems can work with a steam accumulator, steam accumulators are generally infeasible for a storage capacity exceeding 1 hour. Among the largest steam accumulator systems is the PS10 concentrated solar plant, with four tanks providing 20 MWh of discharge power for up to 50 minutes. [108] Though there have been experimental endeavors focusing on latent heat storage for process steam, [105] these efforts primarily targeted smaller-scale systems. More development is required to achieve the necessary cost-effectiveness and thermohydraulic balance for large-scale applications, such as nuclear systems.

Figure 49 suggests a conceptual solution for systems ranging from dozens to hundreds of megawatts and requiring storage durations exceeding 1 hour, and the PFD as shown in Figure 50 illustrates its energy balance model. Charging line extraction is, due to the latent heat storage, only 7 bar above the nominal extraction. A PCM storage is, for modeling purposes, substituted by a water and steam intermediate loop with heat exchangers representing the charging and discharging operation. The discharged process steam from TES is then mixed with the process steam taken from nominal extraction.

Drawbacks of the system include that this system would require controlled extraction at both charging and nominal lines. Limited subcooling on the charging return condensate requires active feedwater temperature control and limits the charging heat diversion ratio to about 17%.

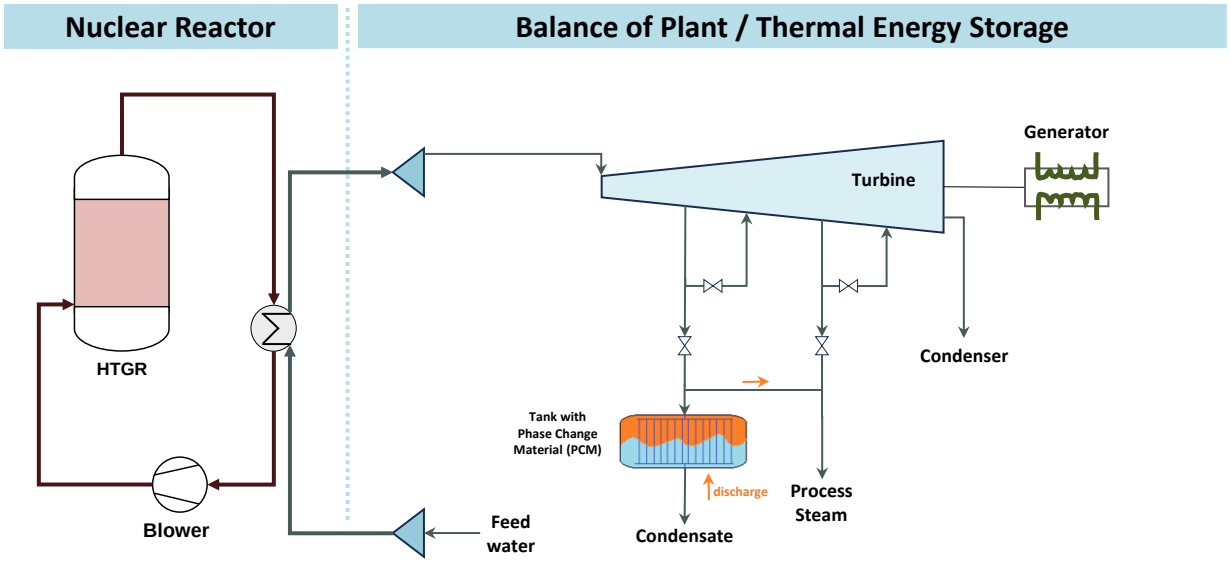

Figure 49. Configuration with a PCM TES that uses turbine extraction steam for charging and discharges into a process steam line.

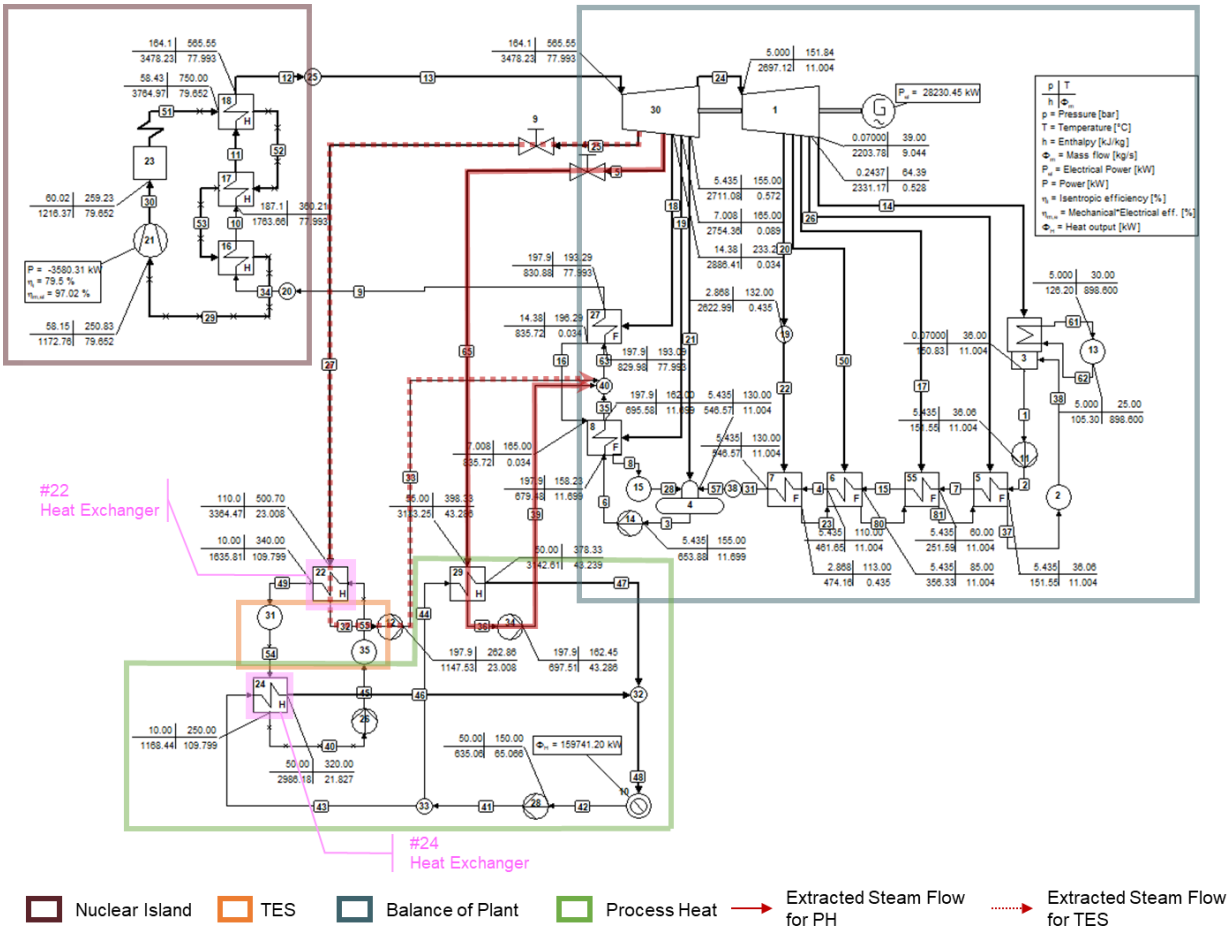

Figure 50. A nuclear-TES coupling approach with extraction-charged TES with PCM, which then discharges into a process steam line.

Table 12. Summary of power conversion systems—NR-POWER / NR-CHP /NR-CHP-TES-POWER / NR-CHP-TES type.

Cycle			Energy Efficiency (%)	Heat production Efficiency (%)	CHP Efficiency (%)	Max Heat Diversion to TES ** (%)	Max Decrease in Power Output (%)	Max Decrease in Heat Output (%)	Pwr. Conversion System Capacity	Note
Reference	Type*	Features								
—	NR-POWER	Elec. power gen.	40.0	0	40.0	0	0	0	Fixed	Current Xe-100 system design
Figure 41	NR-CHP	Elec. power gen. + process heat w/ extracted steam	40.0~13.4	0~76.6	40.0~90.4	0	86.6	100.0	Fixed	Minimum low-pressure flowrate 15% and higher heat production possible by steam bypass operation
Figure 43	NR-CHP	Elec. power gen. + process heat w/ steam after backpressure turb.	9.8~-2.5	89.6~102.5	99.4~99.9	0	100.00	100.0	Fixed	Steam bypass operation is assumed
Figure 46	NR-CHP-TES-POWER	Elec. power gen. + process heat w/ extracted steam TES charged by main steam	40.0~28.0	0~76.6	28.0~90.4	100.0	100.00	100.0	Main fixed, discharging flexible	Max decrease in power output might be practically limited by minimal load ~ 10%
Figure 48	NR-CHP-TES	Elec. power gen. + process heat w/ extracted steam TES (sensible) charged by extracted steam	42.0~11.3	0~81.8 + TES boost	42.0~90.6	25.3	71.5	100.0	Fixed	Minimum low-pressure flowrate 15% and limit values at max; TES extraction together with non-TES extraction
Figure 50	NR-CHP-TES	Elec. power gen. + process heat w/ extracted steam TES (PCM*) charged by extracted steam	40.0~12.8	0~77.2 + TES boost	42.0~90.2	16.8	68.0	100.0	Fixed	Minimum low-pressure flowrate 15% and limit parameters at max; TES extraction together with non-TES extraction

* NR: nuclear reactor; CHP: combined heat and power system; PCM: phase chance material; POWER: power system.

** Equal to max decrease in CHP output.

Appendix D

Conceptual Demonstration of Industrial Energy Park with Individual Industry

D-1. CHP System with Nuclear Power Without TES

D-1.1 Chemical Plant A—Relatively Lower Heat Demand

In general, industrial processes often utilize internal heat sources, such as recovered waste heat from the cooling of exothermic reactions at high temperatures, or internal power sources, such as letdown turbines. When integrating with external sources, these internal sources are incorporated into the net balance of electricity and net balance of heat demand (highest process pressure steam). The output of the letdown turbines can be utilized at different pressure levels. Realistically, the outputs may be controlled, but for the purposes of this analysis, they are regarded as an internal aspect of the industrial process, influencing the net demand for heat and power.

Table 13 outlines the configuration for integrating the energy supply system into Chemical Plant A. Table 14 shows ranges of net power, delivered thermal energy, and system efficiency regarding different CHP configurations. The range of the presented parameter values corresponds to the minimum and maximum steam extraction rate.

Table 13. System parameters for scenarios that integrate an HTGR with Chemical Plant A.

Scenario	Number of CHP: Baseline Turbine Cycle	Number of CHP: Extraction-Condensing Turbine Cycle	Number of CHP Backpressure Turbine Cycle	Max Power Production (MW)	Max Heat Supply (excl. bypass) (MW)
Chem. Plant A	1	2	1	263	509

* Details of CHP types can be found in Table 2.

Table 14. Parameters of applied HTGR systems with different CHP configurations.

	W_{net} (MW)	$Q_{delivered}$ (MW)	Electrical Efficiency	Heating Efficiency	CHP Efficiency
Baseline cycle	81	0	40.0%	0%	40.0%
CHP extr. cycle	81–26	0–164	40.0%–12.9%	0%–80.6%	40%–93%
CHP backpr. cycle	20	182	9.7%	89.6%	99.4%

* Details of CHP types can be found in Table 2.

Figure 51 illustrates the coverage of thermal and electrical demands via the integration of HTGRs with dedicated conversion systems. For Chemical Plant A, the CHP plants utilize steam extraction from a turbine to adjust the heat output to its maximum capacity. The total thermal demands are fulfilled with a backpressure plant (constant output all the time, Line 3 in Table 2) and a two extraction-condensing turbine CHP plants meeting thermal load fluctuation. Together with a power-only production unit, a set of four Xe-100 reactors can supply all necessary heat and electricity most of the time, with a median export of 27 MWe—as indicated by the net electricity balance seen in Figure 52. It is important to mention that peaks in electricity production (export) can be mitigated through curtailment, and extended periods of decreased demand can be accommodated by adjusting the reactor output. These results conclude that TES is crucial for balancing the system.

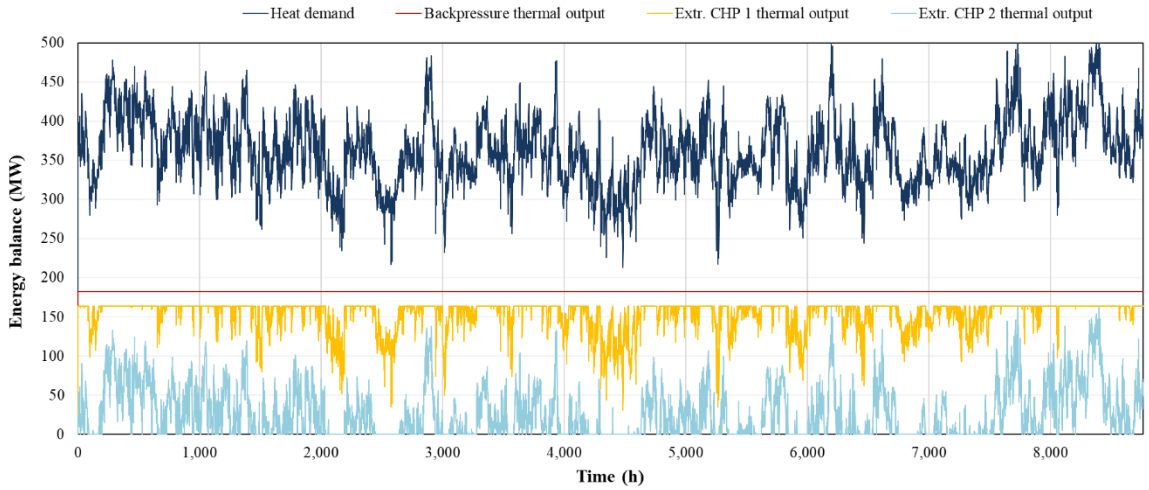

(a)

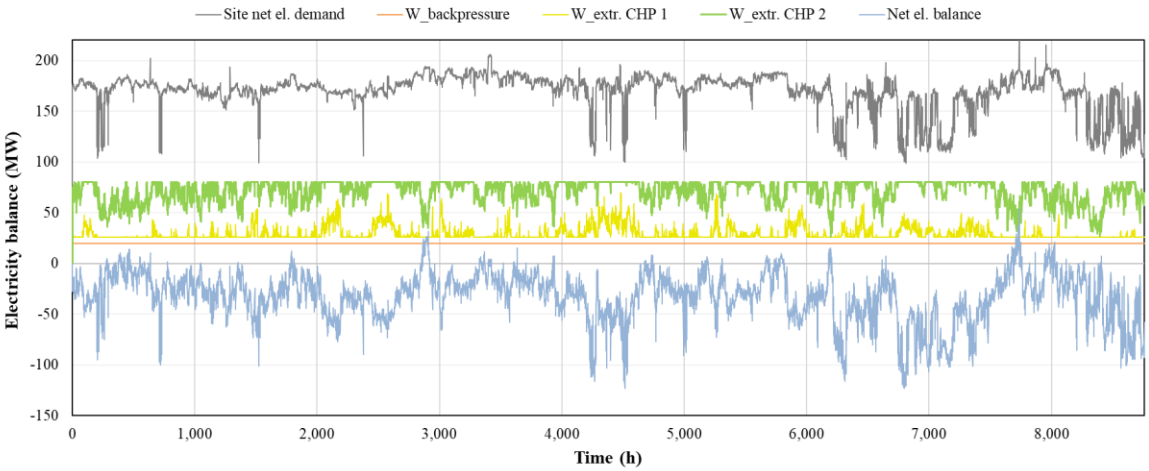

(b)

Figure 51. Heat and electricity demand and supply from HTGRs and their power conversion systems (for Chemical Plant A): (a) heat demand and supply from distinct reactor units and their power conversion systems and (b) electricity demand and supply from distinct reactor units and their power conversion systems.

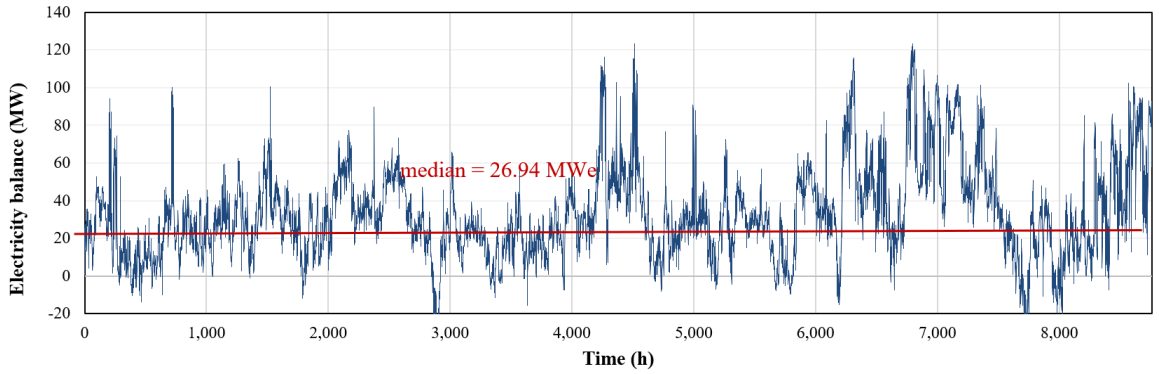

Figure 52. Net excess (positive) or deficit (negative) electricity at Chemical Plant A after providing all heat via the configuration proposed in Table 13.

D-1.2 Chemical Plant B—Relatively High Heat Demand

The nuclear integration strategy for Chemical Plant B, which requires a large amount of heat, is described in Table 15. Figure 12 shows ranges of net-work, delivered thermal energy, and system efficiency for the CHP configuration.

Table 15. System parameters of the scenarios that integrate HTGR with Chemical Plant B.

Scenario	Number of CHP Backpressure Cycle	Number of CHP Extraction Turbine Cycle	Number of Baseline System	Max Power Production (MW)	Max Heat Supply (incl. 1 bypass) (MW)
Chemical Plant B	6	0	0	118.8	1,113

* Details of CHP types can be found in Table 2.

Table 16. Parameters of applied HTGR systems with different CHP configurations.

	W_{net} (MW)	$Q_{delivered}$ (MW)	Electrical Efficiency	Heating Efficiency	CHP Efficiency
CHP backpr. cycle	20 ~ -4	182~203	9.7% ~ -2.0%	89.6%~100%	99.4%

* Details of CHP types can be found in Table 2.

Figure 53 shows how thermal and electrical demands are covered by HTGRs and their conversion systems. The approach applied to Chemical Plant B is that the backpressure systems run at constant load and only the last conversion system can route heat through a bypass if the heat demand is greater than what can be met with full backpressure operation. Note that even a set of six reference Xe-100 reactors cannot meet all the necessary heat and electricity peak demands throughout the year. However, there are periods of surplus, and the net demand frequently fluctuates near a net-zero balance, as shown individually in Figure 54. Adding another reactor unit to meet load peaks could incur excessive costs unless it is justified for the sake of ensuring reliability. Without an additional reactor unit, heat deficits must be covered by external sources (e.g., natural gas peaking boilers), while positive (export) peaks of heat need to be curtailed. Excess electricity can be exported to the grid. If there are extended periods of reduced demand, it can be managed by adjusting the reactor output or scheduling maintenance during these intervals.

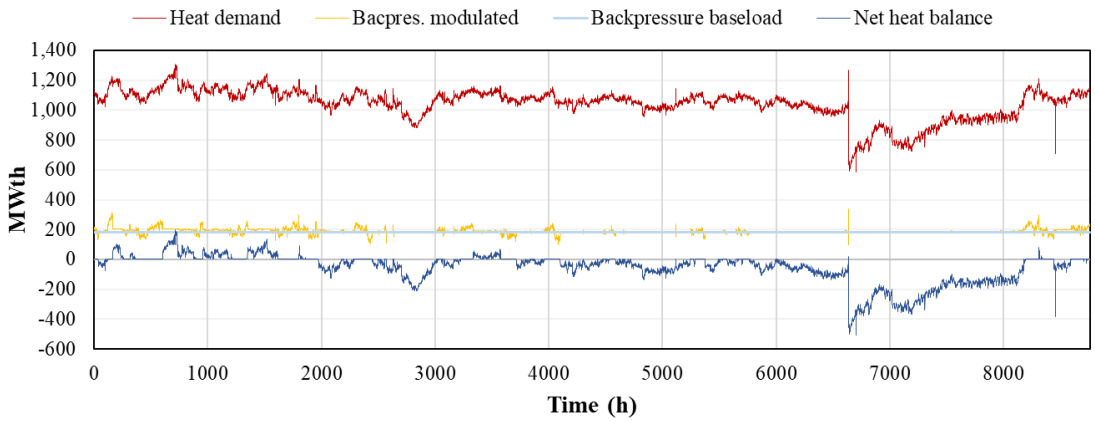

(a)

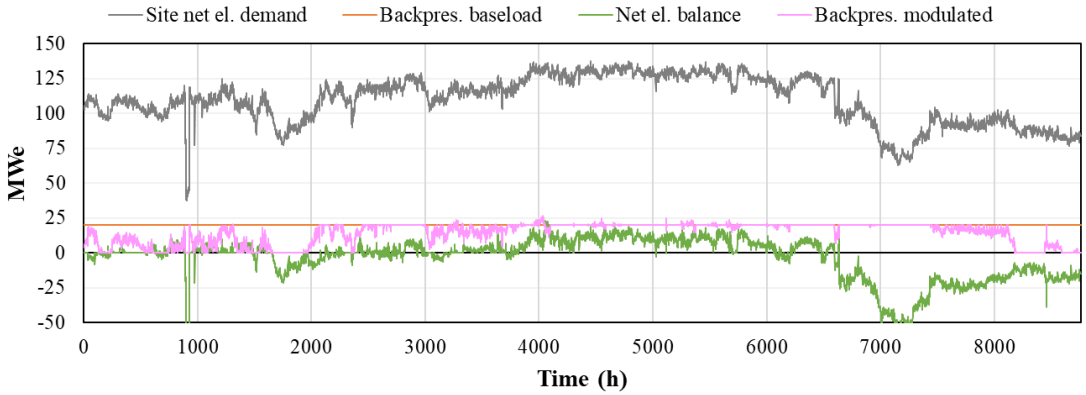

(b)

Figure 53. Heat and electricity demand profiles, supply from proposed systems, and resulting net balance for Chemical Plant B: (a) heat demand and supply from distinct reactor units and their power conversion systems and (b) electricity demand and supply from distinct reactor units and their power conversion systems.

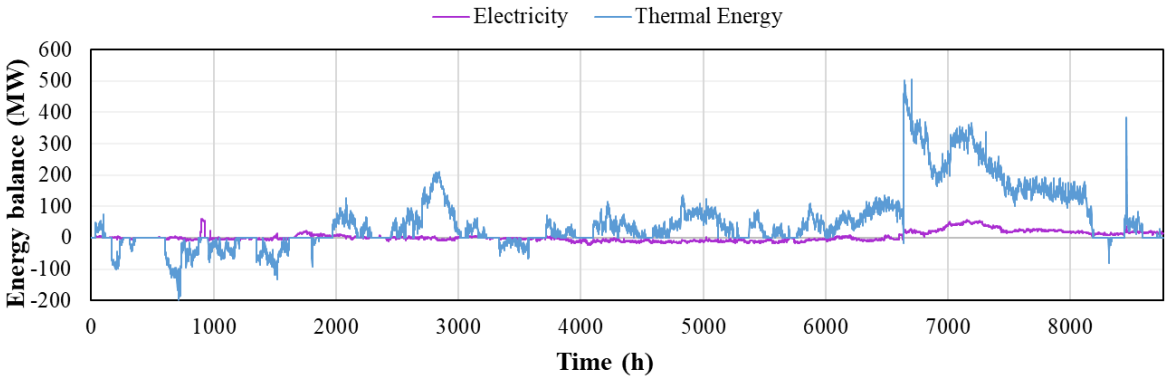

Figure 54. Net surplus (positive) or deficit (negative) electricity and heat at Chemical Plant B, which features the configuration proposed in Table 15.

Another configuration for CHP plants was explored and is detailed in Appendix B. It features one extraction turbine and three backpressure turbines.

D-1.2.1 Petroleum Refinery

The nuclear energy supply steam integrated into the petroleum refinery, with no TES, is described in Table 17. Table 18 shows ranges of net-work, delivered thermal energy, and system efficiency for the CHP configurations. Note that a set of four Xe-100 reactors can provide all the required heat and electricity while exporting nearly 64 MWe to the grid. Since the refinery load is constant, TES integration could improve the system economy by modulating this net power export.

Table 17. System parameters of scenarios that integrate an HTGR with the reference refinery.

Scenario	Number of CHP Systems	Number of Baseline System	Electricity Demand (MW)	CHP Syst. Power Supply (MW)	Baseline Syst. Power Supply (MW)	Net Electricity Balance (MW)
Steam + H2, net export	1	3	225.3	45.3	243.8	63.8

* Details of CHP types can be found in Table 2.

Table 18. Parameters of applied HTGR systems with different CHP configurations.

	W_{net} (MW)	$Q_{delivered}$ (MW)	Electrical Efficiency	Heating Efficiency	CHP Efficiency
Baseline cycle	81.3	0	40.0%	0	40.0%
CHP cycle, refinery + H2 steam demand	45.3	73.0	19.4%	35.9%	55.4%

* Details of CHP types can be found in Table 2.

D-1.2.2 Electric Arc Furnace

The load demand profile for an EAF, as sourced from Reference [28], was adjusted to a reference size of 245 MW. Figure 55 shows that the system experiences significant oscillations due to the high load variability. Without electricity imported from the grid, one or two Xe-100 reactors are necessary to fulfill the demand. The nuclear integration herein is obvious, wherein a baseline nuclear plant strictly provides electricity.

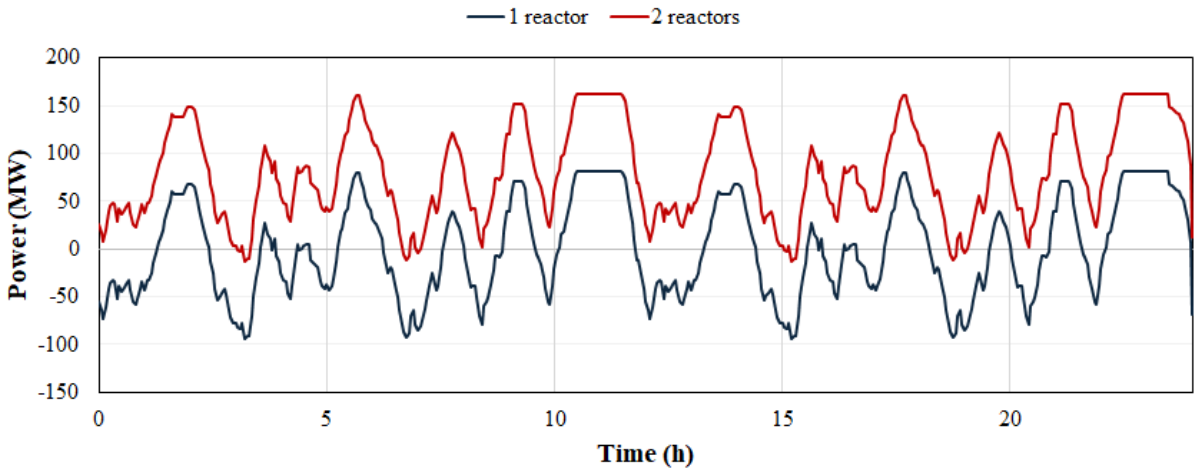

Figure 55. Case involving the integration of Xe-100 reactors into EAF operation over a 24 hour period. Positive power implies energy export.

D-2. CHP System with Nuclear Power and TES for Chemicals

Two chemical plants that were illustrated in the previous section are good examples for showcasing the potential and impact of TES integration. Selecting two chemical plants with significantly different sizes also provides a good demonstration of different technologies, potential control strategies, and the goals of TES operation.

D-2.1 Chemical Plant A—Relatively Lower Heat Demand

TES can be applied either to the CHP system or the electricity-only system, as illustrated in Figure 56. The advantage in implementing TES on the electricity-only system is the simplicity of the overall system controls: three CHPs can meet the thermal demand but cause oscillating electricity demand. Therefore, a single power-only system using TES must balance the overall electricity demand. If TES is instead integrated with the CHP system, the steam extraction rate would have to be constantly adjusted to meet the electrical output. Thus, the configuration connecting TES to the electricity-only system (i.e., Figure 56(a)) may be preferred and will be explored here as the primary option. However, with the highly varying and coordinating thermal and electrical loads, implementing TES with CHP may present its own set of benefits. A dynamic modeling results of nuclear reactor with TES system based on specified electrical power demand can be found in Appendix E.

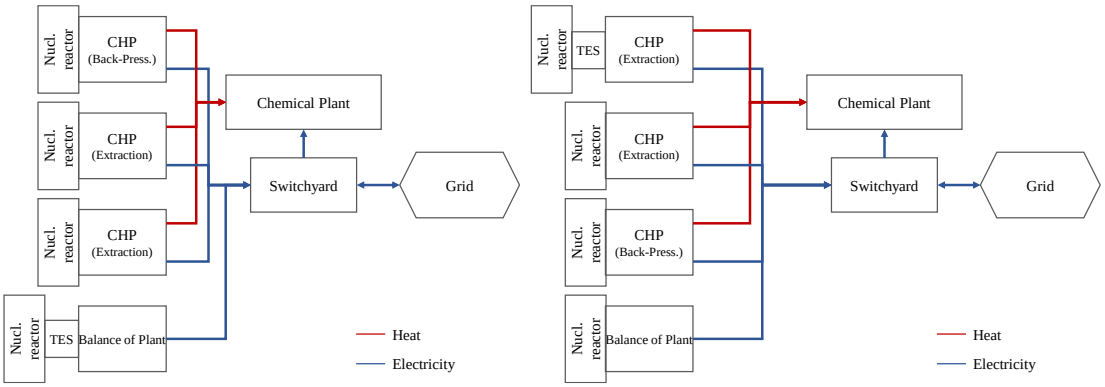

Figure 56. System configurations for nuclear and TES integration into Chemical Plant A (with relatively higher electricity demand): (a) TES coupled with an electricity-only system and (b) TES coupled with a CHP (steam extraction) system.

The findings presented here are obtained from a TES system with an 80 MWe boost limit and 8 hours of storage capacity. The configurations explored in Section D-1 showed that the nuclear CHP systems for Chemical Plant A could meet all the required heat demand and most of the required electricity demand without TES. Instead of meeting fluctuations, the goal of TES integration here is to provide a constant electric output to the grid, improving the reactor economics and minimizing the need for grid ancillary services. By implementing TES, the system can provide a predictable net power output of 25–35 MWe into the grid (see Figure 57) 48% of the time window (i.e., 1 year). Implementing more complex dispatch algorithms using demand prediction can further reduce the number and magnitude of peaks.

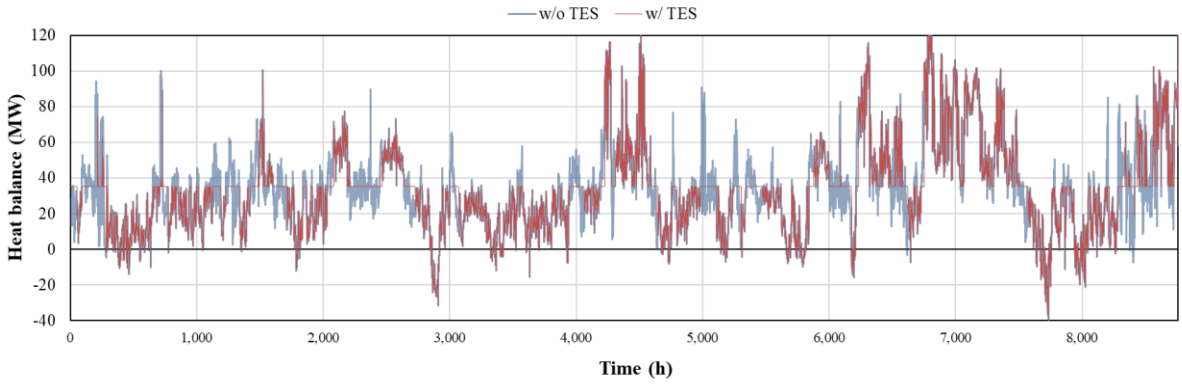

Figure 57. Net electricity balance for Chemical Plant A—both with and without TES—when the operation demand is a steady 35 MWe export (positive sign = export; negative sign = import).

D-2.2 Chemical Plant B—Relatively High Heat Demand

Chemical Plant B has a high heat demand, making the CHP system with a backpressure turbine a better option. Six Xe-100 reactors are considered in this case, as illustrated in Figure 58. They can be coupled with CHPs either with all backpressure turbines or with five backpressure turbines and one steam extraction turbine. A TES system with a 150 MWth boost limit and 10 hours of storage capacity was used for this case.

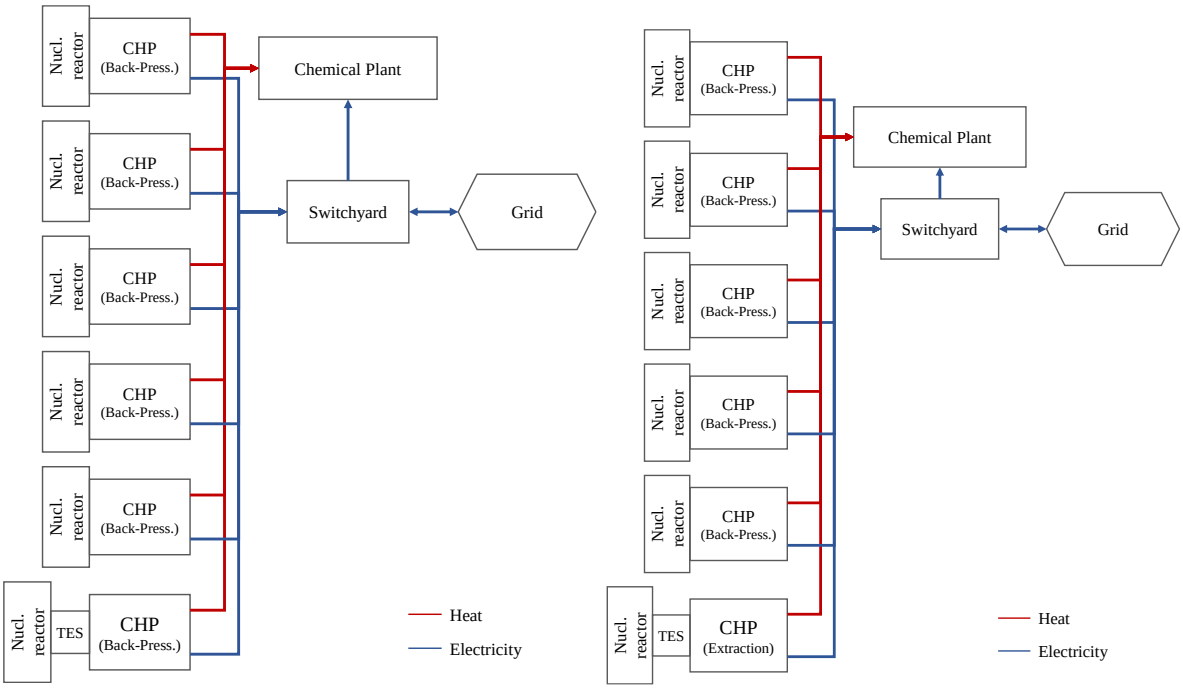

Figure 58. System configurations for nuclear and TES integration into Chemical Plant B (with relatively higher heat demand): (a) TES coupled to a CHP backpressure system and (b) TES coupled to a CHP extraction system.

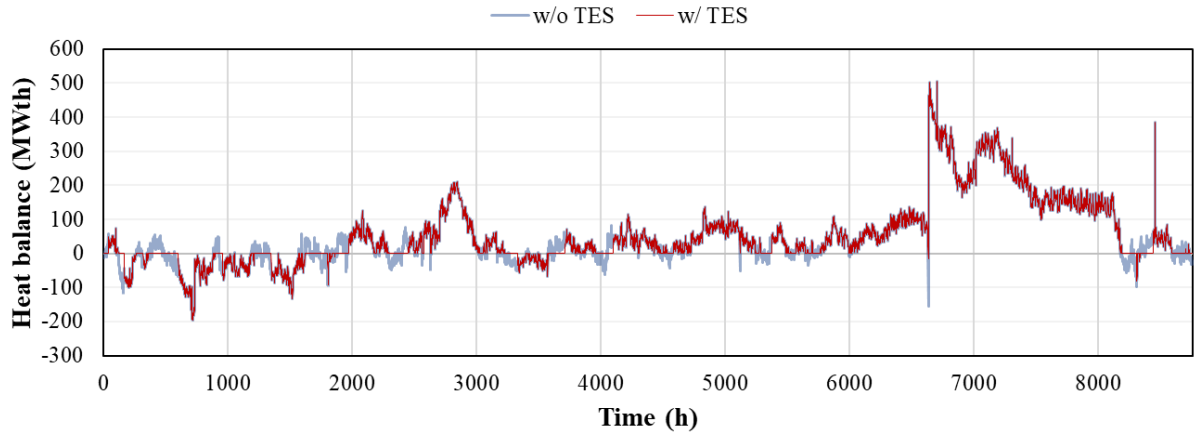

Figure 59. Net heat balance for Chemical Plant B (the case with six backpressure turbine systems), both with and without TES (positive sign = curtailment; negative sign = backup boilers).

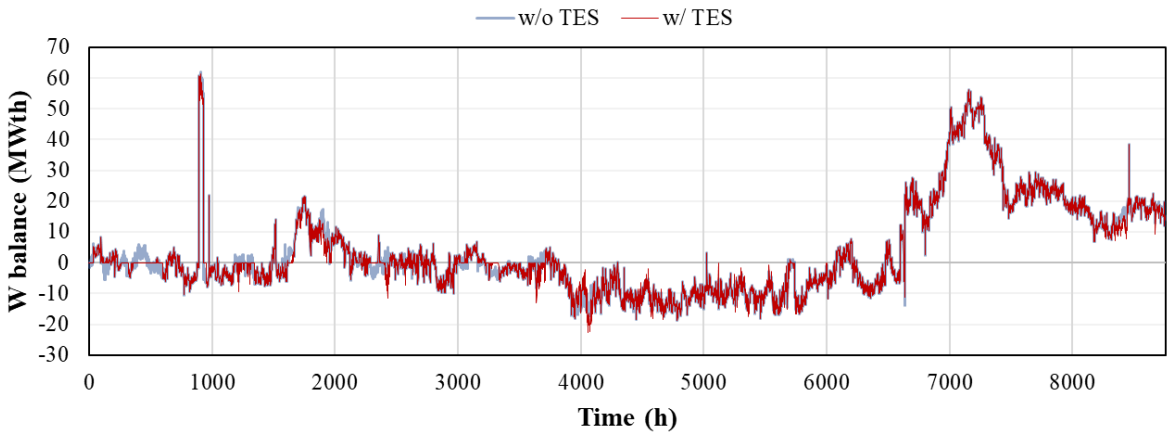

Figure 60. Net electricity balance for Chemical Plant B (the case with six backpressure turbine systems), both with and without TES (positive sign = export; negative sign = import).

The TES implementation results can be observed in Figure 59 (for heat balance) and Figure 60 (for electricity). With TES, there are fewer periods and a smaller extent of thermal energy deficit, even though the auxiliary systems providing heat are still in need. TES reduces the need for external heat sources and mitigates heat curtailment. NG- or fuel-oil-fired systems are low-capital-cost systems that could be used in addition to TES to cover these short-duration demand peaks. TES's impact on the electricity balance is minimal if only backpressure turbines are used, which limits the opportunities for energy export. From Figure 61, only a limited number of charging and discharging cycles occur annually when using a 20-hour-capacity TES. The durations of heat excess or deficit are, however, considerably longer than what TES can accommodate.

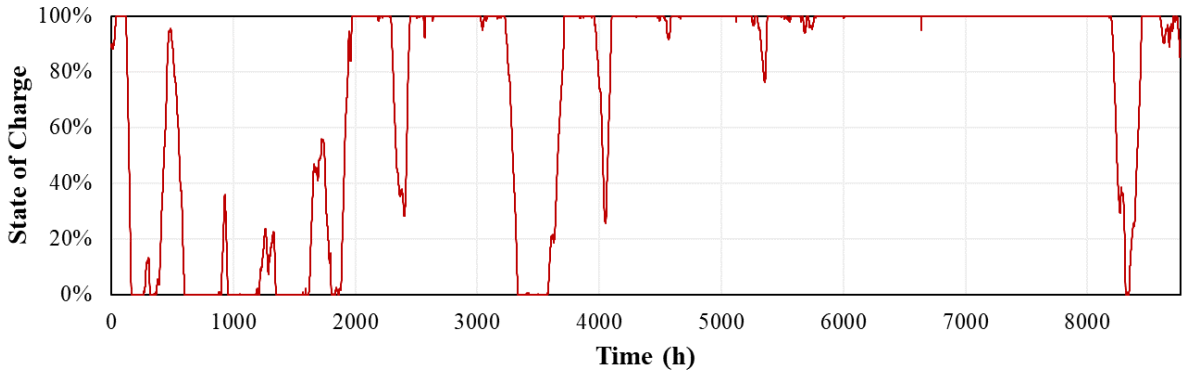

Figure 61. State of charge for the specific TES implemented at Chemical Plant B.

D-2.2.1 Petroleum Refinery

In this area, two possible configurations of TES implementation are considered: one in which TES is implemented on the CHP cycle and one in which it is implemented as an electricity-only system (see Figure 62). Since implementing TES on an electricity-only system is simpler for overall system control, the first configuration (Figure 62(a)) is preferred and will be explored here as the primary option.

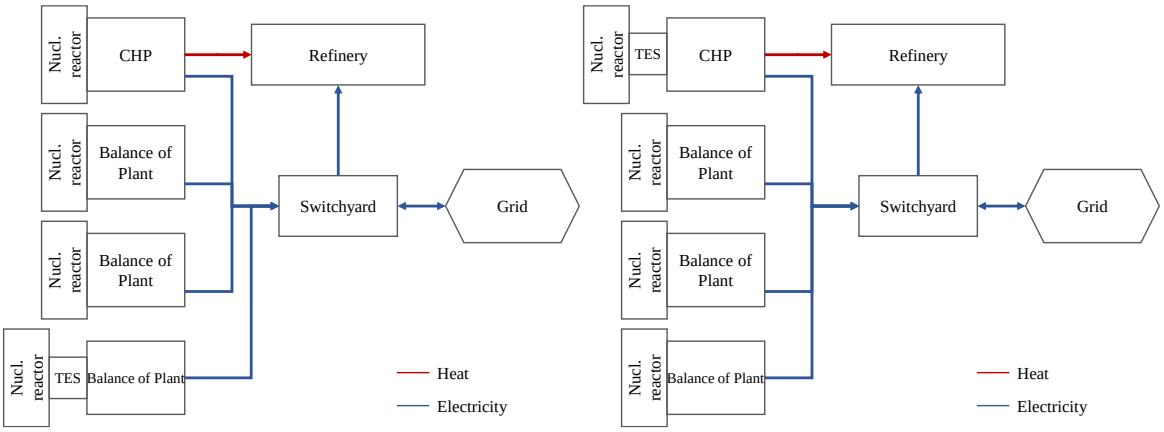

Figure 62. Two configurations for implementing TES into the petroleum refinery system, on a CHP extraction system and on an electricity-only system: (a) TES coupled to an electricity-only system and (b) TES coupled to a CHP extraction system.

The results of the baseline nuclear integration scenario without TES (see Table 17) show an excess of 63.8 MWe. Applying the corresponding conversion efficiency of 40%, this excess thermal power amounts to 159 MWth, which should be equal to or less than the TES charging capacity. The TES discharging magnitude depends on the required power in peak demand. This study assumes identical charging and discharging magnitudes and an additional 64 MWe to power output (thus, the peak excess power is 128 MWe, with a minimum excess power of null). Figure 63 gives the results of daily cycling operation, with an arbitrary export demand profile and a 4 hour maximum discharge capacity.

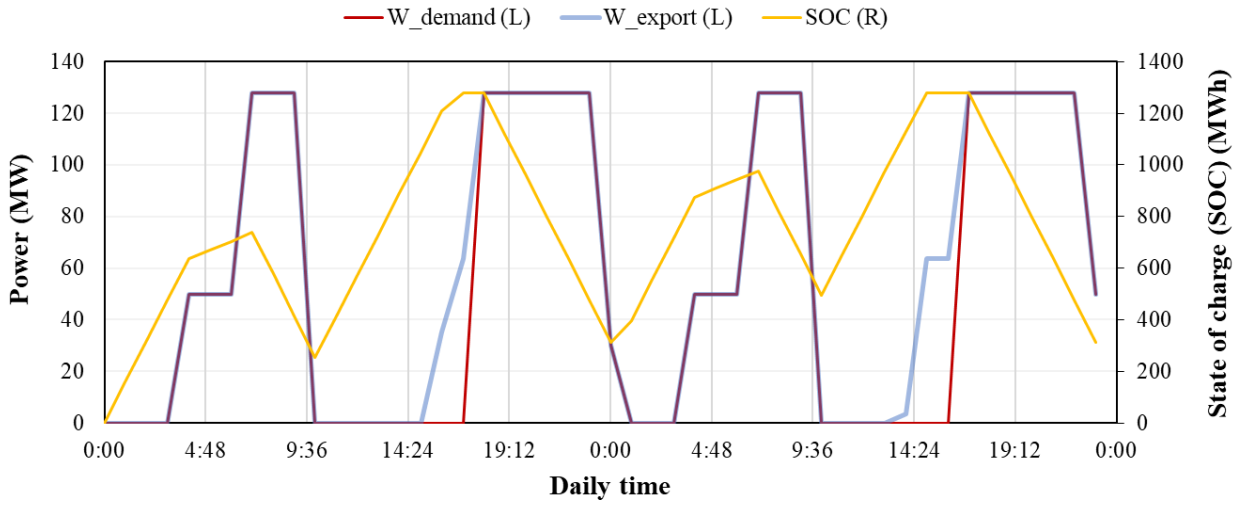

Figure 63. Example of a TES system applied to the excess power from the petroleum refinery integration—in daily cycling operation and with an arbitrary export demand profile.

D-2.2.2 Electric Arc Furnace

The schematics for an EAF facility coupled with a nuclear-powered CHP and TES capability, are illustrated in Figure 64. Figure 65 presents the electricity demand from the EAF facility and the electricity supply from the nuclear reactors integrated with the balance of plant and TES system (output boosting by 65 MW and 300 MWh[th] of storage capacity). The TES size was selected to illustrate that even though the storage is either full or empty at certain short periods, it still fails to fully provide the necessary power during peak demand. Determining the TES size is a cost-based choice between selecting a smaller, more cost-effective system—potentially resulting in penalties for deviating from a consistent energy profile that requires the use of grid—or a larger, more expensive system that will not cause these penalties.

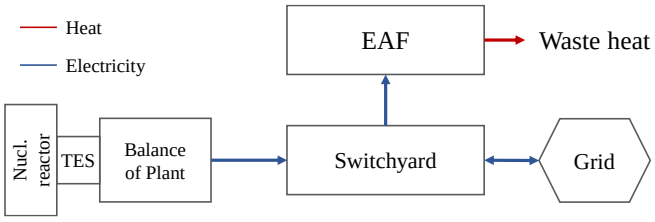

Figure 64. Configuration of nuclear-TES coupling to an EAF.

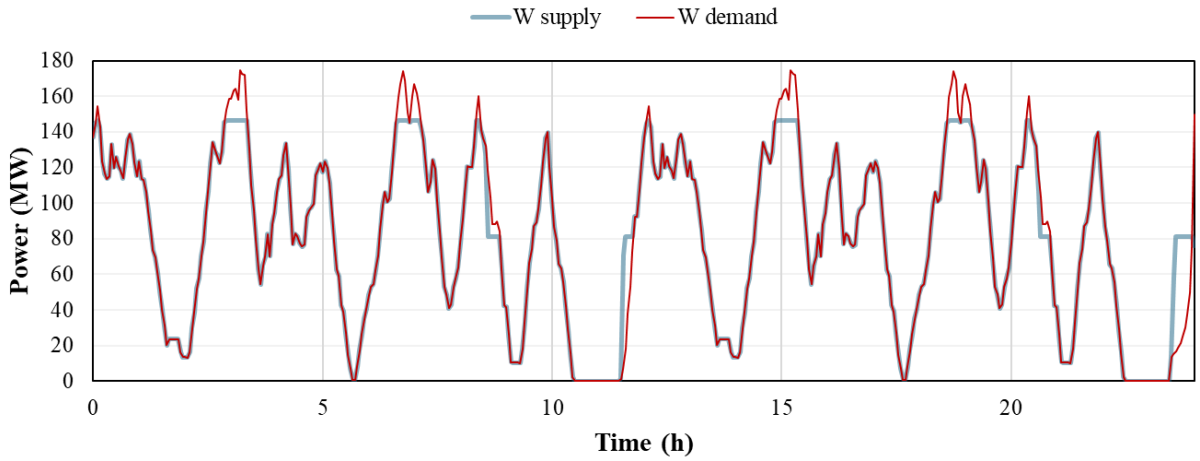

Figure 65. Electricity demand from the EAF facility, and the electricity supply from the nuclear-TES system. Thermal power from a nuclear reactor (245 MWth) and a 1.85 hour (300 MWh_{th}) TES system are assumed.

Appendix E

Framework for Analysis of Reactor with TES System Based on Specified Electrical Power Demand

The industrial energy park gives an interesting use case study in how such flexible operation may affect the nuclear island when thermal energy storage (TES) is implemented. Of particular interest is the coupling with the EAF due to its highly fluctuating energy requirements. Here reactor modules with extraction turbines are providing the flexibility in the heat demand while the electricity balance towards the grid is managed by a separate reactor module with an electrical-power-only steam cycle, as shown in Figure 56(a) where the nuclear island is coupled directly with TES (following the schematic shown in Figure 10(b)). This reactor sees large operational swings in its BOP's electrical power output to meet the demand at the EAF. A dynamic model of such a reactor design was developed in Reference [25] and was adapted in this work to follow the profile at Chemical Plant A. In this previous report, a detailed discussion of the system model and control scheme was given for shakedown testing and this analysis is not reproduced here.

We can however utilize the adapted model to present a framework to understand how the behavior of a rapid load following in the BOP, as is seen in the coupling with the EAF, can be translated towards the nuclear island to assess the feasibility of any such operational scheme. To start with, the demand profile for electrical power for the reactor coupled with TES at hourly intervals can be linearized assuming each power set point is held for the entire hour. Nuclear plants typically have electrical power ramping rates of 1–5% of reactor electrical power output per minute. The presence of TES allows greater power flexibility due to the large thermal buffer to the nuclear island and so, despite the limited control scheme design as was discussed in Reference [25], an ambitious ramping rate for power was assumed at 7.5%/min, a value that should be common in systems with rapid load change as the steam cycle for NGCC. This number is defined as the change in electrical power output per minute as a percentage of the nominal electrical power output. For the Xe-100 reference design with 80 MWe of power boosting coming from the TES, this nominal electrical power output is 161.3 MWe. Using this number as the maximal electrical power we get a total ramping rate of around 12 MWe/min.

Applying 7.5%/min as the chosen electrical power ramp rate, we can adapt the individual hourly setpoints in the yearly data to a full demand profile by taking the ramp rate between the values and holding these for the rest of each hour. An example of this finer grained profile is shown in Figure 66 for a 24 hour period of the data.

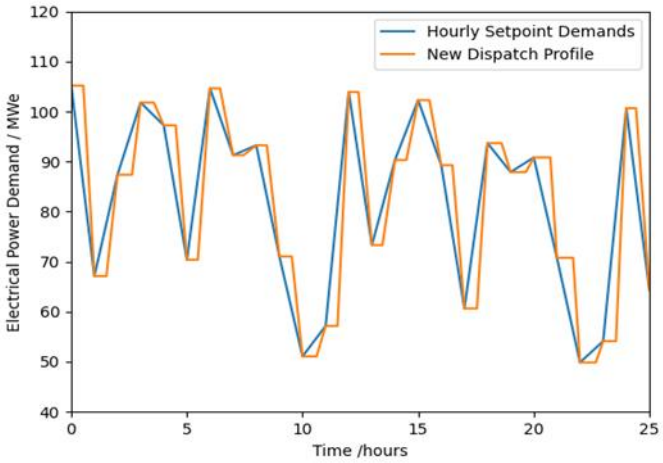

Figure 66. Adaptation of hourly set point demands to new dispatch profile based on a chosen electrical power ramp rate of 7.5%/min.

Applying this to the dynamic system model, we can investigate how the variation in electrical energy demand from the PCC may affect the rest of the systems components. This electrical power output following the new demand profile is shown for a week of operation in Figure 67. Due to the ramp rate, the power can closely match the demand across the period.

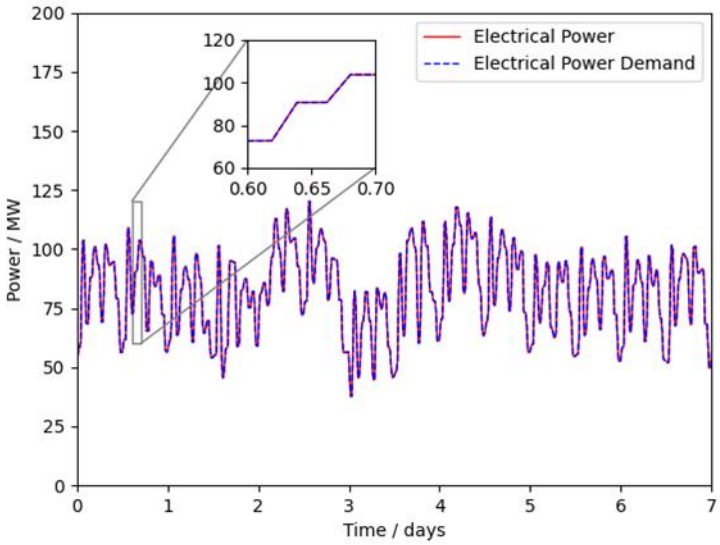

Figure 67. Power demand and electrical power output tracking across the course of a week.

The BOP itself sees the largest impact of this ramping. Figure 68 shows how the inlet pressure to the turbine may be affected due to aggressive ramping of the turbine through partial admission.

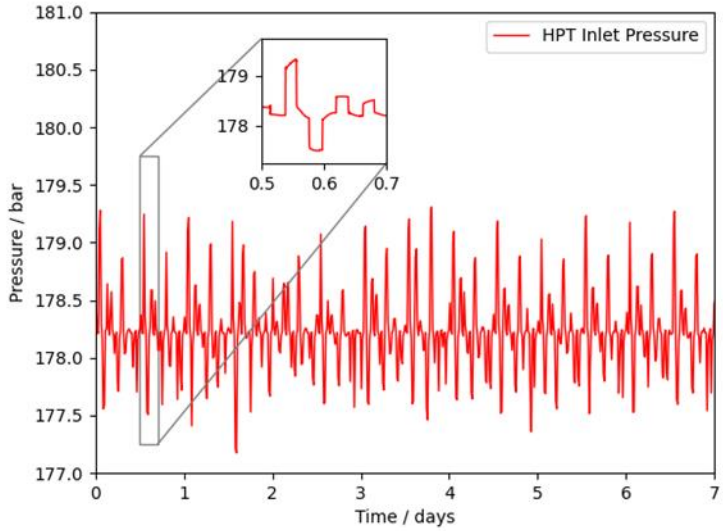

Figure 68. Effect of Chemical Plant A dispatch profile on the HPT inlet within the dynamic modeling.

While this change in pressure remains safely within a satisfactory range despite the control scheme, it is of interest primarily from a component lifetime perspective. Alternative work stemming from this may look to assess how the ramp rate and corresponding pressure and temperature fluctuations at the HPT inlet may impact HPT maintenance outages.

More importantly from a safety perspective is the impact aggressive load following has on TES functionality and the translation of this to reactor primary conditions. The two TES systems and their respective hot and cold tank levels are shown in Figure 69.

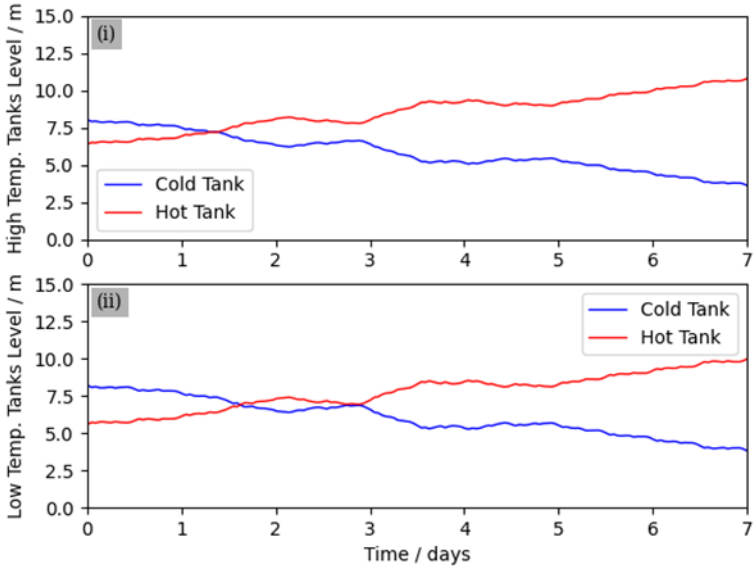

Figure 69. Sensible heat storage system tank levels for week of dispatch examined.

These tank levels fluctuate across the course of the week as the demand switches from over nominal production to under nominal production. The effect of this on the reactor core is low, but there is some gradual feedback such that the core inlet temperature fluctuates with the temperature falling when demand is over nominal and rising as demand falls. This fluctuation is shown in Figure 70. The model is controlled such that core reactivity is adjusted to a similar profile as the core inlet temperature profile to maintain average core temperature.

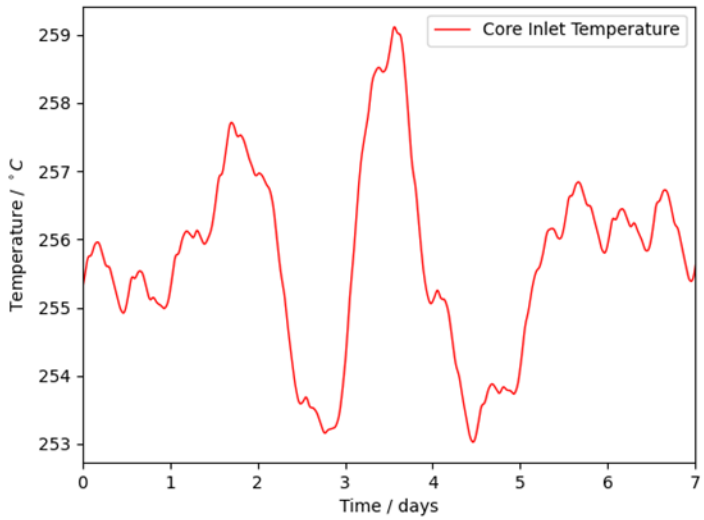

Figure 70. Core inlet temperature variation with the dispatching of the TES in the weekly demand case analyzed.

We can simulate the effect that this core inlet temperature and resulting reactivity changes have on the reactor core. We can see in Figure 71 that any core thermal power changes are minimized over the week with a maximum swing of around 0.0002%.

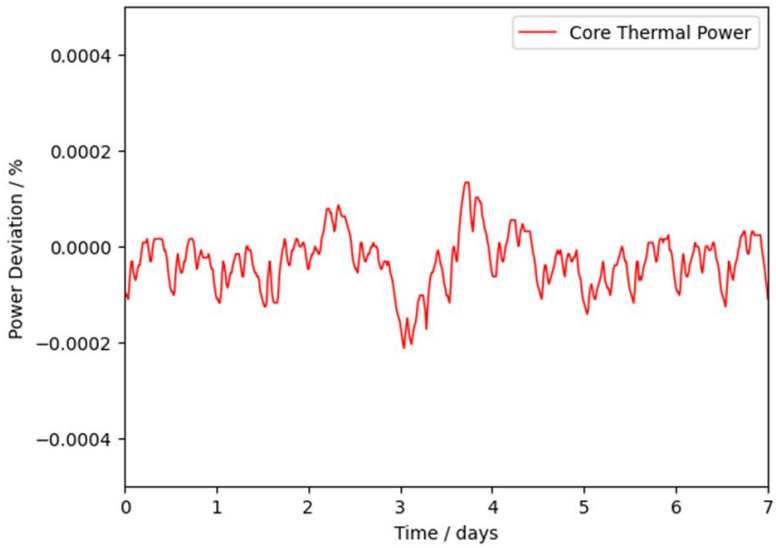

Figure 71. Core thermal power deviation variation with the dispatching of the TES in the weekly demand case analyzed.

While this model only goes a small way toward capturing the entire dynamics of such a complex system, we hope the presented framework allows future analysis of complex thermally integrated energy systems with a demonstration of thermal isolation of HTGRs from rapidly varying demand through integrated TES systems.

Appendix F

Holistic Energy Resource Optimization Network

The Holistic Energy Resource Optimization Network (HERON) is a resource capacity optimization tool developed at INL to determine the statistically optimal sizing and balance approach for various resources within integrated energy networks. [109] The code was constructed as a plug-in to the Risk Analysis Virtual ENvironment (RAVEN), using its underlying methods and capabilities to run a bi-level leader-follower optimization that optimizes unit sizing based on a probabilistic dispatch optimization.

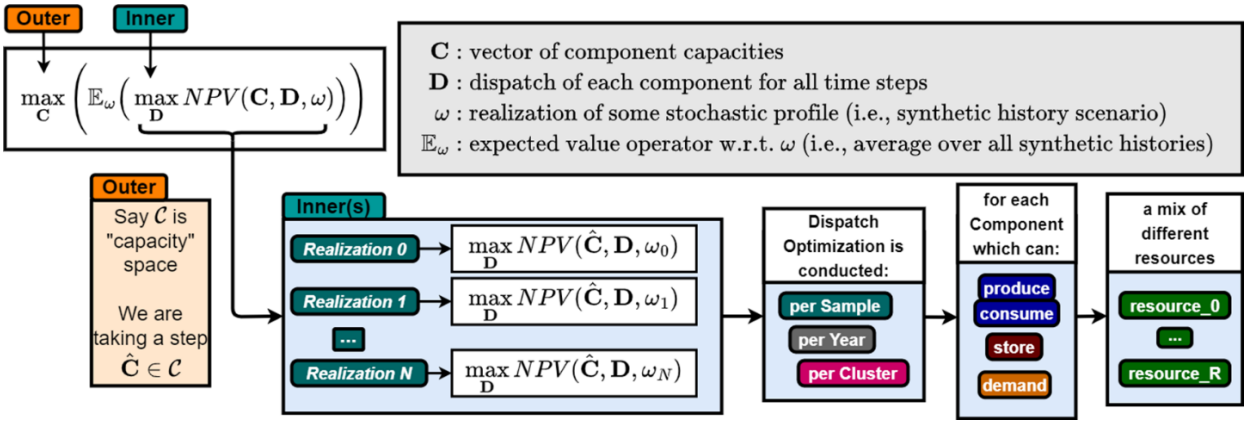

Figure 72. Bi-level optimization scheme used in HERON with multiple realizations. [109]

Figure 72 illustrates the optimization scheme used in HERON. The “outer” leader optimization aims to identify the optimal combination of resource-generating capacities to maximize an objective function, typically the net present value (NPV), for a given system. More specifically, it seeks to maximize the statistical behavior of NPV, such as its expected value, which could involve either minimizing costs or maximizing profits. HERON utilizes an automated stepping parameter sweep, where the code systematically explores various combinations of installed unit capacities, or “portfolios.” It accepts portfolios that improve the economic objective function and redirects the search when the objective function value decreases. This process continues until no further improvements are found, leading to HERON’s convergence on an optimal generation portfolio. In the “inner” follower run of HERON, the selected unit capacities are fixed and dispatched to meet system requirements in a way that maximizes system value. Potential dispatch scenarios for electricity and heat are repeatedly sampled from autoregressive moving average models and run to obtain statistically significant values across multiple possible futures. By combining many independent dispatch scenarios, the statistical value of the fixed capacity set is calculated and reported back to the “outer” loop of HERON, providing a metric for evaluating the expected economic effectiveness of that portfolio.

To optimize the dispatch, each unit in the system is represented algebraically in an optimization language. The dispatches of the units at each time step (nominally hourly) are optimization variables, while technical limitations (e.g., minimum and maximum operation and ramping limitations) are implemented as constraints. The economic impacts of variable operation and maintenance costs, fuel costs, production tax incentives, commodity sales, and other hourly costs and revenues are aggregated to provide the objective function to be optimized. For commodity storage such as electric batteries, TES, etc., the constraints also include minimum and maximum commodity levels, charge and discharge rates, round-trip efficiencies, and initial and final commodity levels for the optimization window. The optimization language is written using the Pyomo library in Python, then solved using one of several optimizers (e.g., ipopt [110] or coincbc [111]).

Appendix G

Input Cost Parameters for HERON Optimization

Table 19. Cost assumptions for HERON optimization.

Item	HTGR	TES	BOP	Charger	NG Boiler
CAPEX [$/kWt]	3,250 (C) [a] 2,500 (M) 1,750 (L)	Cost fn.[b]	Cost fn.[b]	234,181.4.[b]	0[c]
Capacity Recovery Factor [d] (CRF)	0.07500914	0.0805864	0.0805864	0.0805864	N/A
Annualized CAPEX [$/kWt]	244 (C) 188 (M) 131 (L)	Cost fn. × CRF	Cost fn. × CRF	Cost fn. × CRF	0
Fixed O&M [$/kWt-yr]	585 (1-unit) [e] 392 (fleet)	0 [f]	0 [f]	0 [f]	0 [c]
Var. O&M [$/MWt]	12[g]	0	0	0	15[h]

C, conservative; M, moderate; L, low CAPEX assumptions.

a The values are from Reference [112]. While we emphasize our findings for scenarios with a conservative CAPEX estimate for HTGR ($3,250/kWt), the dispatch profiles, such as TES charge and discharge and selecting the source for industrial loads between HTGR and NG boiler, do not change with CAPEX levels at the given HTGR capacity. Rather, they are influenced by their variable O&M costs. However, we include moderate and low estimates to provide target HTGR heat price levels to break even the project investment.

b The cost function, which includes key components for the respective system, is incorporated [25]. Since these cost functions are capacity responsive (i.e., economies of scale), higher capacity yields lower CAPEX per unit capacity. The charger cost function, which includes piping and heat exchangers to transfer reactor heat to TES, is found to be relatively capacity-insensitive in our previous analysis and is thus set as constant. For details, see Reference [25].

c An NG boiler is considered to be a given. Similarly, the fixed O&M cost for the NG boiler is considered a precommitted cost.

d CRF is introduced to derive the annualized CAPEX for each component. This enables the comparison or incorporation of technologies with different lifetimes within the fixed project life [25]. Annualized CAPEX (cost fn. multiplied by CRF) occurs every modeling year, and the sum of their NPVs should be identical to the corresponding nominal CAPEX at the beginning of the modeling year.

e We consider O&M cost reductions in multiunit plants using a cost reduction factor of 0.67 [112]. While this factor is devised for large light-water reactors (LWRs), we consider it applicable since the total HTGR capacities from fleet deployment in our modeling are comparable to those of large LWRs.

f Fixed O&M for TES and BOP are not explicitly modeled in HERON; instead, their costs are assigned to the HTGR [112].

g The value reflects a moderate estimate of fuel costs for HTGR technology, selected from a range of $10–16/MWt as reported in recent literature [112].

h We assume a market where NG prices are higher than HTGR fuel costs, setting up a situation where the two technologies interact: one with high CAPEX but low variable O&M costs and one with low CAPEX but high variable O&M costs. This assumption is based on the past 5 year average Henry Hub NG spot prices: $9.1/MWt (2023), $22.4/MWt (2022), $12.7/MWt (2021), $7.2/MWt (2020), and $8.6/MWt (2019) [45].

Appendix H

Core HERON Optimization Results

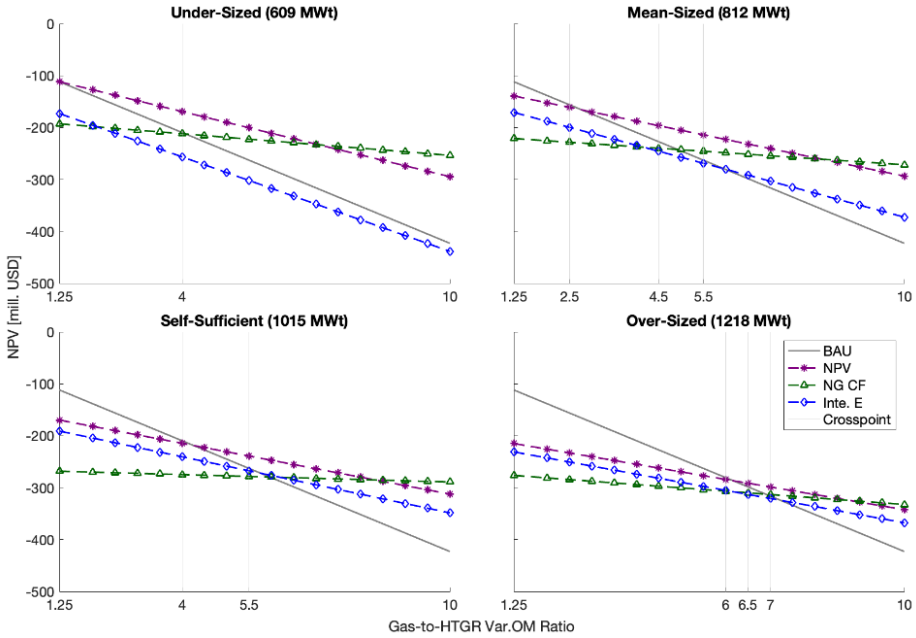

Figure 73. Crossover points where the HTGR-TES system outperforms standalone NG boilers in cost-effectiveness (NPV) for a single industrial process (HTGR CAPEX: $2,500/kWt, $6,329/kWe). Starting from a base cost ratio of 1.25 between NG boiler variable O&M ($15/MWht) and HTGR variable O&M ($12/MWht), crossover points are explored in increments of 0.5 up to a ratio of 10. Any NPV from individual operation goals that outperforms the BAU operation is marked on the x-axis. Due to data point resolution, these points may not match exactly with those derived from interpolation.

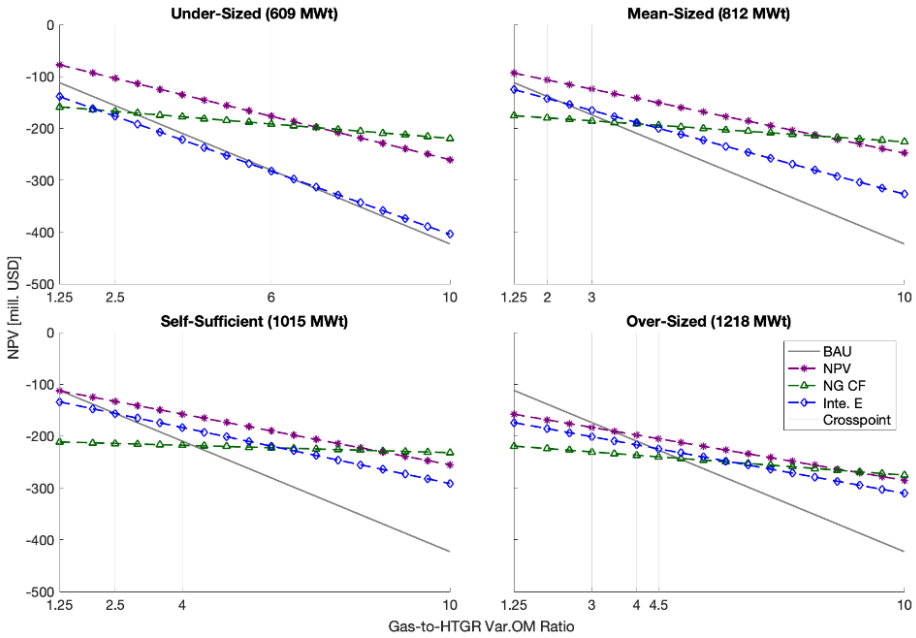

Figure 74. Crossover points where the HTGR-TES system outperforms standalone NG boilers in cost-effectiveness (NPV) for a single industrial process (HTGR CAPEX: $1,750/kWt, $4,430/kWe). Starting from a base cost ratio of 1.25 between NG boiler variable O&M ($15/MWht) and HTGR variable O&M ($12/MWht), crossover points are explored in increments of 0.5 up to a ratio of 10. Any NPV from individual operation goals that outperforms the BAU operation is marked on the x-axis. Due to data point resolution, these points may not match exactly with those derived from interpolation.

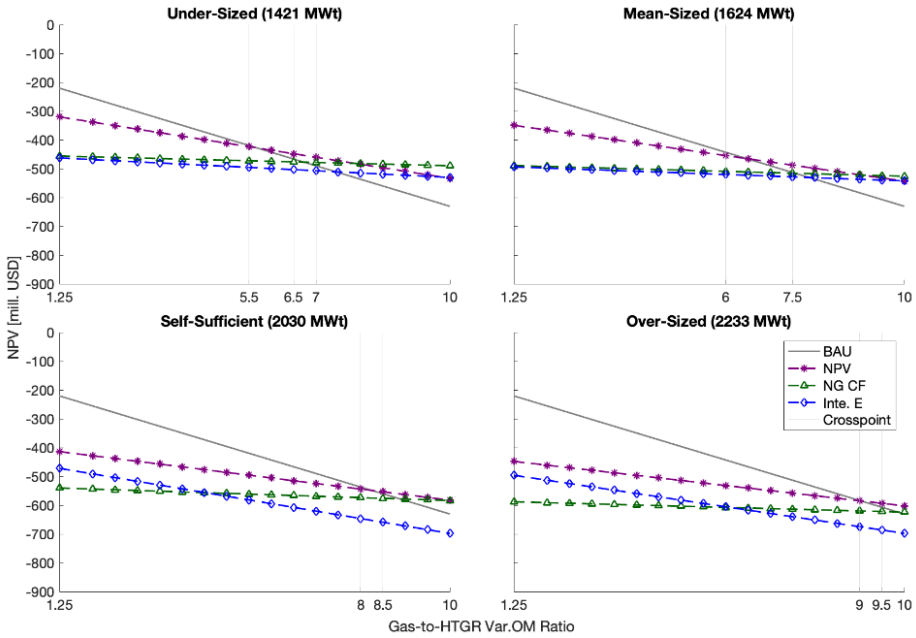

Figure 75. Crossover points where the HTGR-TES system outperforms standalone NG boilers in cost-effectiveness (NPV) for combined industrial processes (HTGR CAPEX: $2,500/kWt, $6,329/kWe). Starting from a base cost ratio of 1.25 between NG boiler variable O&M ($15/MWht) and HTGR variable O&M ($12/MWht), crossover points are explored in increments of 0.5 up to a ratio of 10. Any NPV from individual operation goals that outperforms the BAU operation is marked on the x-axis. Due to data point resolution, these points may not match exactly with those derived from interpolation.

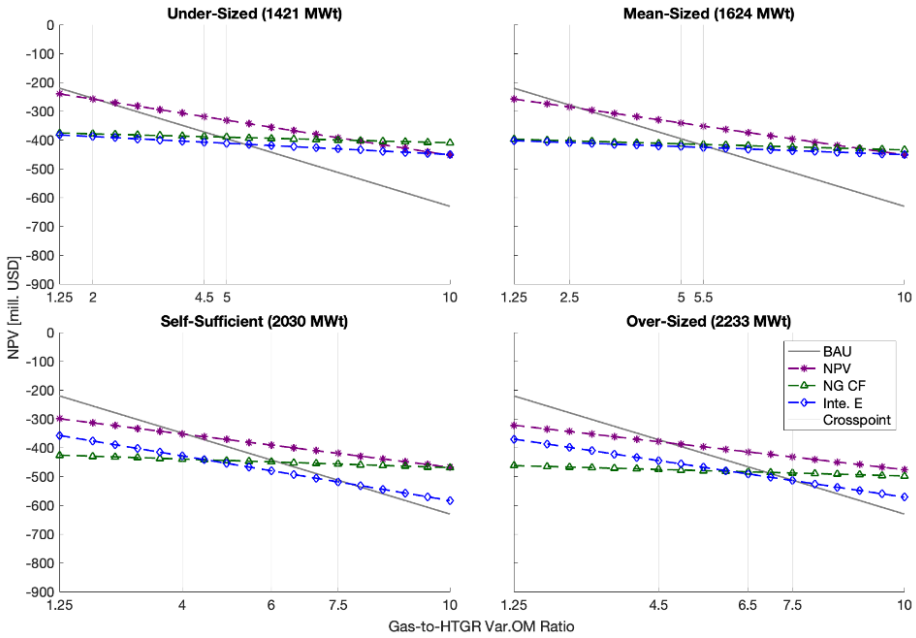

Figure 76. Crossover points where the HTGR-TES system outperforms standalone NG boilers in cost-effectiveness (NPV) for combined industrial processes (HTGR CAPEX: $1,750/kWt, $4,430/kWe). Starting from a base cost ratio of 1.25 between NG boiler variable O&M ($15/MWht) and HTGR variable O&M ($12/MWht), crossover points are explored in increments of 0.5 up to a ratio of 10. Any NPV from individual operation goals that outperforms the BAU operation is marked on the x-axis. Due to data point resolution, these points may not match exactly with those derived from interpolation.

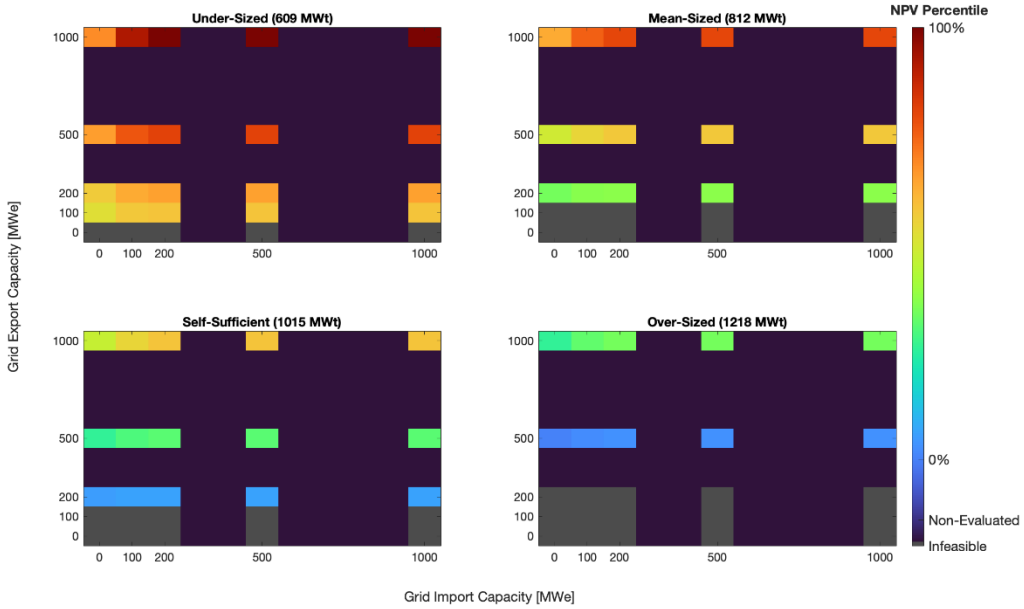

Figure 77. NPV percentile distribution with varying external grid access availability under different deployments (single industrial process). At two to four units deployment, NPVs are optimized for given export-import capacities. NPV percentiles evaluated within four categories: undersized, medium-sized, self-sufficient, and oversized. The dark blue area represents optimization steps not explored area in HERON; dark grey represents areas infeasible in solving the optimization problem.

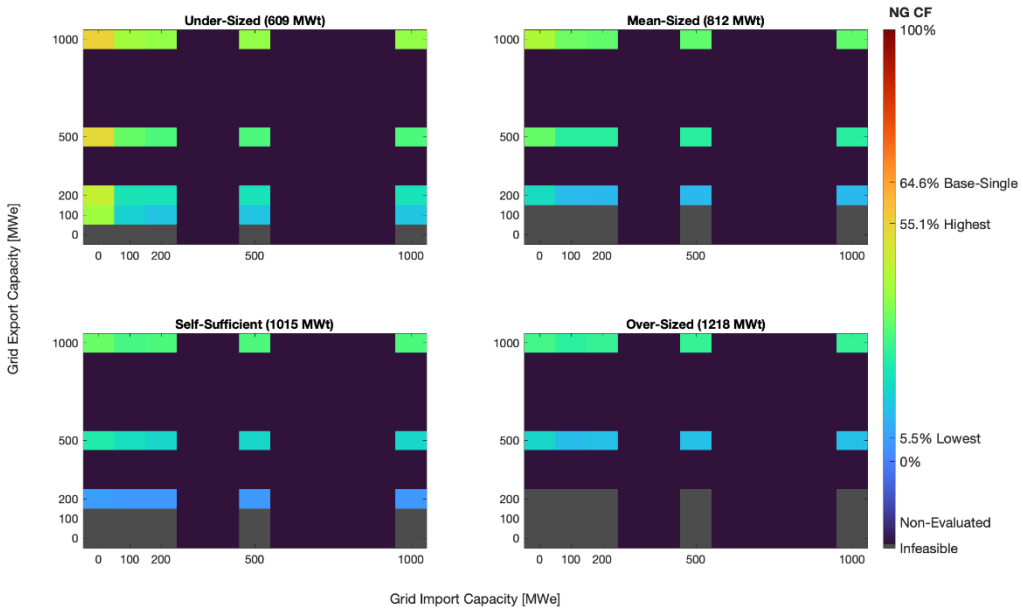

Figure 78. Natural gas boiler capacity factor (NGCF) distribution with varying external grid access availability under different deployments (single industrial process). At two to four units deployment, NGCF values are evaluated within four categories: undersized, medium-sized, self-sufficient, and oversized. The optimal sizing of TES and BOP capacity is identical to that listed in Figure 38. The dark blue area represents optimization steps not explored in HERON, while the dark grey area represents regions infeasible for solving the optimization problem.

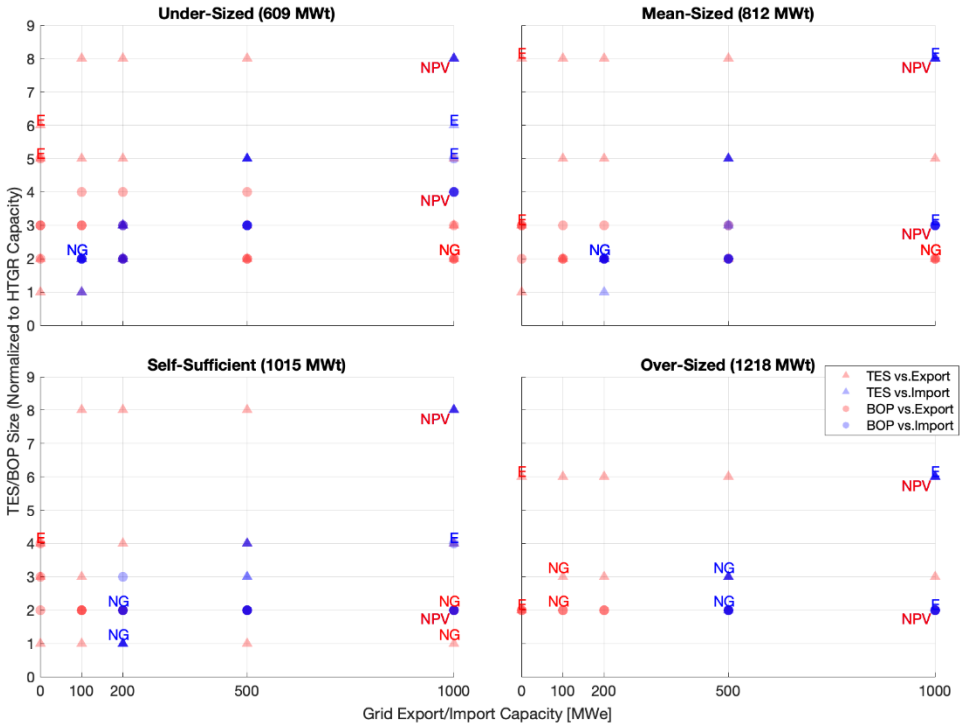

Figure 79. Change in optimal sizing of BOP and TES with varying import and export levels and external grid access availability (single industrial process). Optimal TES (triangle) and BOP (circle) capacities are indicated against considered grid export (red) and import (blue) levels. Corresponding design spaces for maximizing NPV, minimizing the natural gas boiler CF, and maximizing internal electricity supply, are denoted as NPV, NG, and E, respectively.

Note: TES size is represented in terms of charge duration, ranging from 0 to 9 hours, based on the reactor capacity. For instance, if the total reactor capacity is 609 MWt and the optimal TES capacity is eight, the TES capacity would be 609 MWt × 8 = 4,872 MWt. Similarly, BOP size is represented as a fraction of the TES capacity with increments of one-eighth. If the BOP size is represented by 4 (4/8) and the TES capacity is 4,872 MWt, the BOP capacity is calculated as 4/8 × 4,872 MWt = 2,436 MWt. Adding the reactor capacity (1,421 MWt) to this, the total capacity would be 3,045 MWt; we assume the TES can discharge all its stored energy in 1 hour (1 hour discharge duration).

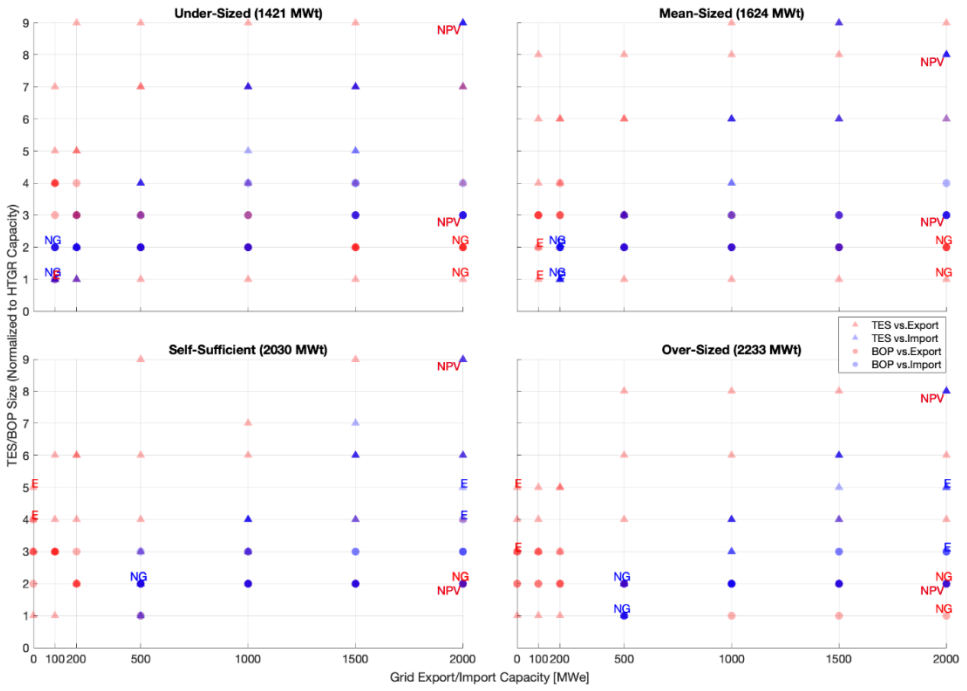

Figure 80. Change in optimal sizing of BOP and TES with varying import and export levels and external grid access availability (combined industrial processes). Optimal TES (triangle) and BOP (circle) capacities are indicated against considered grid export (red) and import (blue) levels. Corresponding design spaces for maximizing NPV, minimizing the natural gas boiler CF, and maximizing internal electricity supply, are denoted as NPV, NG, and E, respectively.

Note: TES size is represented in terms of charge duration, ranging from 0 to 9 hours, based on the reactor capacity. For instance, if the total reactor capacity is 1,421 MWt and the optimal TES capacity is 9 hours, the TES capacity would be 1,421 MWt × 9 = 12,789 MWt. Similarly, BOP size is represented as a fraction of the TES capacity with increments of one-eighth. If the BOP size is 3 (3/8) and the TES capacity is 12,789 MWt, the BOP capacity is calculated as 3/8 × 12,789 MWt = 4,796 MWt. Adding the reactor capacity (1,421 MWt) to this, the total capacity would be 4,796 MWt + 1,421 MWt = 6,217 MWt; we assume the TES can discharge all its stored energy in 1 hour (1 hour discharge duration).

Table 20. Breakdown of the HTGR-TES system operation for a single industrial process under varying operational goals: maximizing NPV and minimizing the natural gas boiler capacity factor (NGCF).

HTGR		TES Capacity [MWht]	BOP Capacity [MWt]	Charge Event	Discharge Event	Avg. Charge Power [MWt]	Avg. Discharge Power [MWt]	Target Goal
Units	Capacity [MWt]							
3	609	3,045	4,872	2,631	599	1,059	4,187	NPV
		914	1,218	1,628	1,417	529	548	NG CF
		2,893	3,654	2,361	299	419	2,981	Inte. E
4	812	3,248	6,496	2,447	737	1,443	4,311	NPV
		1,218	1,624	1,446	1,605	930	754	NG CF
		3,248	6,496	2,863	495	659	3,432	Inte. E
5	1015	3,045	8,120	2,223	912	1,862	4,085	NPV
		1,269	1,015	1,049	1,892	945	472	NG CF
		3,045	4,060	2,578	630	999	3,680	Inte. E
6	1218	3,045	7,308	2,014	1,102	2,262	3,720	NPV

HTGR		TES Capacity [MWht]	BOP Capacity [MWt]	Charge Event	Discharge Event	Avg. Charge Power [MWt]	Avg. Discharge Power [MWt]	Target Goal
Units	Capacity [MWt]							
		2,132	3,654	1,577	1,537	1,671	1,543	NG CF
		3,045	7,308	2,326	844	1,431	3,548	Inte. E

Note: NPV, maximizing NPV; NGCF, minimizing the natural gas boiler capacity factor; Inte. E, maximizing internal electricity demand. The charge and discharge events reflect 1 year of operation.

Table 21. Change in minimum allowable HTGR heat price under varying investment tax credit (ITC) levels for a single industrial process. (HTGR CAPEX: $3,250/kWt, $8,228/kWe).

HTGR		Minimum Allowable HTGR Heat Cost[a,b,c] [$/MWth]					
Units	Capacity [MWt]	ITC 0	ITC 6	ITC 30	ITC 40	ITC 50	Target Goal
3	609	57.6	54.6	42.9	35.9	30.6	NPV
		46.6	45.1	39.0	35.4	32.6	NG CF
		49.2	47.5	40.4	36.2	33.0	Inte. E
4	812	58.5	55.4	42.8	35.3	29.7	NPV
		49.7	47.9	40.5	36.1	32.8	NG CF
		44.5	42.5	34.4	29.5	25.8	Inte. E
5	1,015	64.3	60.8	46.8	38.4	32.1	NPV
		50.4	48.5	40.8	36.2	32.8	NG CF
		46.7	44.4	35.1	29.5	25.3	Inte. E
6	1,218	69.5	66.3	53.7	46.1	40.4	NPV
		60.4	58.2	49.2	43.8	39.8	NG CF
		52.2	49.9	41.0	35.6	31.6	Inte. E

NPV, maximizing NPV; NGCF, minimizing the natural gas boiler capacity factor; Inte. E, maximizing internal electricity demand.

The optimal sizing of TES and BOP capacity is identical to that listed in Table 4.

a The minimum allowable HTGR heat cost is the price at which the selling price must be set to break even on the investment. If the goal is to achieve a market rate of return, these values need to be higher.

b While microreactor CAPEX incurs upfront, the recovery of a portion of the CAPEX occurs at a later point. Thus, it should be refrained from directly multiplying the ITC rates. To account for this effect, we used the tailored parameters for nuclear reactors from Reference [42]: 5%, 27%, 37%, and 46% for the ITC rates of 6%, 30%, 40%, and 50%, respectively.

c Calculating the minimum allowable HTGR heat price involves the following steps, with all items calculated in NPV: (1) calculate the cost items for the HTGR, which include fixed O&M and variable O&M, (2) calculate net electricity sales, (3) calculate ITC-reflected HTGR by multiplying the applicable rate by the HTGR CAPEX (e.g., (1 - ITC rate) × CAPEXHTGR × Capacity), (4) calculate the amount of HTGR heat provided for industrial thermal and electrical demand (thermal-to-electric conversion efficiency: 39.5%), and (5) sum the results from Steps (1) to (3) and divide by the amount of HTGR heat provided, from Step (4).

Table 22. Change in minimum allowable HTGR heat price under varying ITC levels for a single industrial process (HTGR CAPEX: $2,500/kWt, $6,329/kWe).

HTGR		Minimum Allowable HTGR Heat Cost[a] [$/MWth]					
Units	Capacity [MWt]	ITC 0	ITC 6	ITC 30	ITC 40	ITC 50	Target Goal
3	609	44.1	41.8	32.8	27.4	23.3	NPV
		39.6	38.4	33.7	30.9	28.8	NG CF
		41.1	39.7	34.3	31.0	28.6	Inte. E
4	812	44.0	41.6	32.0	26.2	21.9	NPV
		41.2	39.8	34.1	30.7	28.2	NG CF
		35.1	33.6	27.3	23.6	20.7	Inte. E
5	1,015	48.1	45.4	34.6	28.2	23.3	NPV
		41.6	40.1	34.2	30.7	28.0	NG CF
		36.0	34.2	27.0	22.7	19.5	Inte. E
6	1,218	54.9	52.4	42.7	36.9	32.5	NPV
		50.1	48.3	41.4	37.3	34.2	NG CF
		41.8	40.1	33.2	29.1	26.0	Inte. E
					Historical NG price range of mean ± 2σ [b]		

NPV, maximizing NPV; NGCF, minimizing the natural gas boiler capacity factor; Inte. E, maximizing internal electricity demand.

The optimal sizing of TES and BOP capacity is identical to that listed in Table 4.

a The minimum allowable HTGR heat cost is the price at which the selling price must be set to break even on the investment. If the goal is to achieve a market rate of return, these values need to be higher.

b Estimated minimum allowable HTGR heat price that falls into historical NG price ranges is colored in green. The past 5 years' price data (07/22/2019–07/19/2024) from the Henry Hub NG spot prices are used [45].

Table 23. Change in minimum allowable HTGR heat price under varying ITC levels for a single industrial process (HTGR CAPEX: $1,750/kWt, $4,430/kWe).

HTGR		Minimum Allowable HTGR Heat Cost[a] [$/MWth]					
Units	Capacity [MWt]	ITC 0	ITC 6	ITC 30	ITC 40	ITC 50	Target Goal
3	609	30.6	29.0	22.7	18.9	16.1	NPV
		32.6	31.7	28.5	26.5	25.0	NG CF
		32.9	32.0	28.2	25.9	24.2	Inte. E
4	812	29.6	27.9	21.1	17.1	14.1	NPV
		32.7	31.7	27.7	25.4	23.6	NG CF
		25.7	24.6	20.3	17.6	15.7	Inte. E
5	1,015	32.0	30.1	22.5	18.0	14.6	NPV
		32.7	31.7	27.6	25.1	23.2	NG CF
		25.2	24.0	18.9	15.9	13.7	Inte. E
6	1,218	40.3	38.6	31.8	27.7	24.6	NPV
		39.7	38.5	33.7	30.8	28.6	NG CF
		31.5	30.3	25.5	22.6	20.4	Inte. E
					Historical NG price range of mean ± 2σ [b]		

NPV, maximizing NPV; NGCF, minimizing the natural gas boiler capacity factor; Inte. E, maximizing internal electricity demand.

The optimal sizing of TES and BOP capacity is identical to that listed in Table 4.

a The minimum allowable HTGR heat cost is the price at which the selling price must be set to break even on the investment. If the goal is to achieve a market rate of return, these values need to be higher.

b Estimated minimum allowable HTGR heat price that falls into historical NG price ranges is colored in green. The past 5 years' price data (07/22/2019–07/19/2024) from the Henry Hub NG spot prices are used [45].

Table 24. Change in minimum allowable HTGR heat price under varying ITC levels for combined industrial processes. (HTGR CAPEX: $2,500/kWt, $6,329/kWe)

HTGR		Minimum Allowable HTGR Heat Cost [a] [$/MWth]					
Units	Capacity [MWt]	ITC 0	ITC 6	ITC 30	ITC 40	ITC 50	Target Goal
7	1,421	58.5	56.1	46.4	40.5	36.1	NPV
		38.7	37.6	33.0	30.3	28.3	NG CF
		37.9	36.8	32.5	29.8	27.9	Inte. E
8	1,624	57.5	55.0	44.9	38.9	34.4	NPV
		40.3	39.0	34.0	31.0	28.8	NG CF
		38.9	37.7	32.9	30.0	27.8	Inte. E
10	2,030	60.3	57.5	46.4	39.8	34.8	NPV
		47.2	45.5	38.9	34.9	31.9	NG CF
		40.1	38.5	32.0	28.1	25.2	Inte. E
11	2,233	61.8	58.9	47.4	40.4	35.2	NPV
		48.3	46.6	39.7	35.6	32.5	NG CF
		41.3	39.5	32.6	28.4	25.2	Inte. E

NPV, maximizing NPV; NGCF, minimizing the natural gas boiler capacity factor; Inte. E, maximizing internal electricity demand.

The optimal sizing of TES and BOP capacity is identical to that listed in Table 5.

a The minimum allowable HTGR heat cost is the price at which the selling price must be set to break even on the investment. If the goal is to achieve a market rate of return, these values need to be higher.